

# **The Evolution of Multi-Site Small Cracks under Fatigue Loading**

A Thesis  
Presented to  
The Academic Faculty

by

Marcus Domenic Cappelli

In Partial Fulfillment  
of the Requirements for the Degree  
Doctor of Philosophy in the  
School of Aerospace Engineering

Georgia Institute of Technology  
May of 2007

Copyright 2007 by Marcus Cappelli

# The Evolution of Multi-Site Small Cracks under Fatigue Loading

Approved by:

Dr. George Kardomateas, Advisor  
School of Aerospace Engineering  
*Georgia Institute of Technology*

Dr. Robert Carlson  
School of Aerospace Engineering  
*Georgia Institute of Technology*

Dr. Erian Armanios  
School of Aerospace Engineering  
*Georgia Institute of Technology*

Dr. David McDowell  
School of Mechanical Engineering  
*Georgia Institute of Technology*

Dr. Thomas Brussat  
Durability and Damage  
*Lockheed Martin, F-22Structures*

Date Approved: 03/30/2007

To Domenico, Leo and Josephine

## **Acknowledgments**

I would first like to thank God. I would also like to thank my parents Angela and Argante for all of the help they have given me in surviving school as well as the rest of my family, Catherine, Lauren and Victoria for putting up with me. I would like to especially to thank my soon to be wife Kristen. Without her by my side none of this would be possible.

I would like to thank my advisors Prof. George Kardomateas and Prof. Robert Carlson who have not only helped me with my work but also through many difficult times. They have become much more than advisors, they have become true friends. I would also like to acknowledge my committee members who have provided invaluable guidance to my work; Prof. Erian Armanios, Dr. Thomas Brussat and Prof. David McDowell. Finally, I would like to thank my undergraduate assistants Christopher Neglia, Heinrich Souza and Ahroni Karon for their assistance in the lab.

## Table of Contents

	Page
Acknowledgements	iv
List of Tables	vii
List of Figures	viii
List of Symbols and Abbreviations	xi
Summary	xv
<u>Chapter</u>	
1 Introduction/Literature Survey	1
1.1 Small Crack Anomaly	1
1.2 Deterministic Analyses	8
1.3 Non-Deterministic Analyses	13
1.4 Significance of Current Work	21
2 Experimental Procedures	26
2.1 Material Properties	26
2.2 Test Specimen	28
2.3 Grips/Alignment	30
2.4 Test Setup/Crack Measurement Technique	33
3 Data	37
3.1 Preliminaries	37
3.2 Crack Geometry	39
3.3 Cluster Measurements	42

4	Transition Length	49
4.1	Micro-Notches: Results/Summary of Previous Work	49
4.2	Cracks Grown from Smooth Surfaces: Current Work	58
4.3	Discrete Crack Growth Rate Observations	65
4.3	Applications	67
4.3.1	Separation of Crack Growth Regimes	67
4.3.2	Fatigue of Thin Metal Foils	68
5	Bi-Modal Model of Micro Multi-Site Cracking	70
5.1	Introduction	70
5.2	Separation of the Distributions	72
5.3	Confidence Limit Analysis	75
5.4	Life Prediction	83
5.5	Crack Acceleration Analysis	86
6	Continuing Research	90
6.1	Operational Condition Issues	90
6.2	Dual Phase Alloys	92
6.3	Cluster Density	94
7	Conclusions	95
	Appendix A: Micro-Structural Characterization	98
	Appendix B: Specimen Preparation	106
	Appendix C: Crack Cluster Topographical Measurements	109
	References	114

## List of Tables

	Page
Table 2.1: Material bulk properties	27
Table 2.2: Material grain sizes	27
Table 2.3: Particle size distributions	28
Table 3.1: Summary of crack measurements	38
Table 3.2: Observed crack shapes	42
Table 3.3: Crack cluster densities	44
Table 4.1: Average grain dimensions for 6061-T651 rod	50
Table 4.2: Summary of the regression constants of the primary cracks analyzed, for the relationship between surface crack length and load cycle count	59
Table 4.3: Summary of the regression constants for the primary crack growth rate versus loading cycle	60
Table 4.4: Summary of the crack growth rate statistics	61
Table 5.1: Summary of primary crack statistics	75

## List of Figures

	Page
Figure 1.1: Sigmoidal variation of crack growth rate	2
Figure 1.2: Summary of observed small crack behavior	4
Figure 1.3: Kitagawa diagram summarizing the fatigue crack growth threshold	5
Figure 1.4: Abbreviated Monte Carlo simulation flow chart	18
Figure 2.1: Schematic defining the material directions	27
Figure 2.2: Specimen geometry (all dimensions in inches)	29
Figure 2.3: Fully polished specimen	30
Figure 2.4: Assembly views of mechanical grips	32
Figure 2.5: Testing load form	33
Figure 2.6: Photograph of experimental setup	35
Figure 2.7: Illustration of scanning procedure	36
Figure 3.1: Assumed semi-circular crack geometry	39
Figure 3.2: Photograph of non-fatal crack on fractured surface	40
Figure 3.3: SEM micrograph of the fracture surface of a primary crack	41
Figure 3.4: Definition of angular positions	43
Figure 3.5: Topography of the multi-site crack growth on specimen I	45
Figure 3.6: Crack length versus loading cycle for all cracks on specimen F	47
Figure 4.1: Corner Micro-Notch Specimen Geometry	51
Figure 4.2: Corner crack geometry	51
Figure 4.3: Crack length versus cycle count data	52
Figure 4.4: Crack growth rate versus crack length data	53

Figure 4.5: Crack growth rate standard deviation/grain intersections versus crack length	54
Figure 4.6: Standard Deviation of crack growth rates versus the number of grains intersected by the crack front	55
Figure 4.7: Sample crack geometries with a simulated microstructure: (a) corner crack, (b) thumbnail crack, (c) surface crack in bending	57
Figure 4.8: Crack length versus cycle count data for primary cracks of specimen F	59
Figure 4.9: Crack growth rates for the primary cracks of specimen F	61
Figure 4.10: Coefficient of variability of the crack growth rate	63
Figure 4.11: Crack growth rates calculated using secant method	66
Figure 5.1: Example of the distribution separation procedure applied to specimen C	74
Figure 5.2: Normal probability plot of the primary crack data at 45,000 cycles	77
Figure 5.3: Normal probability plot of the primary crack data at 55,000 cycles	78
Figure 5.4: Normal probability plot for secondary cracks at 55,000 cycles	79
Figure 5.5: Primary crack data with confidence limits drawn on the mean	81
Figure 5.6: Primary crack data with confidence limits drawn on the mean behavior of both the primary and secondary cracks	82
Figure 5.7: Assumed crack geometry	84
Figure 5.8: Results of the life prediction analysis	86
Figure 5.9: Crack accelerations for all cracks on specimen F	88
Figure 6.1: Effects of cooling rate on the microstructure of Ti-6Al-4V	93
Figure A.1: Schematic defining the material planes	98
Figure A.2: Longitudinal section, 5x zoom	98
Figure A.3: Longitudinal section, 10x zoom	99
Figure A.4: Longitudinal section, 20x zoom	99

Figure A.5: Short Transverse section, 5x zoom	101
Figure A.6: Short Transverse section, 10x zoom	100
Figure A.7: Short Transverse section, 20x zoom	101
Figure A.8: Long Transverse section, 5x zoom	101
Figure A.9: Long Transverse section, 5x zoom	102
Figure A.10: Long Transverse section, 10x zoom	102
Figure A.11: Distribution of Fe-Al particles in the longitudinal section	103
Figure A.12: Distribution of Mg <sub>2</sub> Si particles in the longitudinal section	103
Figure A.13: Distribution of Fe-Al particles in the short transverse section	104
Figure A.14: Distribution of Mg <sub>2</sub> Si particles in the short transverse section	104
Figure A.15: Distribution of Fe-Al particles in the long transverse section	105
Figure A.16: Distribution of Mg <sub>2</sub> Si particles in the long transverse section	105
Figure B.1: Illustration of horizontal polishing	106
Figure B.2: Illustration of vertical polishing	106
Figure C.1: Topography of the multi-site crack growth on specimen 6	110
Figure C.2: Topography of the multi-site crack growth on specimen F	111
Figure C.3: Topography of the multi-site crack growth on specimen E	112
Figure C.4: Topography of the multi-site crack growth on specimen C	113

## List of Symbols

$\%V_v$		Area Fraction
$a$		Crack length
A, B, C, D, E, F, G		Regression constants
$\alpha$	HCP alpha phase of titanium, confidence level	
Al		Aluminum
$\mathbf{b}$	Burger's vector of a dislocation	
$\beta$	BCC Beta phase of titanium, Bi-modal mixture coefficient	
C, m		Paris law constants
$C_x$		Coefficient of variation
$d$	Ligament length, effective crack length, Average grain dimension	
D	Distance between micro-structural barriers	
$da/dN$		Crack growth rate
$d^2a/dN^2$		Crack acceleration
E		Young's modulus
$\eta$	Zero for plane stress, $\nu$ for plain strain	
Fe		Iron
$f(g)$	Boundary correction factor to SIF	
$\gamma$	Plastic zone size correction factor	
$\Gamma$		Gamma function
$i$		Discrete counter variable
J		Elastic-plastic J-Integral

$K$	Elastic Stress Intensity Factor
$K_I$	Stress intensity factor in mode one loading
$K_{IC}$	Critical stress intensity factor for unstable fracture
$K_J$	Equivalent plastic SIF
$K_p$	Plasticity corrected SIF
$K_{tg}$	Stress Concentration over the ligament stress
$l_1, l_2$	Transition lengths defined on the Kitagawa diagram
$\mu$	Mean, Shear modulus
Mg	Magnesium
$n, p, q$	Crack growth curve constants
$n$	Average number of grains intersected by a crack front, number of dislocations in a slip band, number of measurements
$N$	Loading cycle count
$\nu$	Degrees of freedom in a student-t distribution
$P$	Load
$r$	Notch radius
$R$	Load ratio
$\rho$	Plastic zone size
$R^2$	Coefficient of determination
$S$	Standard deviation
$\sigma$	Stress, Standard deviation
$\sigma_y$	Yield stress
$\sigma_u$	Ultimate stress

Si	Silicon
t	Thickness of specimen , Thickness of finite plate
$\tau$	Applied shear stress
$\nu$	Poisson ratio
W	Specimen width, Width of finite plate
$\bar{x}$	Sample mean
X	Remaining distance to next micro-structural barrier
y	Vertical measurement between a crack and the specimen centerline

## List of Abbreviations

ASTM	American Society for Testing and Materials
BCC	Body centered cubic
CDF	Cumulative Distribution Function
DTMC	Discrete Time Markov Chain
EIFS	Equivalent initial flaw size
FCC	Face centered cubic
GTRI	Georgia Tech Research Institute
HCP	Hexagonal close packed
Hz	Hertz
kN	Kilo-Newtons
Ksi	Kips per square inch
Lbs	Pounds
LEFM	Linear elastic fracture mechanics
PDF	Probability Density Function
s	Seconds
SIF	Stress intensity factor
SEM	Scanning electron microscope
TPS	Thermal protection system

## Summary

The fatigue of aerospace structures poses the significant problem of estimating the total life of a component in order to construct an appropriate inspection schedule that will ensure the safety of the aircraft. Erroneous crack growth analysis results can lead to overly costly maintenance and inspection schedules or worse, an unsafe vehicle. The total component life can be broken into three segments: 1) Initiation of microscopic cracks, 2) the growth of these micro-cracks until they either arrest or reach the macro-scale and 3) the growth of a macro-crack until failure.

While adequate analytical tools exist to quantify the growth of relatively long cracks, the other phases are not well understood. This thesis focuses on the growth of cracks which are small in relation to the material microstructure especially the situation of clusters of small cracks grown from smooth surfaces, termed micro-multi-site cracking, as is frequently the case for components in service. It is these cracks with which current research is concerned. A proper understanding of this regime of crack growth will allow for less conservative maintenance schedules as well as the application of more sensitive health monitoring systems which are currently under development.

To address the problem a significant experimental investigation of micro-multi-site cracking was conducted. Crack cluster geometry, growth rates and anomalous behavior were all optically monitored and recorded by means of a tele-microscope. Tests were conducted from natural cluster initiation through final failure by fracture to allow the complete evolution of the clusters to be observed. The material used was a plate form of 7075-T7351 aluminum alloy.

A micro-structurally based transition crack length is defined to determine the point which separates small and long crack growth. This definition is based upon the observed evolution of scatter in the growth rates of growing small cracks. It is shown that this scatter falls with growth until the transition point is reached where it assumes a constant value for the growth of long cracks. Additionally, applications of the defined transition length are reviewed.

It is then shown that the total population of cracks within the clusters can be considered as bi-modal. One distribution consists of *primary* cracks which can grow and ultimately cause specimen failure. The second distribution consists of *secondary* cracks, the growth of which ultimately arrests. However, these cracks form a neighborhood through which the primary cracks must grow and will thus affect the growth of the primary cracks through crack shielding and other interactions.

Several methods for experimentally separating the two distributions have been developed. The first method relies upon the defined transition point between small and long crack behavior. A second method based upon the second derivative of the crack length versus cycle count data has also been developed.

Since the secondary cracks cannot lead to failure their data must be discarded prior to any fatigue crack growth analysis. It is then shown that failure to do so will lead to erroneous non-conservative predictions of crack growth. With this separation completed, confidence bounds are fit to the small cracks in the primary crack distribution. These bounds are then used as part of a two region analysis of crack growth. Prior to the defined transition length the confidence bounds are used. After transition to long crack behavior

traditional fracture mechanics predictions are appended to the ends of the upper and lower bounds on small crack growth.

Finally, recommendations for continuing research are suggested. It is proposed that the current results are extended with research on the effects of operational condition issues, such as variable amplitude loading and varying levels of surface preparation, on small crack growth. Additionally it is proposed that the small to long crack transition behavior of a dual phase alloy such as Ti-6Al-4V titanium be investigated.

## Chapter I – Introduction/Literature Survey

While predicting the growth of relatively long cracks is a simple matter, the growth of cracks which are small when compared to the material microstructure is inherently more complex. This small crack behavior is evidenced in the high variability in measured growth rates, growth below the traditional stress intensity factor threshold and growth at higher rates than equivalent long cracks. After a summary of the small crack anomaly this chapter contains a brief summary of the many methods developed in the literature to deal with the small crack anomaly. Both deterministic and non-deterministic models will be described and evaluated. Finally, the relation of the current work to the literature and how it addresses deficiencies in the current knowledge will be discussed.

### **1.1 Small Crack Anomaly**

The growth of cyclically loaded cracks under predominantly elastic conditions is well understood [1], provided that the cracks are long compared to characteristic lengths specific to each case of growth. Such cracks satisfy all of the assumptions of Linear Elastic Fracture Mechanics (LEFM) and are thus adequately described by the Stress Intensity Factor (SIF,  $K$ ) which takes the form shown below where  $f(g)$  is a function of the geometry  $\sigma$  is the remotely applied stress and  $a$  is the crack length.

$$K = f(g)\sigma\sqrt{\pi a} \quad (1.1)$$

This parameter completely characterizes the crack tip stress and strain fields. Additionally, the concept of similitude, which LEFM is predicated upon, states that any cracks having the same SIF will also have identical crack tip stress fields, regardless of crack size. For fatigue loading it is useful to define the cyclic SIF or SIF range ( $\Delta K$ ),

which is simply the difference between the maximum and minimum stress intensity values for a single loading cycle.

Subject to these assumptions, the growth of a crack can then be described by a sigmoidal curve of the form presented below in figure 1.1. As shown, this curve contains three distinct regions.

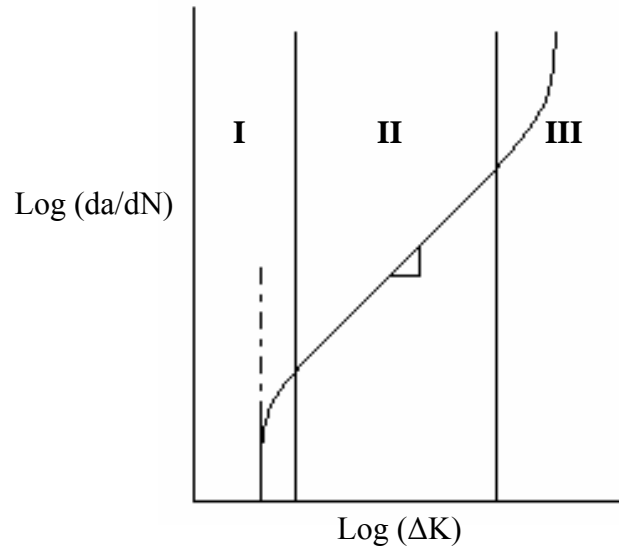


Figure 1.1: Sigmoidal variation of crack growth rate

Region III is defined by very large crack growth rates as the crack grows towards unstable fracture and thus comprises only a small portion of the fatigue life. Region II is the so called Paris region. The growth rates of cracks which fall in this category tend to obey an exponential function of the SIF range. This function is presented below, where  $C$  and  $m$  are experimentally determined constants.

$$\left(\frac{da}{dN}\right) = C(\Delta K)^m \quad (1.2)$$

This equation can easily be integrated to obtain a history of crack growth.

Region I is the near-threshold region. Here, complexities can arise which depend on the crack length, not only the SIF. Long cracks in this region generally grow at smaller rates than the Paris equation predicts. Additionally, below the threshold SIF ( $\Delta K_{th}$ ), where the growth curve is vertical, long cracks will not grow under cyclic loading. Attempts have been made to model the entire growth curve with a single equation. One such equation is presented below [2]:

$$\left( \frac{da}{dN} \right) = \frac{C(1-R)^m \Delta K^n (\Delta K - \Delta K_{th})^p}{[(1-R)K_{IC} - \Delta K]^q} \quad (1.3)$$

In the above equation  $K_{IC}$  is the material fracture toughness,  $R$  is the load ratio and  $n$ ,  $p$  and  $q$  are additional experimentally determined constants.

However, when cracks are small compared to the pertinent characteristic lengths they no longer follow the growth curve that longer cracks follow. The characteristic lengths that define a crack as either small or long can be of several types. The first of these is a geometrical length. An example of this would be size of the plastic zone created by a notch. The second type of characteristic length is that of the material microstructure, such as the width of a grain. The current work will focus on such cracks such which are not large compared with the material microstructure or micro-structurally small cracks. At these small lengths there is a breakdown in the concept of similitude, the very foundation that LEFM relies upon. This means that the behavior of these small cracks is no longer uniquely determined by the SIF. It is this breakdown that leads to the observed small crack anomaly.

The abnormal behavior of small fatigue cracks was first quantified by Pearson in 1975 [3]. He noted that a micro-structurally small crack will grow at a significantly greater rate than a long crack with an identical SIF. This included small cracks that would grow below what was considered to be the threshold SIF range below which long cracks could not grow. After significant growth however, the small crack behavior merged with that of long cracks.

This anomalistic behavior is summarized below in figure 1.2 [4]. The behavior observed by Pearson is evidenced in the “U” shaped small crack growth curves and the fact that they lie above the LEFM long crack growth curve. In addition to this behavior, Lankford and Tanaka et al. [5, 6, 7] have made more in-depth observations on the growth of small cracks. They have observed that the growth of small cracks does not progress along a smooth growth rate curve. Rather, the growth is a sequence of accelerated growth/retardation occurrences.

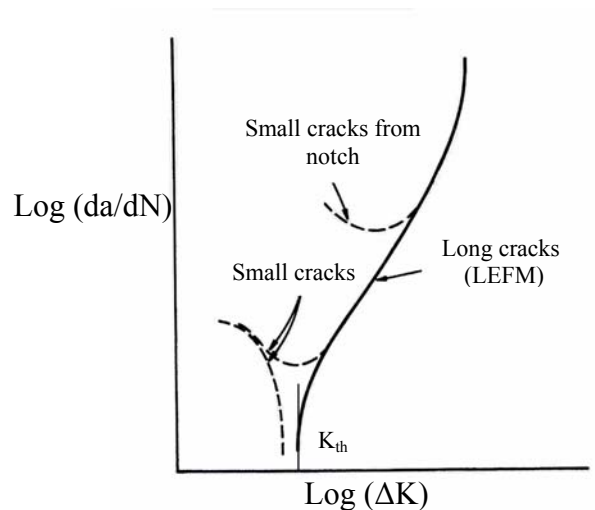


Figure 1.2: Summary of observed small crack behavior

It is also evident in the above figure that the growth of some portion of small cracks simply arrests. This phenomenon is a special case of the retardation/acceleration transients found in the growth of small cracks and has been observed by many researchers [8]. Additionally shown is the possibility of small crack growth both above and below the threshold SIF for long cracks.

The threshold behavior of small and long cracks can be summarized in a Kitagawa diagram [9], an example of which is shown below in figure 1.3.

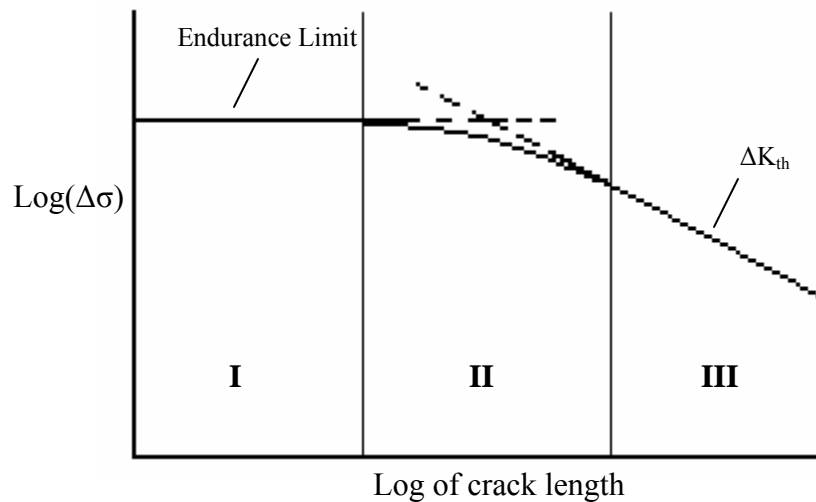


Figure 1.3: Kitagawa diagram summarizing the fatigue crack growth threshold

This diagram plots the logarithm of the stress range versus the logarithm of the crack length. Crack growth is only possible for a crack/loading system that lies above the curve. It is shown then that there are three distinct regions of threshold behavior. In region III cracks are long and obey the LEFM assumption of a constant threshold value of the SIF range. However, in region I small cracks instead obey a threshold defined by a constant maximum tensile stress range. This stress range is related to the fatigue limit. Region II represents a transition region between the two threshold limits. If the constant

SIF threshold were extrapolated into the small crack regime in region I it can be noted that a small crack can grow below what would be predicted by LEFM as the lowest stress range possible for growth.

While some scatter is inherent in any crack growth data, even for long cracks, small crack data tends to be significantly more dispersed. Just as other small crack growth parameters tend towards that of long cracks with growth, so does the level of scatter. It is therefore expected that as small cracks grow scatter is expected to fall. This is contrary to the behavior of long cracks where the width of scatter bands is generally fairly constant. The retardation/acceleration transient effects are the cause of the additional scatter found in small cracks. These effects are themselves caused by the influence of the local microstructure of the material on crack growth. Each grain in the material is inherently anisotropic, having a specific crystallographic orientation. This means that each grain will either favor or discourage crack growth to a different degree. Additionally, inhomogeneities in the microstructure such as inter-metallic particles and triple points [10, 11] between grains will affect the growth of cracks. These micro-structural effects then cause the breakdown of similitude for small cracks. Much research has been conducted on this topic.

In work on fatigue crack initiation and early propagation in 3% Silicon Iron, Tanaka et al. [7] directly observed the microscopic behavior of small cracks as they interact with the material microstructure. By etching specimens prior to observation they were able to not only observe when cracks interacted with the local microstructure but also the mechanism of crack propagation. By observing several corner cracks where two perpendicular sides of a single grain were observable they were able to obtain a limited

amount of crack growth data with knowledge of the crystallographic orientation of the cracked grain. It was found that while grain boundaries did pose a barrier to crack growth, additional anomalies in crack growth rates were observed when cracks transitioned between growth mechanisms. The mechanisms observed were growth along slip bands, inter-granular grain boundary growth and Stage II growth (non-crystallographic). From the observed corner cracks it was also determined that the growth mechanism could be a function of the crystallographic orientation of the cracked grain and that of its neighbor.

A similar study was performed by Lankford on small cracks grown from a smooth surface in an aluminum alloy [5]. It was found that many of the observed periods of accelerated growth were caused by localized micro-plasticity contained within a single favorably oriented grain. The opposite case of an un-favorably oriented grain would result in retarded crack growth. Additionally, through a fractographic analysis on a surface that had been etched to reveal grain boundaries, it was determined that for small cracks, grain boundaries represent a barrier towards growth. While the strength of the barrier depends on the orientation of the two grains, it was observed that at a boundary cracks would stop and be forced to re-nucleate into the new grain.

It has also been argued that the accelerated growth of small cracks could be the result of a lack of crack closure [12, 13, 14]. This transient effect raises the effective SIF range, which would cause the observed accelerated growth, until crack closure can develop as a crack becomes longer. However, even crack closure effects are subject to irregularities caused by interaction with the local microstructure. Morris has shown that the crack

closure stresses for small cracks vary from grain to grain [15]. Additionally, the closure stresses were dependent on the proximity of crack tips to the nearest grain boundary.

Due to the complex nature of determining the behavior of small cracks, a large number of methods have been developed to aid in the prediction of their growth. These methods include both deterministic and non-deterministic analyses. What follows is a brief summary of the various classes of work on the topic.

## **1.2 Deterministic Analyses**

Several researchers have investigated the concept of a transition crack length between small and long crack behavior. These lengths have been defined by observing several aspects of small crack growth. If defined properly, this transition length would be of tremendous importance as it would supply an initial crack length where LEFM analyses become applicable.

One such definition has been suggested by Taylor and Knott in an investigation on a cast nickel aluminum bronze alloy [16]. In observing small crack threshold behavior they have defined several critical lengths,  $l_1$  and  $l_2$ . These lengths correspond to the points on the Kitagawa diagram where the fatigue threshold deviates from a constant stress and from a constant SIF respectively. The value of  $l_2$  then becomes a convenient transition length as it represents the crack length, below which LEFM assumptions of a threshold SIF lead to a non-conservative analysis. It was also observed that the growth of cracks whose lengths were below this value were dominated by micro-structural effects. Above this length the small crack growth data began to agree with long crack data.

It was found that the value of this transition parameter could be loosely correlated with the characteristic micro-structural dimensions. For instance, cracks in a high

strength steel with fine grains would become transition to long cracks before cracks in a coarse grained aluminum alloy. For their tests on a nickel aluminum bronze alloy they found that cracks transitioned when their surface length reached approximately three grain diameters.

In an investigation of the results of around ten sets of experiments performed by other researchers, Taylor and Knott have summarized the transition behavior found in a wide range of materials. They have done this by applying the definitions of  $l_1$  and  $l_2$  and attempting to compare these values to the micro-structural dimensions pertinent to each material being studied. It was found that there was a correlation between the transition sizes and the scale of the microstructure. The transition crack lengths were found to range between approximately five to 100 times the size of the applicable micro-structural dimensions. However, there was no clear consensus on which micro-structural features to choose. Grain sizes, the width of individual lamellae in dual phase metals and even the average width of inclusions were used.

Additional deterministic methods of handling the small crack anomaly have been proposed that do not rely on a transition crack length. These methods rely instead on characterizing the entire range of crack lengths in a single parameter, rather than breaking an analysis into multiple regimes which require different methods of analysis. This would significantly simplify the engineering problem of predicting crack growth rates from initiation through failure. The majority of these methods rely on applying corrections to previously developed continuum methods of fracture mechanics.

For instance, some level of success has been had in correlating the growth of small cracks using the elastic-plastic J-Integral and the related  $\Delta J$ -Integral [17], even though

some of the fundamental assumptions used in their derivation, such as the use of the Hencky deformation theory of plasticity, may be violated. However, since J-Integral solutions for complex crack shapes may be hard to come by, Newman [18, 19] has suggested a simpler model of a plastically corrected SIF,  $K_p$ . This parameter is an attempt to estimate values for an equivalent plastic SIF,  $K_J$ , which is proportional to the square root of J. These equations are presented below.

$$K_J^2 = \frac{JE}{(1-\eta^2)}, \quad K_J \sim \sqrt{J}$$

$$K_p = \sigma \sqrt{\pi d} f(d) \tag{1.4}$$

$$d = a + \gamma \rho$$

This plastically corrected SIF is evaluated at an effective crack length,  $d$ , which is taken to be equal to the physical crack length plus some proportion,  $\gamma$ , of the plastic zone size,  $\rho$ . In fatigue where SIF range values are used, it is the cyclic plastic zone size which must be used to evaluate SIF's. With a properly selected value of  $\gamma$  this method has been shown to provide a fair approximation of J over the majority of stress levels.

For the purposes of life prediction, Newman has combined the above analysis with a plasticity closure model based on the Dugdale model of crack tip yielding. The Dugdale model has been modified by leaving a plastically deformed wake of material behind the crack tip. Additionally, the flow stresses in the plane stress Dugdale model were adjusted by a constraint factor, which varies from unity under plane stress conditions to three in perfect plane strain conditions, to account for plasticity induced constraints. This model is then used to calculate the crack opening stress for various heights of initial defects

present from inclusions which are often found to be cracked prior to loading due to the thermo-mechanical processing of the material. These values can then be used to create an effective plastic SIF range,  $\Delta K_p$ , which only includes stresses where the crack is open. The results of the analysis showed that even with very small flaw heights crack closure can be delayed until further crack growth. This leads to a higher effective SIF and thus the faster growth that is observed in small cracks.

However, unlike in plastic wake models of closure, Halliday et al [12] have suggested that small cracks may not be completely closure free. They have shown that small cracks may still close at positive stresses due to fracture surface roughness caused by discrete asperities. These effects can reduce, but not completely nullify the plasticity induced closure phenomena.

An alternate method of quantifying aspects of the small crack regime has been suggested by Suresh [20]. He has proposed that nonlinearities in the morphology of small cracks can cause the observed retarded growth and even arrest. These nonlinearities naturally occur as cracks intersect grain boundaries and turn to align themselves with the local crystallographic texture. Simple linear elastic analyses have been conducted to obtain SIF's for the cases of kinked cracks. These show that the crack driving force can be significantly lowered for such cracks. For example, for a crack that contains a kink that is turned  $45^\circ$  from the tensile axis, the effective stress intensity range is only 78% of the full range that would be expected for a planar crack of the same length. This effect could lead to the retarded growth observed when a crack front impinges on a grain boundary. Additionally, it is possible that the crack driving force can also fall below threshold levels causing crack arrest.

In addition to the many continuum analyses that have been proposed, several micro-mechanical models have also been developed. One such model has been developed by De Los Rios et al [21] which includes the effects of both mechanical and micro-structural aspects of crack growth. They have observed that small cracks often grow in slip bands within grains that are favorably oriented towards the maximum shear stress. By equating the mechanical energy release rate to the energy released in the slip plane with crack extension, the following equation was developed for crack growth.

$$\frac{da}{dN} = f \sqrt{\pi a D} \left( 1 - \frac{\phi[D - X]}{D} \right)^3 \frac{\tau}{\mu} \quad (1.5)$$

The slip band was modeled as a linear distribution of close packed dislocations, with its strength equal to the number of dislocations multiplied by their burgers vector,  $\mathbf{nb}$ . The length of the slip band was modeled as the remaining length to the next grain boundary,  $X$ .  $D$ , represents the average length between barriers and  $f$  is a scaling constant. The function  $\phi$ , which ranges from zero to one, represents the difference in crystallographic orientations of the two adjacent grains, zero representing perfect misalignment which halts growth and one being the case of similar alignments.

While the results of this model did not match experimental results perfectly, it did exhibit the proper trends. Cracks either slowed or were completely arrested at boundaries. Analyses of this type highlight the importance micro-structural features have on the growth of small cracks.

A fairly distinct model has been proposed by McDowell [22] which attempts to describe a set of crack growth laws for small cracks that are normalized by traditional strain life models of crack initiation as well as by the established long crack threshold

SIF. This leads to the advantage that most of the constants required by the model can be obtained by standard fatigue tests, which are tabulated for many materials. The model differs from most small fatigue crack growth models as it separates small fatigue crack growth into three regimes, each of which is handled separately. These three regimes, which correspond to the three regimes in the Kitagawa diagram described above, are the micro-structurally small crack, the transition to micro-structural insensitivity and the mechanically small crack. The micro-structurally small crack regime is modeled by an approximation of a slip transfer model between adjacent, misoriented grains. Both the transition regime and the mechanically small crack regime are modeled with the crack growth rate being linearly dependent on crack length as suggested by observations. However, the models for both regimes are defined in a manner which reproduces the proper fatigue crack growth threshold as defined by the Kitagawa diagram. Additionally, all models have been modified to include the effects of biaxial loading. When applied to simple uniaxial loading the general behavior of small cracks is captured, including the characteristic dip in crack growth rate which is observed in the growth of small cracks.

### **1.3 Non-Deterministic Analyses**

As discussed above, the growth of small cracks depends on many parameters such as grain size and orientations that are stochastic in nature. It is therefore reasonable that non-deterministic analyses would be applied to the problem. These methods vary in nature and have been widely developed.

One of the simplest non-deterministic models of crack growth depends on a stochastic process termed a Discrete Time Markov Chain (DTMC) [23]. The DTMC has two fundamental assumptions: that the state of the system (in this case the crack length or

other measure of damage) is discrete and that the future states of a system depend only on the current state and not the systems history. These assumptions imply that the state of the system at any given time can be determined from the initial conditions of the system and a probability transition matrix,  $P_{ij}$ . The elements of this matrix represent the probability of transitioning from state  $i$  to  $j$  in a given interval. Simple approaches such as this have been applied to crack growth problems [24].

More sophisticated stochastic processes have also been applied to the problem of crack growth to account for the inhomogeneous behavior observed in fatigue tests. For instance, Ortiz et al [25] have modeled crack growth by a random growth law, such as a Paris curve with random values for the constants  $C$  and  $m$ , multiplied by a stochastic process. The random growth law models the differences observed between similar fatigue tests while the stochastic process models the irregularity inherently observed in the growth of a single crack in a fatigue test. Once the model is completed the distribution of fatigue lives is calculated by methods of stochastic integration.

Cox and Morris [26] have attempted to create a direct link between micro-mechanical models of small fatigue crack growth and the statistics of the measured growth rates. This was done using a semi-Markov process otherwise known as an embedded Markov chain. Unlike other analyses however, the chain does not describe the evolution of the crack length or other measure of damage. Instead, the chain describes the evolution of a damage control variable which is related to the local value of a material's resistance to fracture. This variable can be interpreted in any number of ways for a given problem, depending on what mechanisms are known to control the growth of cracks in a specific material/environment system. For example it can be related to the material grain size,

local applied strain or the distribution of inter-metallic particles. This variable, in addition to the crack length is then fed into a postulated growth law. The authors point out the foreseen weakness in this method to be its inability to account for the periods of crack arrest and subsequent re-initiation often observed at grain boundaries.

The authors go on to apply this model to the growth of small fatigue cracks in Ti-6Al-2Sn-4Zr-6Mo titanium alloy [27]. In the analysis it was assumed that the anomalous behavior of small cracks in this alloy was caused by fracture surface roughness induced closure. The growth control variable in this analysis was taken to be related to the distance between crack deflections. It was assumed that crack deflections were created whenever the tip of a growing crack intersected a micro-structural boundary. The distribution of boundaries could then be easily measured. For this particular dual-phase alloy, these assumptions lead to a bi-modal distribution from the sizes of both the  $\alpha$ -phase and  $\beta$ -phase grains. The crack growth law is then taken to be a function similar to the Paris growth law, but with a fraction of the growth control variable added to the SIF range. The authors note that the form of the crack growth function will have little influence on the final analysis, after a calibration of all constants in the function has been completed.

Non-deterministic analyses not based upon the use of stochastic processes have also been proposed. For example, a simple statistical model of small crack growth in an aluminum alloy has been proposed by Halliday et al [28] for modeling small fatigue cracks naturally initiated on smooth surfaces. Using standard testing methods including the use of acetate replicas, small crack growth rate data was obtained for a significant number of cracks. At various crack lengths, 95 percent confidence limits on the growth

rates were constructed assuming the rates possess a normal distribution. For predictive analyses, the small crack regime was subdivided into a large number of intervals. The number of cycles needed for a crack to grow an interval in length was calculated by assuming a constant growth rate in that interval. This growth rate was randomly chosen between the 95 percent confidence limits from the small crack data utilizing the assumed normal distribution of rates. Multiple simulations of crack growth would then be run and averaged to form a prediction of growth. Additionally it was suggested that based on SIFs, the upper bound of small crack growth compared well with high load ratio, low closure long crack growth and the lower bound compared well with low load ratio long crack data. Therefore in the framework of this analysis, long crack data could be, and was used to simulate the small crack growth regime data.

A similar analysis was performed by Kitagawa et al [29] as part of a method to characterize the amount of accumulated damage on a smooth surface utilizing only small cluster crack data. A large amount of crack cluster data, including crack sizes, positions and growth rates, was collected for cracks generated by corrosion on a smooth surface. The data was collected at several loading levels and at multiple stages in the life of each specimen. While this initial data was generated as corrosion cracks on a smooth surface, the developed methodology is just as applicable to fatigue cracking.

It was found that crack lengths at each load level and fraction of total lifespan tested exhibited a normal probability distribution. Additionally, it was found that the individual cracks grew approximately according to a Paris-like power law, the parameters for this power law obviously differing than those for long cracks. Using this model for growth and the knowledge that crack lengths were normally distributed at each load count, a

simple transformation formula could be used to show that the average crack lengths at an arbitrary loading cycle would also be normally distributed with known values of the mean and standard deviation. Finally, it was also suggested that while corrosion cluster cracks generally followed normal distributions, fatigue cluster cracks would follow a skewed distribution such as the log-normal.

Another body of work utilizes one of the most popular and widely applied stochastic methods of analysis, the Monte Carlo simulation. The Monte Carlo simulation represents a class of numerical methods used to solve mathematical problems by the repeated simulation of one or more random variables [30]. These methods have been applied to a multitude of engineering applications which include both stochastic and deterministic systems. Several groups of researchers have applied these methods to micro-cracks in metallic materials.

The first step in any Monte Carlo analysis is to model the system, for example the growth of a fatigue crack, as a function of random variables. These variables can be simple discrete functions representing events such as whether or not a crack will arrest when intersecting a grain boundary. They can also be any arbitrary continuous function representing more complex events such as the amount of crack growth occurring during a given interval. For each iteration of the system these variables are simulated. Any arbitrarily distributed random variable can be simulated by transforming a uniformly distributed random variable, either numerically or analytically to the assumed distribution. After a significant number of iterations have been obtained, their distribution statistics can be used to approximate the distribution statistics of the physical system being analyzed.

Utilizing methods such as these, Lawson et al. [31] are one of a number of groups of researchers to create a numerical stochastic simulation of small fatigue crack growth. The model essentially relies on four events: initiation, Paris law growth, arrest/escape and coalescence. An abbreviated flow chart of simulated crack growth is provided below in figure 1.4. For this analysis crack growth was assumed to be controlled by a Paris law, modified to include stress singularities. The singularities used were shown to exist by Picu [10, 11], under purely elastic conditions in a material with randomly oriented anisotropic grains.

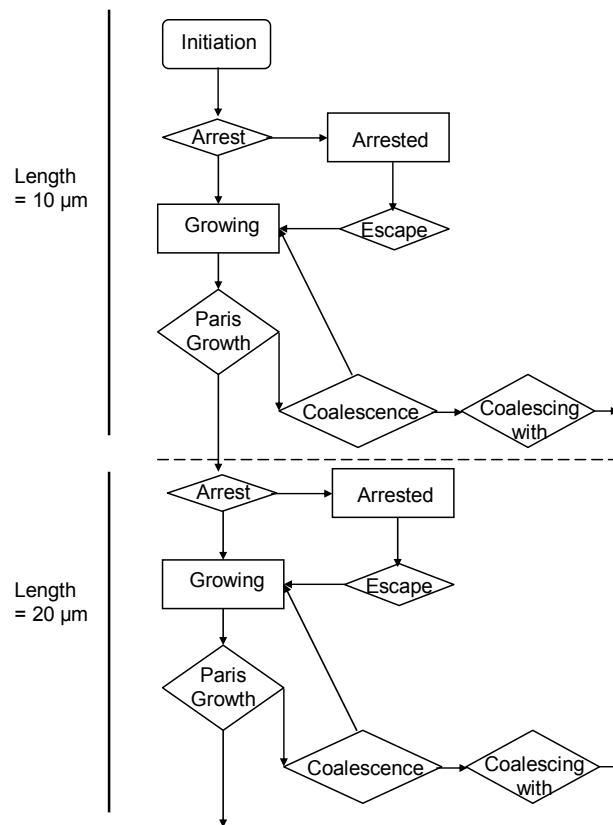


Figure 1.4: Abbreviated Monte Carlo simulation flow chart [31]

This simulation was found to be capable of reproducing the distribution of micro-crack sizes from actual tests run on 304 Stainless Steel with a fair amount of accuracy. In order for the simulation to be run, each event in the simulation must be assigned a probability at each growth step. For this particular model these include the probabilities of arrest, escape, coalescence with a randomly sized micro-crack and the probabilities of growing a particular amount. All of these values must be estimated in some way. Most are found through correlation with experimental data.

Another example of a Monte Carlo method used to simulate the growth of small cracks was developed by Cox and Morris [32, 33]. However, unlike other analyses that simulate only the surface crack length, this analysis simulates the advance of the entire crack front. Additionally, this crack front is propagated through a randomly generated microstructure rather than a homogeneous continuum.

The first step in the analysis consists of generating a randomly oriented grid of polygonal grains with a chosen density. A crack is then assumed to initiate within a single grain and its front is divided into segments by nodes. The growth rate of the crack front at each node is then assumed to be dependent on a local SIF and the distance from the node to the next grain boundary. The local SIF at each node is estimated using various analytical corrections for crack shape abnormalities [34]. Growth arrest at any given node is also allowed and the duration of the arrest period is estimated as a function of the local stress state. Using this method the effects of crack front irregularity and micro-structural influence can be investigated.

A similar analysis was performed by Steadman [35] to model the complex growth morphologies of small crack fronts. As in the Cox and Morris analysis, crack fronts were

assumed to be planar. However, unlike that analysis where deviations in the crack front stemmed naturally from a stochastically generated microstructure, deviations in the crack front in this analysis were forced onto the crack by a graftal algorithm developed for research on the growth of biological plants. During each iteration the crack front was grown, with the allowance that some segments may be temporarily arrested. The number of cycles needed to grow the crack to its new length were then calculated using a deterministic analysis similar to the one used by Cox and Morris. Upon completion of both models, cases of crack growth can then be compiled and used in a Monte Carlo simulation.

The importance of interactions between cracks in a cluster were highlighted by Chen et al [36, 37]. In their experiments on an Al-SiC metal matrix composite the effects of crack shielding and anti-shielding, leading to decelerated and accelerated growth respectively, were investigated. An attempt was also made to develop an understanding of the occurrence of coalescence between cracks within a cluster. For the purpose of a Monte Carlo simulation a probabilistic model of coalescence was created. This model was based upon Buffon's needle problem, which involves calculating the probability that a needle randomly dropped onto an array of parallel, equal width strips will land on a borderline between two strips. In this model the needle represents the growing crack and the borderline is an average of any cracks the growing one may coalesce with. The authors also point out that the small crack data is fit well by the lognormal distribution. It is proved that with this distribution continually fitting the data, small cracks cannot grow according to a Paris like power law.

Many researchers have attempted to include the small crack regime into fatigue life prediction by selecting a “proper” initial crack which is then propagated using linear elastic fracture mechanics principles. This constitutes the so-called equivalent initial flaw size method (EIFS). Laz et al. [38, 39] developed such a method, through extensive testing, for 2024-T3 aluminum alloy. The distribution of initial crack sizes was assumed to be equal to the distribution of the cracked inter-metallic particles from which each crack initiated. Thus a distinction was made between the distribution of crack nucleating particle sizes and the distribution of all particle sizes. While there was significant stress dependence, it was found that the nucleating particles mainly fell in the upper 30 percent of all particles.

With the distribution of initial crack sizes determined, a Monte Carlo simulation was used to choose an initial crack size from that distribution and an experimentally determined number of cycles to crack nucleation. In each case the resulting initial crack was propagated using FASTRAN II [40] and the values of propagation and nucleation lives combined. The distributions of fatigue lives calculated using this method corresponded well with the measured distributions.

#### **1.4 Significance of Current Work**

The small crack anomaly is of great importance to the application of damage tolerance principles towards aerospace structures as they can spend a large portion of their total fatigue life initiating and growing small cracks [41]. For this reason, the small crack regime must be included into life prediction methodologies. Failure to compensate for the faster and more erratic growth of small cracks in a fracture analysis can lead to dangerous over-predictions of fatigue lives. Additionally, as non-destructive test methods improve

in capability, small cracks may routinely be found during periodic inspections. In order for this data to be used to obtain an accurate knowledge of when the structure must be inspected again to ensure safety, an accurate prediction of small crack growth must be made.

Of the many deterministic methods used to describe the growth of small cracks, most tend to include the effects of only a single phenomenon. For instance, elastic-plastic analyses as well as plastically corrected SIF models address the effects of plasticity induced crack closure transients. Other models address the topic of crack kinking and the mixed mode solutions that it presents. Some models will even take into account the micro-mechanics of crack growth. While many of these models will reproduce some general features of small crack growth, none have yet reproduced all of them. This is because few, if any models combine the effects of many of the various complications found in the growth of small cracks.

Material microstructure obviously has a great effect on the growth of small cracks. In fact it may even be seen as the primary driving force in the breakdown of similitude which causes the small crack anomaly. Even crack closure arguments are subject to material inhomogeneity, as the plastic zones of small cracks will be contained in a small number of randomly oriented grains with slip systems that may or may not be preferentially oriented. Additionally, as shown by Taylor and Knott [16], the transition from small to long crack growth can also be dependent on the material microstructure present. For these reasons, the influence of the material microstructure on the growth of small cracks will be central in the analyses in the current work. For instance, a definition

of transition length will be defined based upon the measured scatter and the amount of microstructure sampled by growing crack fronts.

An additional weakness of deterministic methods is their failure to predict the variability of small crack growth. While this may be acceptable for long cracks which are relatively reproducible, it is not acceptable for small cracks where measured scatter can be quite large. For this reason a non-deterministic approach is needed to properly describe the small crack anomaly. Even micro-mechanical models which may appear to include the effects of a stochastic material microstructure only produce solutions for specific cases of micro-structural orientations and inhomogeneity. These methods would need to be extended to allow for the true case of a stochastically chosen micro-structural field in order to develop predictions of scatter. It is for these reasons that non-deterministic procedures were used in the current work.

It is desired that any non-deterministic method developed will have several key characteristics. Methods should be as physically based as possible. They should also require the fewest amount of constants that cannot be simply measured or do not have a clear physical meaning. This will not only allow for a better understanding of the phenomena under study but also facilitate the application of the developed methodology as a predictive algorithm on a variety of material/loading systems.

This uncovers a major weakness in the models which utilize Markov processes, of which several examples were discussed above. The individual elements of the transition matrices must be filled even though they do not have a definite physical meaning. For this reason, while these models may be used successfully to fit data, their use as a predictive methodology may be limited.

Monte Carlo simulation methods can often suffer from the same deficiencies. Any simulation of crack growth will contain multiple events, which may or may not be physically based, for which probability distributions must be defined. Such events include the probability of crack arrest or the amount of cycles needed for a crack to grow a given increment. These probability distributions must either be estimated from test data or otherwise approximated. At this point the model can become an exercise in curve fitting, where many parameters can be altered to obtain a given distribution function result. While these methods can provide much insight into the complex problem of small crack growth, their usefulness in predicting the sizes of micro-cracks in multiple material/loading situations is questionable.

There have been several attempts to model and understand the situation of multi-site small crack growth which rely on empirically based distributions instead of Monte Carlo simulations or stochastic models. These methods offer promise in that the fitted distributions are a simple analytical description of physically measurable quantities that maintain knowledge of the variability found in the data. They also inherently include the effects of all complications that can possibly arise in the growth of small cracks. However, researchers often blindly include the data from all measured cracks even though it is widely recognized that a substantial portion will simply arrest. These non-propagating cracks cannot lead to failure, they simply introduce the possibility of crack coalescence and form a neighborhood through which propagating cracks must grow. Therefore, when these cracks are included in the crack data that will be used for analysis they serve only to skew the measured distributions in a non-conservative manner.

For this reason the current work will develop a bi-modal model of multi-site cracking. Experimental procedures based upon the physical behavior of the observed cracks will be developed to separate out the non-propagating or slowly propagating cracks. These cracks, termed secondary cracks, will be excluded from analysis leaving only the growing cracks that can actually contribute to specimen failure, termed primary cracks. The distributions of these primary cracks can then be used to characterize the growth of small cracks within a cluster. This characterization can be used until the micro-structurally defined transition length from small to long crack growth is reached. From this point forward traditional deterministic methods of LEFM can be used to predict the propagation of the now long cracks.

## Chapter II - Experimental Procedures

The material chosen for testing was 7075-T7351 aluminum alloy. A full microstructural census was ordered from the GTRI on a sample of the material prior to testing. The results of this study are presented below. A test specimen was chosen that allows for the natural initiation of clusters of cracks on a smooth surface. Each specimen is carefully polished prior to use to ensure the statistical accuracy of the experiments and to facilitate optical crack measurements. The specimens were loaded in tension by a constant amplitude sinusoidal waveform with a maximum load of approximately 5,000 pounds and an R value of 0.1. The testing was performed on a hydraulic test stand using both hydraulic and mechanical grips. An optical tele-microscope was used to track crack growth.

### **2.1 Material Properties**

The material chosen for all tests was 7075-T7351 aluminum alloy. This high strength-low weight alloy is widely used throughout the aerospace industry. The material was purchased as a hot rolled plate with a thickness of 0.25 inches. As in any rolled plate material, sections can be taken in three representative orthogonal orientations where intrinsic differences in the microstructure and material properties are exhibited. These are the long transverse, short transverse and longitudinal directions and are defined below in figure 2.1. Bulk properties were supplied by the manufacturer, Alcoa, and are provided below in table 2.1.

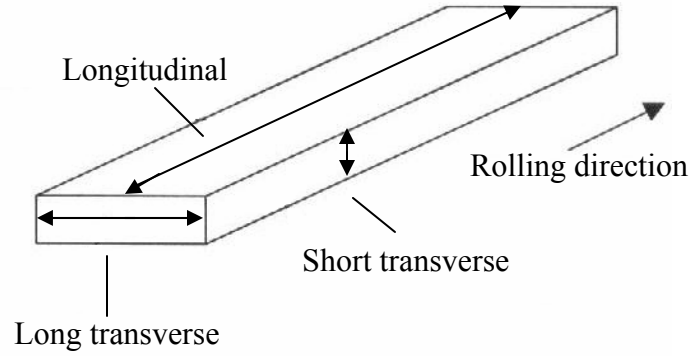


Figure 2.1: Schematic defining the material directions

Table 2.1: Material bulk properties

$\sigma_y$ (ksi)	$\sigma_u$ (ksi)
64.0	75.3

Prior to testing the Georgia Tech Research Institute (GTRI) was commissioned to perform a full micro-structural analysis on a specimen taken from the bulk plate [42]. In order to determine the grain sizes the specimen was etched with Keller’s reagent which reveals grain boundaries. The grain structure of the plate, which can be described as “pancake like”, necessitated the use of a cycloid method in estimating the grain size [43]. The more commonly used line intercept method would have produced inaccurate results on the elongated grain structure present. A summary of the grain sizes found is presented below in table 2.2. Micrographs of the material microstructure in all three orientations are presented in Appendix A.

Table 2.2: Material grain sizes

Longitudinal*	Transverse*	Short Transverse*
58.8	76.1	15.0

\*All dimensions in microns.

Along with the grain sizes, the GTRI provided an analysis of the large number of inter-metallic particles present in the matrix. It was found that the particles were primarily composed of two compounds: Mg<sub>2</sub>Si and Fe-Al. The area fractions of the particles in the primary material orientations are presented below in table 2.3. Micrographs of the particles as well as particle size distribution plots are presented in appendix A.

Table 2.3: Particle size distributions

Section	Area Fraction (%Vv)		Total Particles
	Mg <sub>2</sub> Si (Dark Particles)	Fe-Al (Gray Particles)	
Longitudinal	0.11	0.70	0.81
Transverse	0.07	0.66	0.73
Short Transverse	0.07	0.65	0.72

## **2.2 Test Specimen**

The specimen design used for this series of experiments was chosen over many of the more common specimen geometries because it holds several key advantages. The goal of this specific specimen geometry is to provide a smooth surface where cracks can initiate naturally in clusters, while at the same time keeping the area that must be scanned for cracks at a reasonable level. The geometry must also be reasonably easy to machine and allow for easy hand polishing.

The geometry of choice is shown below in figure 2.2. The notched section will localize fatigue damage while only creating a slight stress concentration of 1.2 over the ligament stress. This value was calculated using the formula shown below [44].

$$K_{tg} = \frac{W}{d} \left[ 3.065 - 3.472 \left( \frac{2r}{W} \right) + 1.009 \left( \frac{2r}{W} \right)^2 + 0.405 \left( \frac{2r}{W} \right)^3 \right] \quad (2.1)$$

$$\sigma_{\max} = \sigma \cdot K_{tg} = \frac{P \cdot K_{tg}}{tW} \quad (2.2)$$

Here  $K_{tg}$  is the stress concentration over the ligament stress,  $W$  is the width of the specimen,  $d$  is the ligament length,  $r$  is the semi-circular cutout radius,  $t$  is the specimen thickness,  $\sigma$  is the base stress and  $P$  is the load. A total of 12 specimens were manufactured.

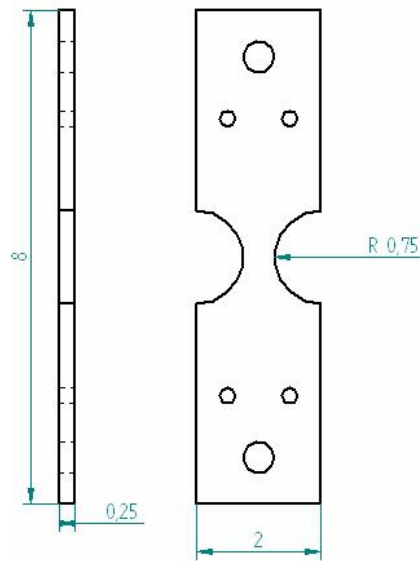


Figure 2.2: Specimen geometry (all dimensions in inches)

Prior to being tested, all specimen gauge sections required extensive polishing. The specimens were prepared first with the use of three abrasive papers of the following grits: 240, 320 and 600. This treatment removed any surface imperfections and scratches introduced during machining. Preparation was then completed by a careful polishing procedure using 15, six and one micron diamond pastes. During the entire process the

specimen surface was kept as clean as possible. Each stage of polishing was performed perpendicular to the previous. To determine when each stage of polishing was completed and it was proper to move to a finer medium, the specimen surface was viewed under magnification to assure that all marks left by the previous stage had been removed.

This level of polishing was required for several reasons. It first ensures that each specimen begins testing in an identical condition. The highly polished, mirror like surface also facilitates the detection of cracks with the optical detection system used. The detailed procedure used to polish the specimens is provided in Appendix B. A photograph of a fully polished specimen is shown below in figure 2.3.



Figure 2.3: Fully polished specimen.

### **2.3 Grips/Alignment**

Two methods of installing the specimens into the test machine for loading were used throughout the experiments. The first method utilized Instron manufactured hydraulic

wedge grips with a maximum capacity of 200 kN. After testing four specimens the above mentioned wedge grips developed a leak caused by the breakdown of internal hydraulic seals. At that point it was decided to replace the hydraulic grips with custom designed and machined mechanical grips. Upon completion of testing no systematic differences in the data obtained using the hydraulic wedge grips versus the mechanical grips were found.

Both methods of gripping the specimens required their own careful loading procedure to insure proper specimen alignment. When using the hydraulic wedge grips the specimen was first placed into the bottom grip. A 90° angle level was then used to assure that the specimen was properly aligned. At this point the lower grip was closed to lock the specimen into place. The specimen would then be raised to the correct height to sit in the upper grip, which would then also be closed.

When functioning properly the hydraulic wedge grips are more than adequate to perform the relatively short fatigue tests under consideration here. However, they do have several weaknesses, the first being the susceptibility of the moving parts to damage. Additionally, unless further precautions are taken, over the course of a fatigue test the specimen can slip in the grip and slowly lose alignment. The custom-made grips do not suffer from either of these weaknesses.

Machined from high-strength steel the mechanical grips consist of three major components: a body, an insert and a cover plate. The specimen is installed into the body with three lubricated pins made of hardened tool steel. The pins fit into the pattern of three holes seen on the top and bottom of the specimen in figure 2.2. These patterns are replicated on the grip body, the insert and the cover plate. After the specimen is loaded

into the body the insert and cover plate are installed over the pins. The cover plate is secured to the body with six bolts. The insert is cut such that upon tightening of the bolts, the grip section of the specimens will be compressed and lead to a large friction load that will assist the pins in transferring the load to the specimen. An assembly drawing of the grip is provided below in figure 2.4.

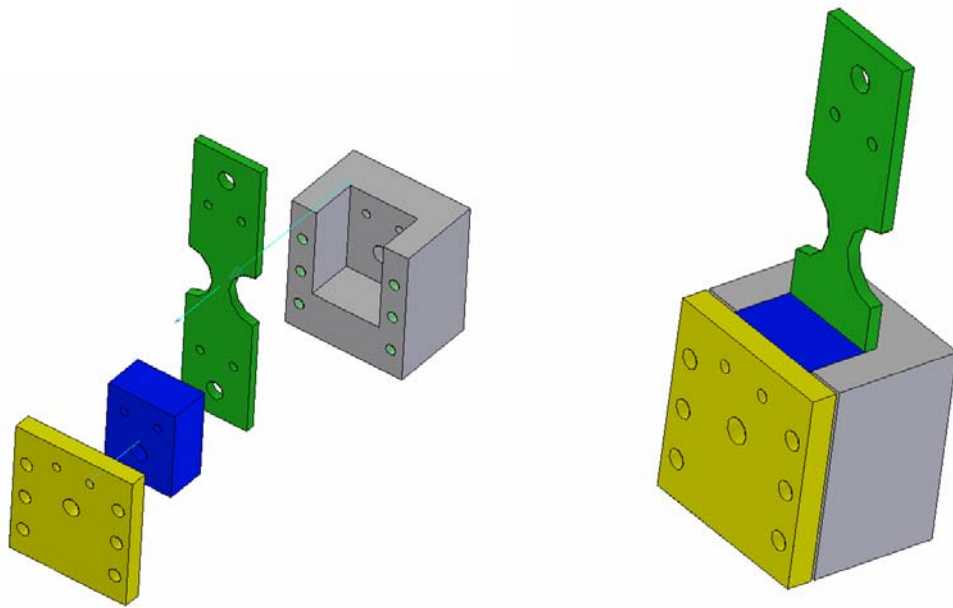


Figure 2.4: Assembly views of mechanical grips

To insure that the specimen will not experience any bending loading due to misalignment, the grips were machined such that when the specimen is lying flat on the rear surface of the body cutout the centerline of the specimen is directly above the centerlines of both the grip and that of the loading peg of the test stand. To further insure proper alignment when using the mechanical grips a careful loading procedure was established. Prior to loading a set of machining parallels were installed into the grips and held tightly in place with shim stock. The grips were tightened and all surfaces of the

parallels were checked to be lying flush with the grips. A steel beam could then be secured between both grips to maintain that alignment until the parallels could be removed and the specimen properly installed.

## **2.4 Test Setup/Crack Measurement Technique**

All tests were conducted on a digitally controlled Instron hydraulic test stand under load control in pure tension. As previously mentioned both hydraulic and custom-made mechanical grips were used on this machine and no discrepancies were found in the data for the different gripping methods. The load form used for all tests was sinusoidal of constant amplitude with a load ratio,  $R$ , equal to 0.1. A maximum load of 22241 Newtons or approximately 5,000 pounds was used, leading to a maximum stress ( $\sigma_{\max}$ ) of 75 percent of the material yield strength. All tests were run at a cyclic frequency of 10 Hz. This led to specimen fatigue lives of around 70,000 cycles, which could be spanned in a reasonable length of time. A one second interval of the loading waveform is presented below in figure 2.5.

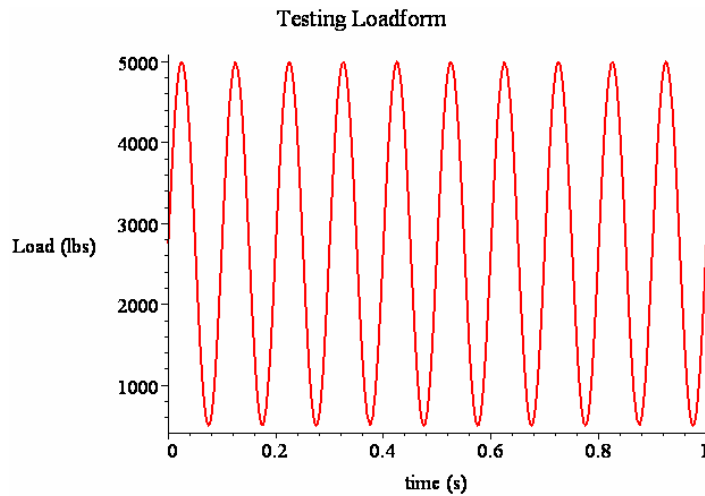


Figure 2.5: Testing load form

At the point when the first fatigue cracks would initiate and grow to an observable size, and again at intervals of 5,000 and 2,500 cycles, depending on the specific test, cycling was halted to allow for the measurement of cracks. The average initiation point was found through experimentation to occur at approximately 40,000 cycles. At these points the specimens were brought to the maximum load to ensure that all cracks were fully open to aid in locating them and to allow a proper measurement of their length.

The cracks were measured optically using a Questar, QM 1 tele-microscope. The microscope had an optical resolution of 2.5 microns and a working range of 0.55 – 1.7 meters. The image was picked up through a video camera mounted to the microscope and displayed on a high resolution (570H/485V) black and white monitor. The video feed was run through a video enhancement unit that allowed for the superposition of a cross-hair onto the image as well as the manual adjustment of contrast, brightness, sharpness and a white hot/black hot selector.

The microscope was mounted to a three-axis translation stage with digital position transducers. With this setup the position of the crosshairs could be used to measure lengths of any features in the image. These position measurements were accurate to 0.00005 inches. The intense lighting required for proper viewing was provided by a high intensity fiber-optic spotlight. A photograph of the experimental setup is provided below in figure 2.6.



Figure 2.6: Photograph of experimental setup

A method of scanning the specimen surface using the Questar was developed to minimize the possibility of failing to detect a crack. The specimen surface is scanned horizontally. Upon completion of each run across the surface the microscope is moved vertically through a distance of slightly under half of the vertical viewing area. Scanning is then restarted in the opposite horizontal direction. This procedure is shown below in figure 2.7. This method assures that all points on the surface of the specimen are scanned at least twice and in multiple directions.

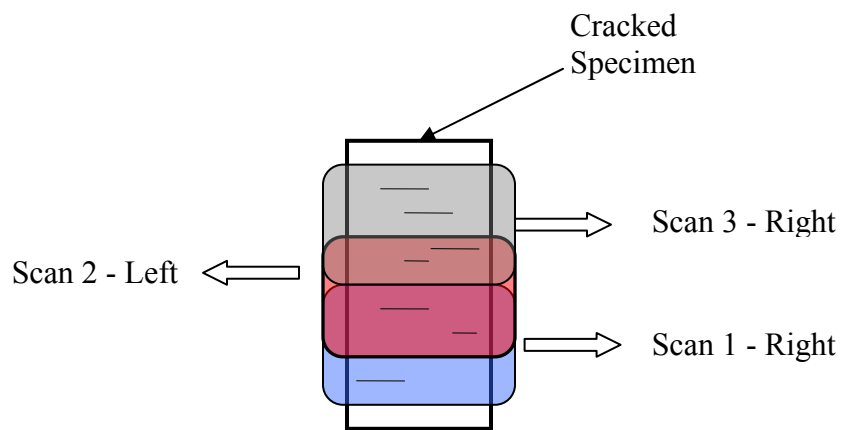


Figure 2.7: Illustration of scanning procedure

## Chapter III - Data

Preliminary tests were conducted to determine the time to crack initiation and the proper crack inspection intervals. The data collected are then summarized and discussed. A total of 57 cracks were observed; 14 of these primary cracks and 43 were secondary cracks. For purposes of analysis cracks were assumed to have a semi-circular geometry. This assumption has been confirmed through fractographic analysis. Not all cracks however conformed to this planar geometrical assumption. The unique geometries observed are presented and their implications on statistical analyses are discussed.

Additionally crack cluster measurements are discussed. Crack cluster densities are calculated and shown. Plots of crack cluster topography are also presented. These plots allow visualization of the cluster evolution. Conjectures on crack coalescence are suggested through observation of the cluster behavior.

### **3.1 Preliminaries**

Prior to the collection of any data, two specimens were selected for preliminary testing. The purpose for these tests was twofold. They first allowed for the evaluation and refinement of the test procedures to be used. In addition they also provided valuable data on the cycling required for the initiation of cracks and the proper intervals between crack measurements. It was found that the earliest cracks would initiate and grow to a measurable size after approximately 40,000 cycles. It was also initially determined that the remaining fatigue life of the specimen could be adequately documented by measuring cracks every 5,000 cycles. However, after several tests it was decided that acquiring data every 2,500 cycles would provide a much more complete and clear picture of the crack

growth histories without forcing the tests to take an unreasonable amount of time to be completed.

Throughout the testing program useable data was collected from a total of five specimens with ten testing surfaces. However, one of the testing surfaces was scratched voiding all data from it. Additionally, one specimen was broken for the purposes of subsequent fractographic examination, one specimen was used for another project, one was accidentally damaged and two were left untested. With these specimens a total of 57 cracks were observed. Of these 14 were deemed to be primary cracks which left 43 as secondary cracks. This makes the proportion of the total number of cracks that were found to be propagating primary cracks approximately 24.6 percent.

The number of cracks, as well as the proportion of those cracks that were primary cracks varied for each specimen surface. Prior to failure, surfaces were observed that contained as few as zero cracks and as many as 15. A summary of measurements on all specimen surfaces is presented below in table 3.1.

Table 3.1: Summary of crack measurements

Specimen		Crack Counts		Total
		Primary	Secondary	
F	Side 1	2	3	5
	Side 2	2	2	4
C	Side 1	2	9	11
E	Side 1	1	8	9
	Side 2	0	0	0
I	Side 1	2	3	5
	Side 2	3	12	15
6	Side 1	1	3	4
	Side 2	1	3	4
Totals		14	43	57

While a careful effort was made to detect every crack present in each specimen, using the optical scanning method described in chapter II, it is inevitable that at some point in the course of testing some cracks would remain undetected. As large cracks are easily detected, any crack passed by in a given scan would have to be small. If such a small crack were to be missed from early in the fatigue life of a specimen, this would mean that the crack has not grown a significant amount by failure. If detected, cracks such as this would be placed into the secondary crack distribution and not included in any of the analyses to follow, making the failure to detect these cracks inconsequential. Small secondary cracks detected late in the fatigue life of a specimen will likely have little effect on the fatigue life of a specimen. Therefore the failure to detect these cracks as well will not have an effect on any performed analyses.

### **3.2 Crack Geometry**

All of the analyses that follow require an assumption to be made regarding the geometry of cracks. The geometry chosen, termed a thumbnail crack, is a planar semi-circle. The dimensions of such a crack are presented below in figure 3.1.

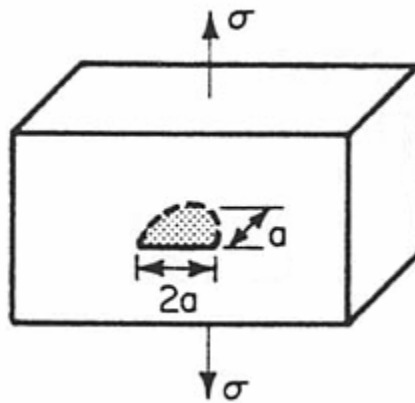


Figure 3.1: Assumed semi-circular crack geometry

This geometrical configuration was confirmed through several means. The first of these was fractographic analysis of several failed specimens. Only one crack can grow unstably to cause catastrophic failure in each specimen. This leaves many non-fatal cracks which are often opened and exposed during the final tearing of the specimen since they present planes of weakness in the material. These cracks can be plainly seen by the naked eye and offer the opportunity to measure the crack front shape at various crack depths. A photograph of one such crack is presented below in figure 3.2.



Figure 3.2: Photograph of non-fatal crack on fractured surface

However, these non-fatal cracks offer only glimpses of the shape of a growing crack. Therefore, SEM micrographs were taken of the fracture surface of a failed specimen. One such micrograph is presented below in figure 3.3. The semi-circular crack shape can be confirmed by observing the parabola-like ray patterns extending from the crack initiation point in the direction of local crack growth. The crack initiation point is highlighted by an arrow.

This crack geometry has also been noted by Lankford [5] in 7075-T6 Aluminum alloy. Those small cracks were generated naturally on a free surface similar to the cracks in the current experiments.

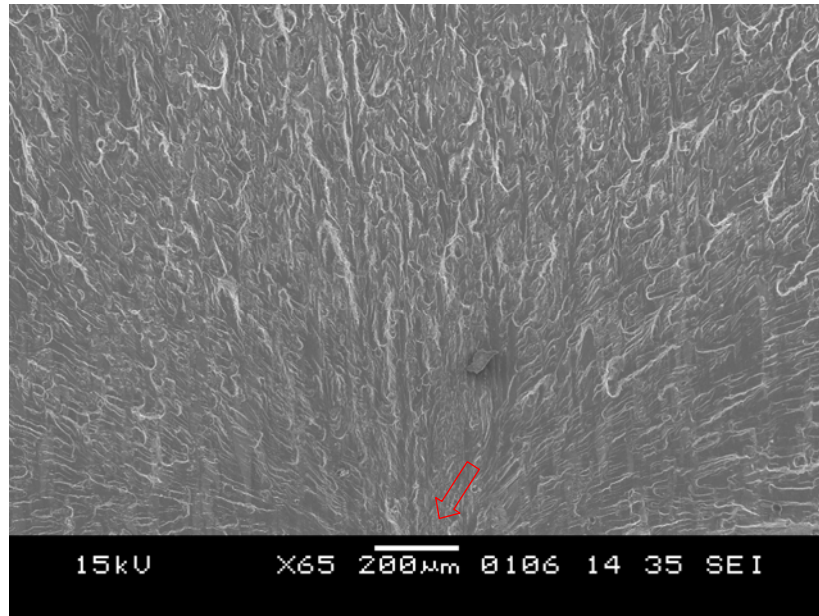
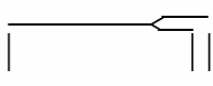
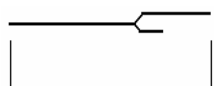

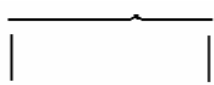

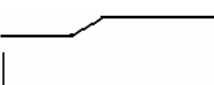


Figure 3.3: SEM micrograph of the fracture surface of a primary crack

While most cracks remained largely planar, other than minor aberrations in the crack path, some observed cracks grew with more complex features. Examples of such features are crack branching and kinking. Complex crack morphologies such as this were observed and documented by Steadman [35, 46] in 6061-T651 Aluminum alloy. During the course of the current tests several complex crack geometries were documented. A table summarizing these is presented below in table 3.2. These situations are often the result of the coalescence of several cracks.

Table 3.2: Observed crack shapes

Name	Stage 1	Stage 2	Description
Forked Crack			<ul style="list-style-type: none"> <li>• One fork arrests, one grows.</li> <li>• Length is measured to longer fork.</li> </ul>
Kinked Crack			<ul style="list-style-type: none"> <li>• Formed through coalescence.</li> <li>• Tabulated as one crack after coalescence.</li> </ul>
Stepped Crack			<ul style="list-style-type: none"> <li>• Formed through coalescence, which does not always occur.</li> <li>• Tabulated as one crack after coalescence.</li> </ul>

For each one of the above cases the crack in question must be assigned a proper length in order to be included in statistical analyses. The methods used to determine measurements for cracks such as these are summarized in table 3.2. In general, prior to coalescence each crack is counted separately and after coalescence the crack is only counted a single time. Additionally, with several of the geometries lengths cannot be assigned until significant crack growth has occurred and been documented. For instance, both forks in a forked crack must be observed to determine which will grow and become dominant and which will arrest.

### **3.3 Cluster Measurements**

In addition to the crack lengths the locations of all cracks relative to the center of the specimen test surface were also measured. All cracks measured were found between the angular positions  $-13.7^\circ$  and  $15.4^\circ$  degrees as defined below in figure 3.4. Within this

range the stresses with which the surface cracks are loaded are not expected to vary by a large amount.

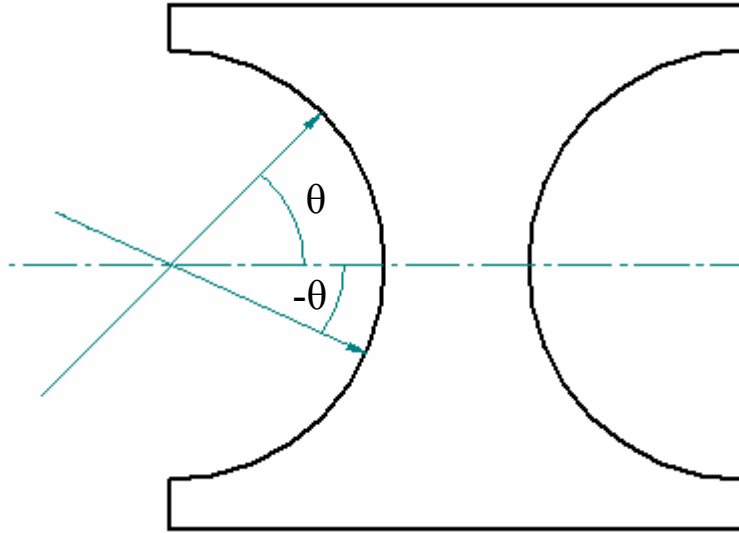


Figure 3.4: Definition of angular positions

The values of  $\theta$  were calculated using the equation shown below where  $y$  is the vertical distance above the specimen centerline and  $r$  is the radius of the semi-circular notch in the specimen.

$$\theta = \sin^{-1}\left(\frac{y}{r}\right) \quad (3.1)$$

These angular measurements allowed for the calculation of the crack cluster density. This quantity is a measure of the amount of cracks per unit surface area. The area used in each measurement was the area between the two cracks with the greatest and least angular measurements from the centerline for each respective surface. A table summarizing the densities for all test surfaces just prior to failure is presented below in table 3.3.

Table 3.3: Crack cluster densities

Specimen		Crack Cluster Densities*		
		Primary	Secondary	Total
F	Side 1	106.6	160.0	266.6
	Side 2	103.4	103.4	206.9
C	Side 1	32.5	146.0	178.5
E	Side 1	18.3	146.0	164.3
	Side 2	0.0	0.0	0.0
I	Side 1	44.8	67.1	111.9
	Side 2	37.6	150.4	188.1
6	Side 1	48.8	146.4	195.1
	Side 2	25.7	77.2	103.0
Averages		46.4	110.7	157.2

\*All densities expressed in cracks per square inch

While these density measurements will not be used directly here, they can provide some valuable insight into the problem of micro-multi-site cracking on smooth surfaces. These uses will be described below in chapter VI on future work.

The positional measurements of cracks were also used to track the evolution and growth of crack clusters. Plots of the topography of each specimen surface and the cracks it contained were made for each cycle count measurements were taken. One such plot is shown below in figure 3.5. Plots for the remaining specimens are provided in appendix C.

In this figure, each row of plots represents one side of the specimen. Each plot in the row represents the state of that surface at a specific cycle count. The X and Y axes represent the horizontal and vertical directions on the specimen test surface. The origin is located at the left edge of the specimen centerline. Cracks that were placed into the primary crack distribution are shown in red while secondary cracks are shown in blue.

*40,000 Cycles  
Cycles*

*45,000 Cycles*

*50,000 Cycles*

*55,000 Cycles*

*60,000*

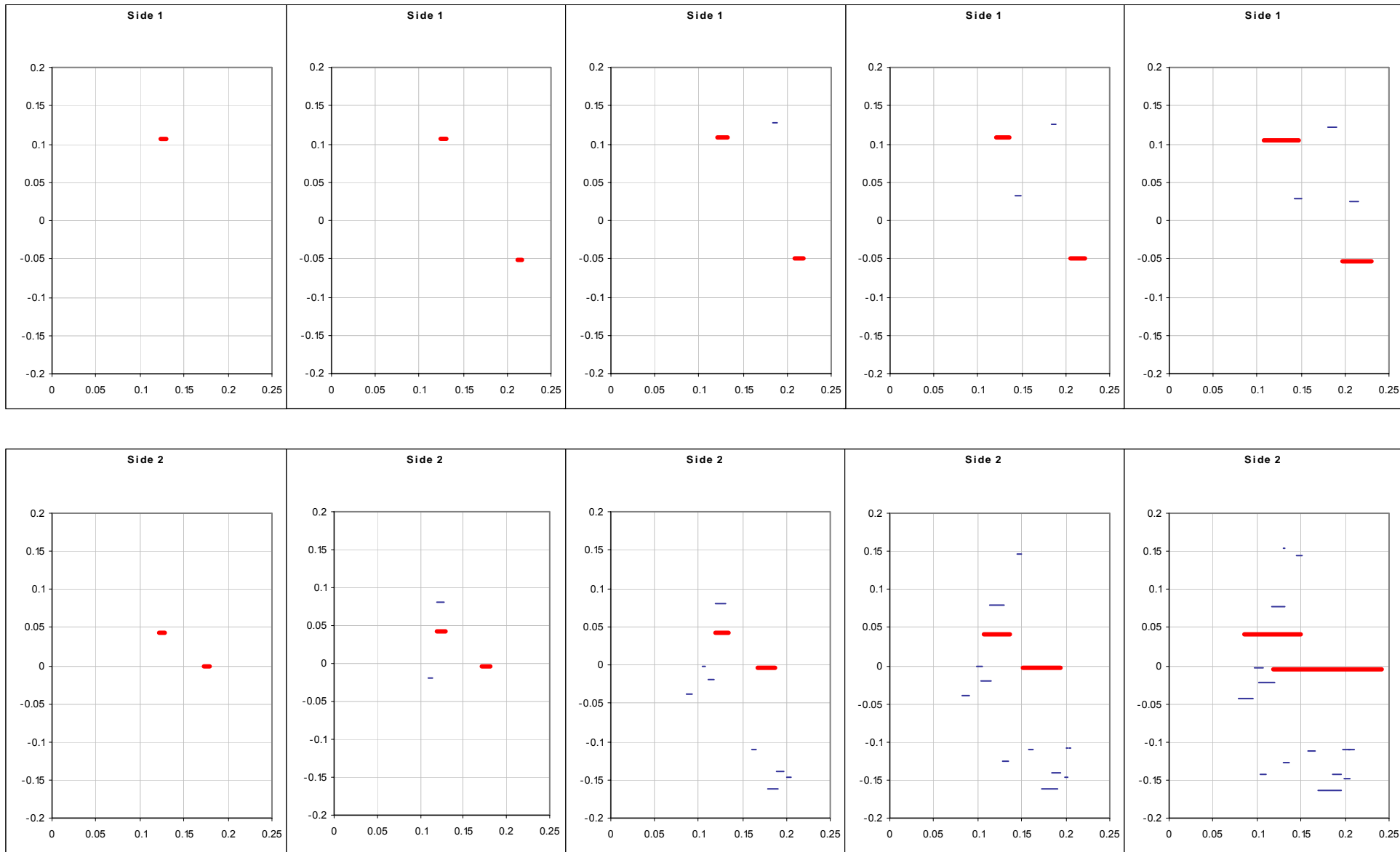


Figure 3.5: Topography of the multi-site crack growth on specimen I

These topographical measurements highlight the inherent complexity involved in any attempt to model a cluster of cracks. The reason for this complexity lies in the measured separation of cracks in clusters. Many cracks are separated by relatively large distances where continuum methods of analysis would be applicable. However, often cracks are separated distance whose magnitude is on the order of the grain size of the material. The material in-between these cracks may contain only a few grains, or perhaps only a single grain and thus cannot be represented by an isotropic continuum. An exact deterministic analysis of this problem would quickly become intractable. Thus, statistical methods in which these effects can be accounted for must be used to address the problem of multi-site cracking.

However, despite the complexity of the problem some qualitative conclusions can be drawn from the crack cluster data. Many of the cracks, but not all, will be affected by other cracks through crack shielding and coalescence. This was also noted by Swain who developed a method to ensure that crack data that came from cluster measurements was free from these effects [47]. A crack's driving force can either be raised or lowered due to the presence of a randomly arranged cluster around it. This creates a randomly distributed neighborhood through which each crack must grow. The random crack clustering is therefore an additional physical cause for the scatter observed in small crack growth.

A small portion of the cracks will also undergo coalescence. Of these pairs, one caused a significant rise in crack growth rate which caused specimen F to fail much sooner than would have been expected in the absence of cluster effects. An example of this behavior is presented below in figure 3.6.

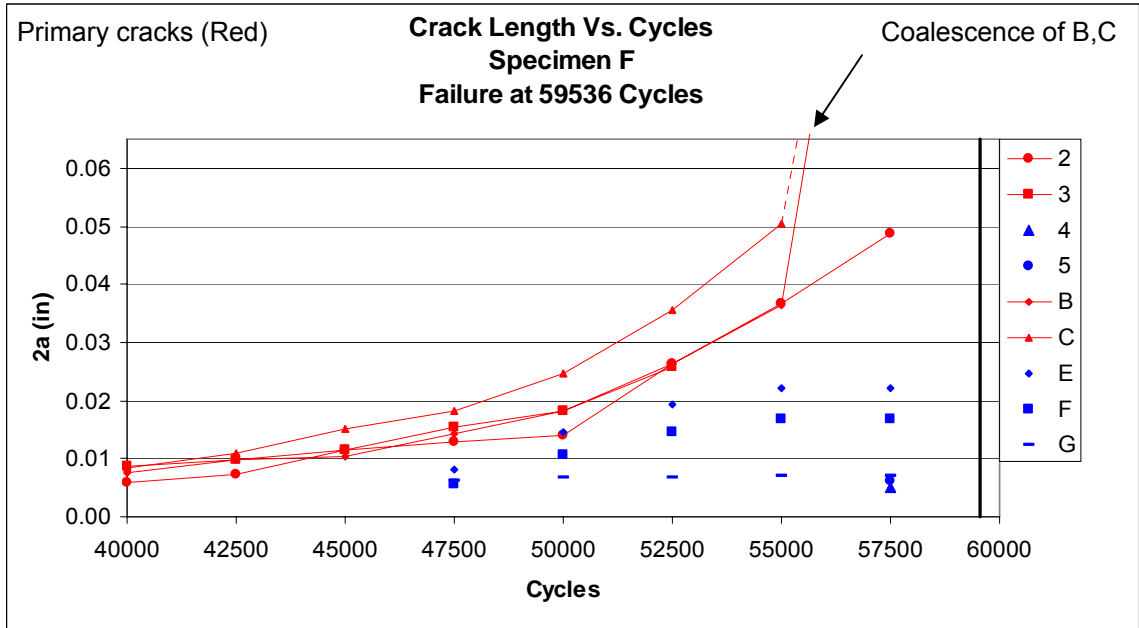


Figure 3.6: Crack length versus loading cycle for all cracks on specimen F

This figure plots the growth history of all cracks on a single specimen. As can be seen cracks B and C coalesce at some point between 55,000 and 57,000 cycles. At initiation these cracks were completely independent of each other. However due to the random locations in which they were initiated, after crack growth the two cracks eventually interfered with each other. This coalescence instantly created a single very large crack that failed the specimen much sooner than would have been expected had the cracks remained separate. Effects such as these continue to highlight the importance of approaching the problem of small fatigue crack growth on smooth surfaces through the use of non-deterministic methods.

While no analysis was conducted to directly predict the occurrence or failure of two cracks to coalesce, several qualitative conclusions can be drawn through observation of the current data. It was observed that as two crack tips grew toward each other with only a small vertical separation on the specimen surface there were two possible outcomes.

The first possibility leads to coalescence by the creation of a nearly vertical crack segment that connects the two original ones. This connection generally occurs very quickly. The second possibility occurs when the cracks simply fail to join and continue to grow parallel to each other.

Both of these possibilities were observed on several occasions. It was apparent that the possibility of coalescence was dramatically higher for relatively large cracks. Many times smaller cracks, below approximately 250 to 300 microns, would not coalesce even though some would eventually grow to large lengths. This suggests an energy criterion for coalescence dependent on the size of the ligament separating the two crack tips and the size of the respective cracks. Larger cracks will have higher amounts of strain energy available to offset the surface energy and plastic deformation required to separate the ligament. When sufficient energy is available the crack fronts will coalesce unstably until an equilibrium crack front is achieved. This was shown for the case of two planar semi-elliptical cracks by Murakami and Nemat-Nasser [34] through the use of the body force method.

## Chapter IV– Transition Length

In this chapter a micro-structurally based transition length between small and long crack behavior is defined. The motivation for this work was a study of small corner cracks in which the evolution of scatter with crack growth was tracked. This work will be presented first.

A similar analysis will be presented on the current test data. It was found that the scatter, measured by the statistical coefficient of variation falls with the growth of small cracks. At the defined transition point this scatter obtains a minimum value which remains essentially constant for the remainder of crack growth. The crack growth behavior of individual cracks will also be presented to directly illustrate what is physically occurring on the specimen surface which leads to such results. Additionally, several applications of the defined transition length are highlighted.

### **4.1 Micro-Notches: Results/Summary of Previous Work**

Work on small cracks was previously conducted at the Georgia Institute of Technology School of Aerospace Engineering by Carlson et al [48, 49]. Unlike the current work where cracks were initiated on smooth surfaces, cracks in this research were initiated and grown from micro-notches carefully cut into each specimen. The ease of locating the single crack per specimen allowed for significantly more detailed observations of each crack in the tests than could be practical for tests where entire crack clusters must be measured. Unfortunately data was only collected for a limited number of specimens. Therefore definitive conclusions cannot be concluded from these tests. However, the following results do provide the motivation for the current work on the evolution of scatter during small fatigue crack growth.

The material chosen for testing, from which all specimens were machined, was 6061-T651 aluminum alloy in rod form. Unlike the bulk plate material from which the current specimens were cut from, bulk rods tend to have a “needle” like grain pattern which is elongated along the axis of the rod. This grain geometry can be described by two characteristic dimensions: longitudinal and transverse. The longitudinal dimension is the average length of the elongated grains along the axis of the rod, while the transverse dimension is the average diameter of the grains when looking at a cross section of a cut through the rod. A metallographic analysis, similar to the one described above for the 7075-T7351 plate, was conducted and provided the following average grain dimensions which are presented below in table 4.1:

Table 4.1: Average grain dimensions for 6061-T651 rod

<b>Longitudinal</b>	<b>Transverse</b>
350 microns	200 microns

The specimen geometry chosen contained a square cross section and is presented below in figure 4.1. The specimens were loaded using a standard three-point bending configuration oriented for bending around the cross section diagonal, such that the maximum tensile stress would be put on a corner fiber of the specimen. Micro-notches were cut into these corner edges of each specimen to a depth of 150 microns, using a digitally controlled slitting saw. This allowed for the growth of corner cracks, the geometry of which is shown below in figure 4.2.

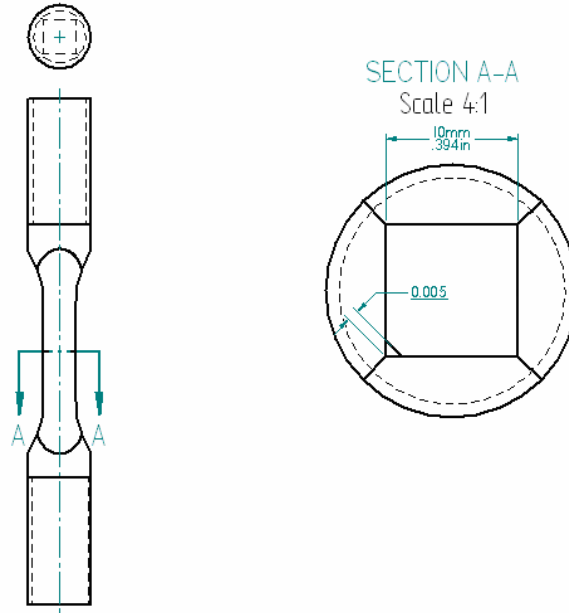


Figure 4.1: Corner Micro-Notch Specimen Geometry

Prior to testing the specimens were polished in a manner similar to the current procedure. This treatment eliminated any alternate crack initiation sites and allowed cracks to be measured optically using a Questar tele-microscope. The maximum applied load gave a tensile stress of 80 percent of the yield strength of the material and was applied with a sinusoid waveform having a frequency of 10 Hz.

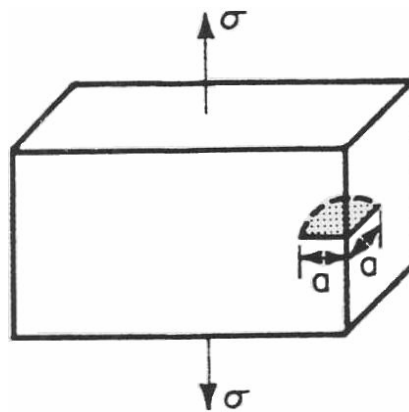


Figure 4.2: Corner crack geometry [50]

The crack length versus cycle count data collected from the limited amount of tests run is presented below in figure 4.3. A cubic regression of the form:

$$a = A \cdot N^3 + B \cdot N^2 + C \cdot N + D \quad (4.1)$$

was performed on the crack length ( $a$ ) versus loading cycle ( $N$ ) data for each crack, where  $A$ ,  $B$ ,  $C$  and  $D$  were the unknown regression constants. These equations were then differentiated to provide the crack growth rate ( $da/dN$ ) in terms of cycles. This data is provided below in figure 4.4 as a plot of the crack growth rate versus the crack length.

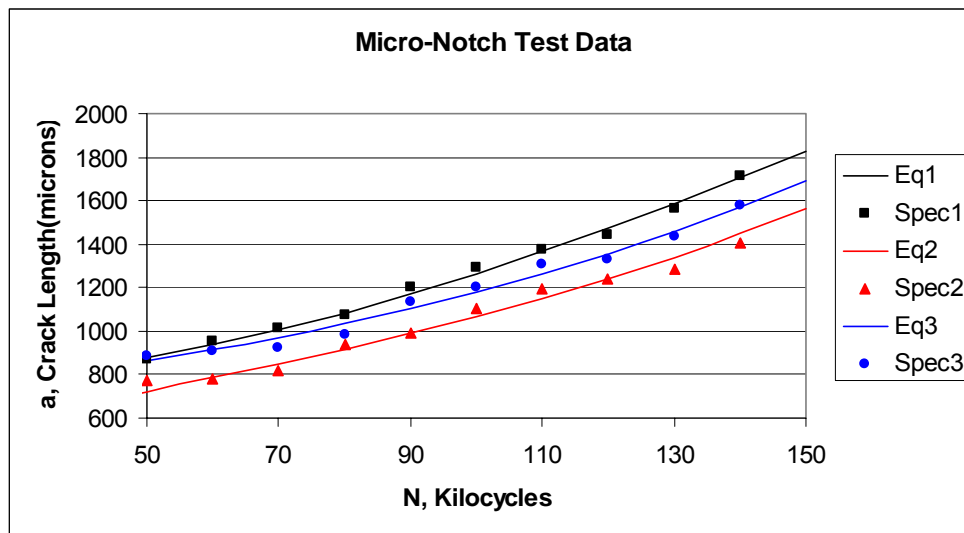


Figure 4.3: Crack length versus cycle count data

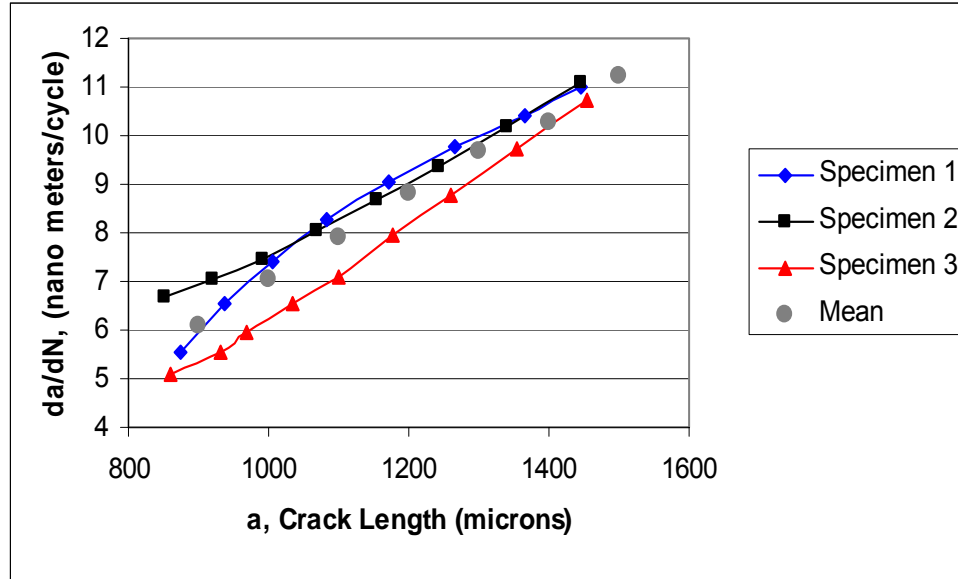


Figure 4.4: Crack growth rate versus crack length data

A plot of the standard deviation of the crack growth rates versus crack length is provided below in figure 4.5. Also on this plot is the linear relation between the average number of grains intersected by the crack front ( $n$ ) and the crack length. In order to derive this relationship the corner crack front was assumed to be a quarter arc of a circle. Fractographic examinations of fracture surfaces confirm this to be a valid assumption. By simple geometry the number of grains intersected by the crack front is then given by the equation:

$$n = \frac{\pi}{2} \left( \frac{a}{d} \right) \quad (4.2)$$

where  $a$  is the crack depth and  $d$  is the average grain diameter normal to the specimen axis.

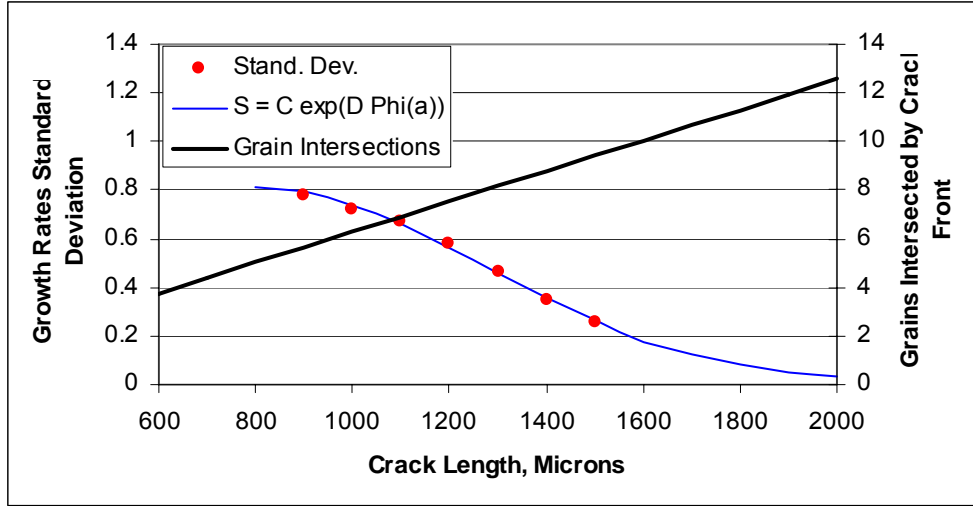


Figure 4.5: Crack growth rate standard deviation/grain intersections versus crack length

The trend of the data indicates that initially the rate of decrease in the standard deviation increases with increasing crack length. Ultimately, however, the rates of decrease begin to decrease with increasing crack length. This behavior is reasonable because it would be expected that the standard deviation should tend to approach an asymptotic value as the long crack regime is approached.

The features of the standard deviation in figure 4.5 indicate that it is possible to represent the observed behavior by an exponential function of the form:

$$S = Ce^{D\Phi(a)} \quad (4.3)$$

where  $S$  is the standard deviation,  $a$  is the crack length, and  $C$  and  $D$  are constants. The constants were determined by the application of a nonlinear regression analysis [49] and provide the final form of the equation shown below.

$$S = 0.81e^{[-2.299 \cdot 10^{-6}(a-800)^2]} \quad (4.4)$$

When equation 4.4 is combined with the linear relation between the crack length ( $a$ ) and the number of grains intersected by the crack front ( $n$ ) equation 4.2, it is evident that the standard deviation of the crack growth rates ( $S$ ) can also be represented as a function of  $n$ . The resulting substitution is shown below and has been used to obtain the plot in presented in figure 4.6.

$$S = 0.81e^{-2.299 \cdot 10^{-6} (.6366 \cdot d \cdot n - 800)^2} \quad (4.5)$$

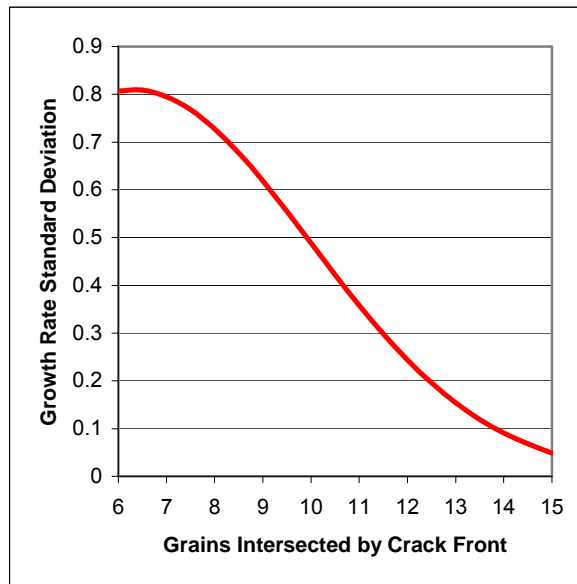


Figure 4.6: Standard deviation of crack growth rates versus the number of grains intersected by the crack front

In figure 4.6 it is apparent that after the crack fronts have intersected approximately 15 grains the standard deviation of the crack growth rates and thus the measured scatter becomes exceedingly small, below 0.1 nano-meters per cycle. At this point the standard deviation and thus scatter has reached its stationary value, signifying that the cracks have begun to act as long cracks and can be treated deterministically using standard fracture

mechanics principles. This micro-structurally defined point is then said to be the transition point from small to long crack behavior.

This behavior can be explained simply when one considers the non-homogeneous, anisotropic medium within which small cracks grow. The front of a small crack will sample only a limited amount of grains, each of which is randomly oriented with respect to the plane of the crack. This means that while some grains may be favorably oriented for crack growth others will not be. It has been suggested [5,15] that the accelerated crack growth in some grains is caused by the presence of micro-plasticity in favorably oriented grains, while the lack thereof is the cause of retarded growth in less favorably oriented grains. It has also been suggested that crack deflections can be caused by a crack orienting itself to the local crystallographic texture [20]. Additionally, it has been shown that grain boundaries pose as micro-structural barriers to fatigue crack growth [5, 7, 15] but it also acknowledged that this effect may simply be an implication of the abrupt alteration in the crystallographic texture that occurs across the boundary.

While a crack is small the afore-mentioned micro-structural phenomena will control the growth of the crack. Thus, fast growth-arrest and deflection behavior is the root cause of the increased scatter found in the growth rates of small cracks as each small crack will sample completely different micro-structural features. However, as the crack grows longer and samples additional grains these effects will begin to average out, approaching the long crack, bulk behavior of the material. This is evidenced by the drop and eventual leveling of the measured scatter and the corresponding drop and leveling of the standard deviation of the crack growth rates.

The above micro-structural definition of a transition point between short and long crack behavior also provides a basis for anticipating differences in the evolution of scatter for different crack surface shapes and micro-structural textures such as pancake and needle. For example, it is shown in figure 4.7, a and b, that in samples with identical material microstructure the crack front of a semi-circular crack intersects twice as many grains as a corner crack of the same depth. The scatter for the semi-circular crack is therefore expected to diminish more rapidly than for the corner crack of the same depth. However, when both cracks transition from small to long crack behavior the average number of grains intersected by the crack front for both geometries will be the same.

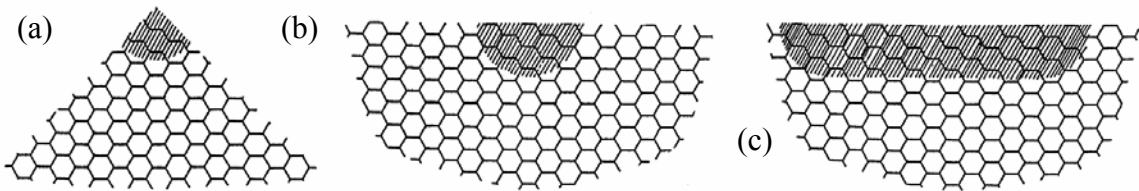


Figure 4.7: Sample crack geometries with a simulated microstructure: (a) corner crack, (b) thumbnail crack, (c) surface crack in bending

When counting the grains intersected by the crack front, it is necessary to only include those grains through which the crack is actively growing. For most cases this will be a simple matter, but in other cases such as the crack geometry shown in figure 4.7, c, care must be taken. This crack can be created by the initiation and growth of a thumbnail surface crack into the decreasing stress field associated with bending about an axis and can be expected to only grow mainly outward towards the sides. Therefore only the intersections of the grains on the sides of the crack front should be counted, which means the crack will act more like a thumbnail crack than its geometry indicates. In other words,

while the crack may appear to be a long crack which samples a large portion of material microstructure, it can in fact still behave as a small crack.

#### **4.2 Cracks Grown from Smooth Surfaces: Current Work**

A similar analysis on the evolution of scatter in small fatigue cracks has been carried out using the data obtained from the current experiments. However, not all crack data was used. First, only the cracks in the primary crack distribution were considered because, as it will be discussed fully in chapter V, only these cracks will continue to grow out of the small crack regime towards failure. Therefore the scatter in the growth rates of secondary cracks will be inconsequential. Additionally, out of the 14 primary cracks measured, two were ignored. These cracks initiated late in the fatigue lives of their respective specimens and so only limited growth data was obtained for them. With such limited data it was not possible to fit meaningful regression curves to the data.

As in the previous case of the micro-notch data, a cubic regression analysis with the form of equation 4.1, was performed on the crack surface length ( $2a$ ) versus the cycle count data. The regression constants for all of the primary cracks analyzed are presented below in table 4.2. For illustrative purposes, a plot showing all of the primary cracks of specimen F with their respective regression lines is presented below in figure 4.8. Close regression fits for the data of the remainder of the primary cracks were also obtained. This is evidenced by the coefficient of determination ( $R^2$ ) values for the regression lines which are provided below in table 4.2. This constant, which ranges between zero and one, is a measure of the goodness of fit of the regression curves. The values obtained, being very close to one indicate that a good fit to the data has been achieved.

Table 4.2: Summary of the regression constants of the primary cracks analyzed, for the relationship between surface crack length and load cycle count

$$2a(N)=AN^3+BN^2+CN+D$$

**Regression Constants**

Number	Crack ID	A	B	C	D	R <sup>2</sup>
1	F-2	0.18062	-22.05204	911.36006	-12572.21381	0.9878
2	F-3	0.14149	-19.16289	878.28026	-13395.81889	0.9920
3	F-B	0.19868	-24.61381	1031.27427	-14389.79548	0.9982
4	F-C	0.34996	-44.90236	1948.79887	-28292.90881	0.9994
5	C-A	0.47413	-67.41886	3212.35010	-51021.70571	0.9995
6	C-B	0.31308	-49.62031	2644.18905	-47052.74405	0.9846
7	E-1	1.43477	-183.26368	7838.90698	-111858.53938	0.9998
8	I-1	0.85598	-116.24491	5265.66493	-79235.93500	0.9981
9	I-2	0.33274	-44.46814	1992.22179	-29673.93100	0.9993
10	I-A	0.28025	-38.69871	1783.11326	-27204.28900	0.9881
11	I-B	0.27263	-40.66540	2045.12333	-34380.17000	1.0000
12	S6C2	1.04648	-155.24480	7680.70600	-126398.02000	1.0000

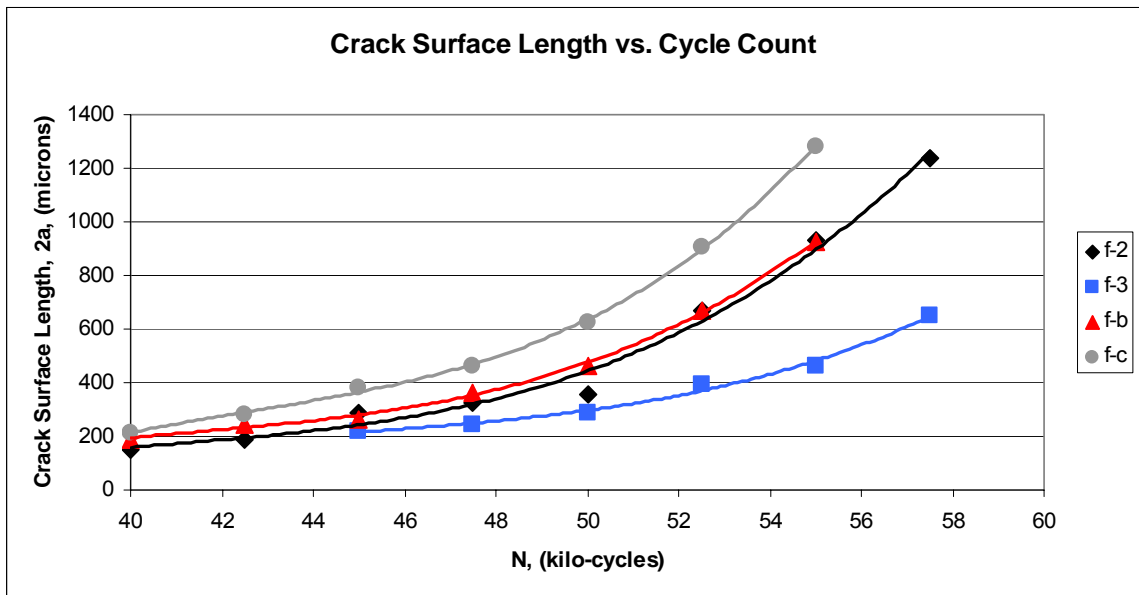


Figure 4.8: Crack length versus cycle count data for primary cracks of specimen F

As in the previous analysis these regression equations were differentiated to provide equations for the crack growth rates as a function of the number of loading cycles. These equations were of the form:

$$\frac{da}{dN} = E \cdot N^2 + F \cdot N + G \quad (4.6)$$

$$E = 3A, \quad F = 2B, \quad G = C$$

where  $A$ ,  $B$  and  $C$  are the regression constants described above. A summary of the growth rate constants for the analyzed cracks is presented below in table 4.3.

Table 4.3: Summary of the regression constants for the primary crack growth rate versus loading cycle

Number	Crack ID	Growth Rate Constants		
		E	F	G
1	F-2	0.54186	-44.10408	911.36006
2	F-3	0.42447	-38.32578	878.28026
3	F-B	0.59604	-49.22762	1031.27427
4	F-C	1.04988	-89.80472	1948.79887
5	C-A	1.42239	-134.83772	3212.35010
6	C-B	0.93924	-99.24062	2644.18905
7	E-1	4.30431	-366.52736	7838.90698
8	I-1	2.56794	-232.48982	5265.66493
9	I-2	0.99822	-88.93628	1992.22179
10	I-A	0.84075	-77.39742	1783.11326
11	I-B	0.81789	-81.33080	2045.12333
12	6-2	3.13944	-310.48960	7680.70600

Having relationships for both the crack lengths and the crack growth rates in terms of the loading cycle it is possible to associate a growth rate to any crack length. This procedure was used to obtain crack growth rates for values of crack lengths throughout the lifecycle of each specimen. A range of values from 200 to 900 microns was chosen,

which includes both micro-structurally small and long cracks. In order to illustrate the results of this procedure plots of crack growth rates versus crack length for the same cracks shown above in figure 4.8 are presented below in figure 4.9.

With this data it was a simple matter to compute any relevant statistics of the crack growth rate at the various crack lengths. In this case only the average and the standard deviation were needed. These were used to calculate the respective coefficients of variation ( $C_x$ ). A summary of these values is shown below in table 4.4.

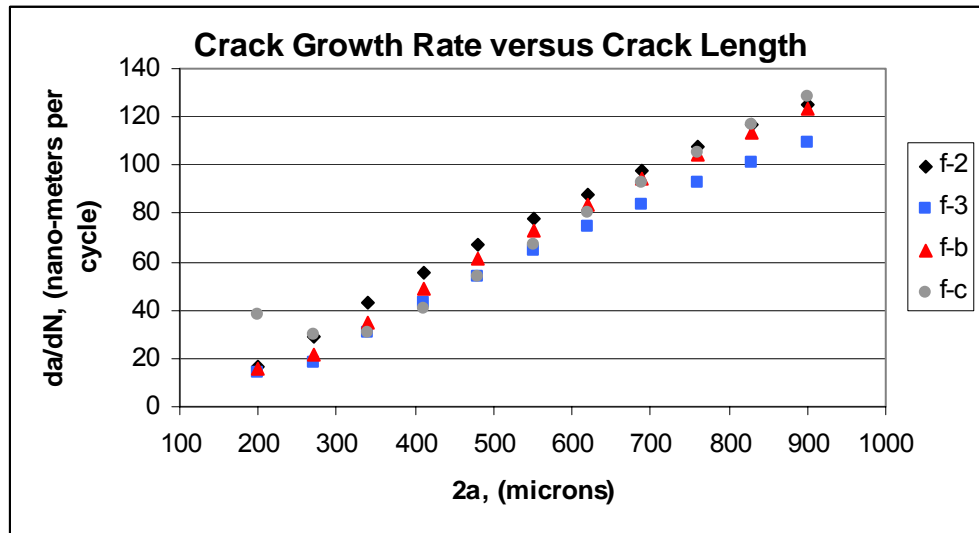


Figure 4.9: Crack growth rates for the primary cracks of specimen F

Table 4.4: Summary of the crack growth rate statistics

Crack Length (Microns)	200	270	340	410	480	550	620	690	760	830	900
S	28.483	16.491	12.534	9.021	12.602	15.153	18.091	21.300	24.585	27.851	31.056
$\mu$	37.927	30.550	31.955	47.784	63.722	79.504	94.432	108.538	121.947	134.766	147.083
$C_x$	0.751	0.540	0.392	0.189	0.198	0.191	0.192	0.196	0.202	0.207	0.211

The coefficient of variation is a non-dimensional, positive quantity that provides a measure of the scatter found in a set of data. It is found by dividing the standard deviation of a set of data by that set's mean:

$$C_x = \frac{S}{\mu} \quad (4.7)$$

Calculated in this manner this quantity provides information about the spread of data relative to the middle value, with large values signifying a large variability and small values meaning the opposite. This allows for the variability of smaller growth rates to be compared with that of the larger rates.

As previously mentioned, the surface cracks measured have been assumed to grow with semi-circular crack fronts as shown in figure 3.1. Using simple geometry it can be shown that the average number of grains intersected by these crack fronts is given by the linear relationship presented below:

$$n = \frac{\pi a}{d} \quad (4.8)$$

where in this case  $a$  is the crack half length or depth. As described earlier, this formula shows that for the same crack depth, a surface thumbnail crack will sample twice the amount of grains as a corner crack. As shown above, any relationship that is a function of the crack length can now be transformed to be a function of the number of grains intersected by the crack front.

Unlike the rod material analyzed above where only one characteristic grain dimension was needed to determine the amount of grains intersected by the crack front, the plate

material used in the current tests demands the use of two. Since any wrought plate will have three characteristic micro-structural dimensions, any two-dimensional crack must grow through two of them. The way the current specimens were machined, all cracks grew into the longitudinal-short transverse plane of the plate. The manner in which this was rectified was that the two values were simply averaged to provide the value for  $d$  in equation 4.8. For this case  $d$  was found to be equal to 0.00145 inches. This value provides the average size of grains sampled by the crack front.

A plot of the coefficient of variation of the crack growth rates, which showcases the evolution of scatter throughout the crack growth process is presented below in figure 4.10. Both  $C_x$  and the number of the grains intersected by the semi-circular crack fronts are plotted versus the crack lengths.

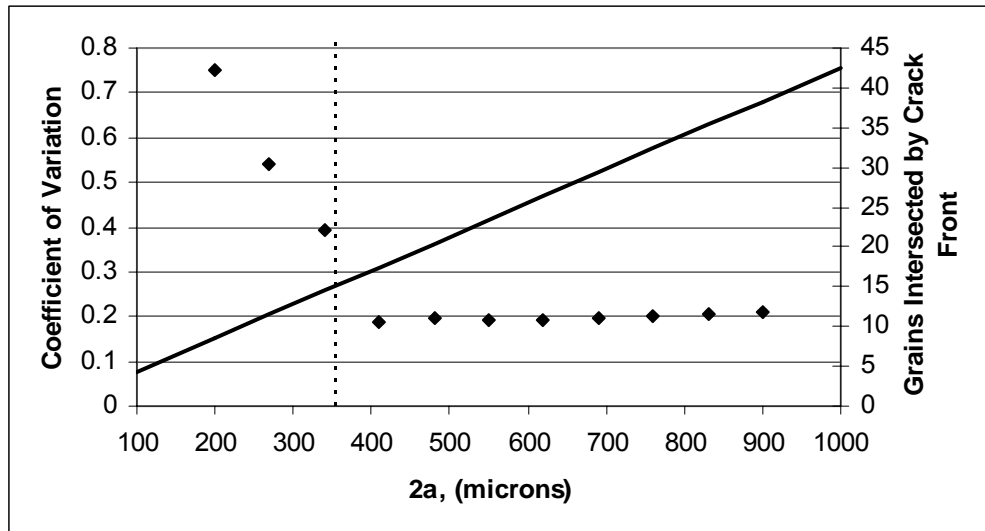


Figure 4.10: Coefficient of variation of the crack growth rate

This plot shows that the scatter present in the current experiments behaves in the same manner as that of the previous experiments run on corner cracks. In the early stages of crack growth a large amount of scatter is present, signifying a strong small crack effect.

As the crack grows this scatter falls off quickly until a certain point at which the amount of scatter observed in the growth rates levels off and maintains a fairly constant value. In these experiments, after the scatter leveled off at a low value it was observed to rise again with crack growth. This rise, however, was very gradual and did not lead to large changes in the observed scatter by the end of the fatigue life of the specimens.

This type of behavior is a product of each crack's varying interaction with the local material microstructure. As discussed above, when the cracks are small the crack fronts will only sample a small number of grains and the growth of the cracks will be dominated by micro-structural phenomena. This leads to the large amounts of scatter observed. As the cracks grow and sample an increasing amount of micro-structure these effects will begin to average out and the scatter will fall. This will continue to happen until enough microstructure is sampled to allow the cracks to approach the bulk long crack behavior expected in the material. Here scatter should stay fairly constant through failure.

As discussed above, a micro-structural transition point between small and long crack behavior has been defined as the point when the growing front of a crack intersects 15 grains. Using equation 4.8, it can be found that this value is reached for cracks in the current experiments when the surface crack length reaches a value of approximately 0.0138 inches or 352 microns. This value, shown as a solid line in figure 4.10, corresponds well, within approximately 0.002 inches, with the actual point where the scatter in the crack growth rates reaches its steady state value. Therefore, the micro-structurally based transition point defined using data from corner cracks in one alloy has successfully predicted the transition point in a second alloy containing cracks of a different geometry.

The observed gradual rise in scatter after reaching the steady state value is most likely an artifact of the specific crack growth environment created in these tests. All cracks in these tests were grown in clusters from smooth surfaces. Consequently, as the cracks grew longer the probability of growth rates being altered by the interaction with other cracks rose.

Additionally, depending on where each crack initiated, the free surface of the side of the specimen would interfere with the growth of some cracks. Initially the free surfaces will be far enough from all cracks when compared to their lengths so as to have negligible effects. However as some cracks grow larger the un-cracked ligament between the crack and the side becomes small enough to alter the stress field around the crack tip. To illustrate this effect the solution for the stress intensity factor of the surface tips of a thumbnail crack in a finite plate is given below [51]. This shows that the crack driving force is a function of the distance from the tips of the crack to the sides of the specimen.

$$K_I = 0.6371\sigma\sqrt{\pi a} \cdot \sec^{1/2}\left(\frac{\pi a^{3/2}}{2W\sqrt{t}}\right) \left[ 1.04 + 2.0167\left(\frac{a}{t}\right)^2 - 0.1061\left(\frac{a}{t}\right)^4 \right] \left( 1.1 + 0.35\left(\frac{a}{t}\right)^2 \right) \quad (4.9)$$

In the above equation  $t$  is the plate thickness and  $W$  is the width of the plate.

### **4.3 Discrete Crack Growth Rate Observations**

The procedures to obtain the crack growth rates used above relied on a polynomial regression curve. This in effect smoothed out the finer perturbations in the crack growth rate which show the true growth-arrest phenomena. For this reason the growth rates of the cracks were also calculated using the secant method, a discrete numerical technique

defined by ASTM standard E647-95a [52]. With this method the crack growth rate in between each pair of crack length measurements is given by the equation shown below.

$$\left(\frac{da}{dN}\right)_a = \frac{(a_{i+1} - a_i)}{(N_{i+1} - N_i)} \quad (4.10)$$

This method was used to calculate the growth rates of all cracks tracked in order to observe their true behavior.

To illustrate this behavior, the crack growth rates of all primary cracks of which more than six data points had been collected are plotted below in figure 4.11. These cracks provide the clearest picture of the primary crack behavior. The plot has been divided into two sections: small crack growth prior to the transition point and long crack growth after the transition point.

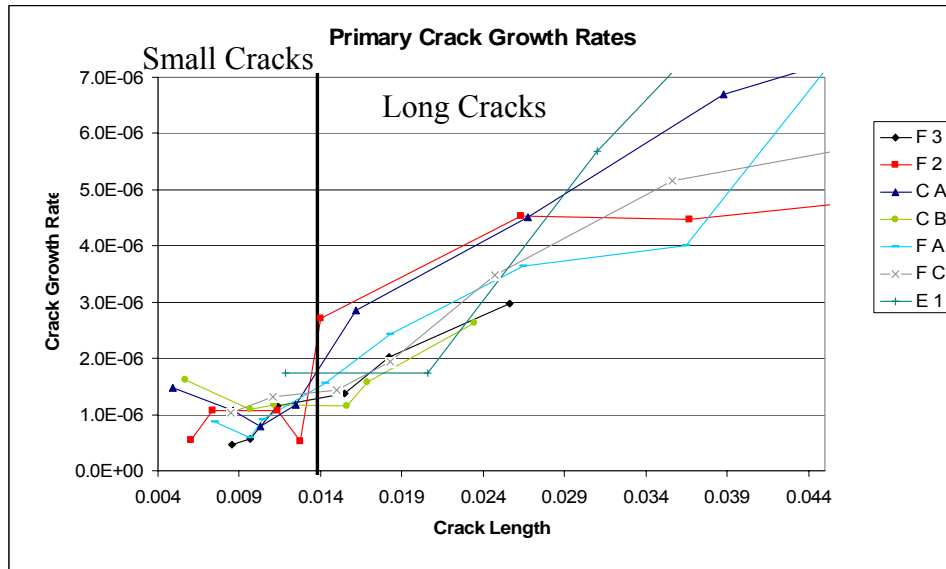


Figure 4.11: Crack growth rates calculated using secant method

As can be seen in figure 4.11, the growth rates for small cracks fluctuate wildly, sometimes even including periods of crack arrest. However, as is also evidenced in figure 4.11, after the micro-structurally defined transition point the growth rates tend to be significantly more stable signifying that the growth of the cracks is no longer dominated by micro-structural inhomogeneities. This shows that the defined micro-structurally based transition point predicts not only the point where scatter drops but that this point corresponds closely to where cracks cease to act as unpredictable small cracks and begin to act as deterministic long cracks.

#### **4.4 Applications**

The micro-structurally based transition point is not solely of academic interest but rather has the potential to be of wide applicability. The only parameters required for its use are the crack geometry and grain size of the material being investigated. For any crack growth analysis the shape of a crack will either be known or previously assumed. The material grain sizes represent easily obtained values which in the case of many materials have already been tabulated. Several examples of such applications will be presented below.

##### **4.3.1 Separation of Crack Growth Regimes**

As previously discussed the growth behavior of small cracks differs greatly from that of long cracks. This difference persists even when cracks are compared not simply by length but by fracture mechanics singularity parameters such as the SIF and the J-Integral. Some authors have attempted to include the small crack regime of growth in the

same analysis as that of long cracks [19] through the use of various corrections to the traditional growth laws. However, the absolute success of these methods is questionable.

Due to the uncertainty in the accuracy of these methods, the analysis of crack growth could be significantly simplified if the small crack growth regime could be separated and analyzed on its own. The micro-structurally based transition point defined here provides a simple crack dimension at which the analysis can be split. This would be similar to the way flow over an airfoil is modeled and analyzed. First the bulk flow is modeled and when this is completed the analysis is used to define the boundary conditions for the analysis of the more complex boundary layer that lies close to the airfoil surface. In much the same way the small crack regime can be modeled and the cycle count for the crack to grow from initiation to the transition point can be obtained. The crack size and cycle count can then be used as a starting point for a traditional long crack analysis. An example of such a procedure will be presented below in chapter V.

#### 4.3.2 Fatigue of Thin Metallic Foils

In work on thin metallic foils, Lamberson [53] concludes that fatigue crack growth in such materials occurs faster than would be expected from fracture mechanics parameters such as the SIF. As-rolled Al-Mg foils with thicknesses which ranged from 30 to 250 microns were tested. Amongst many other applications such foils have found use as components in aerospace thermal protection systems (TPS), as well as in fuel cells. As the applications of such foils are so far reaching it is of importance to understand their fatigue behavior.

It is suggested that the anomalous behavior of fatigue cracks in such thin metallic elements could actually be caused by the small crack phenomena. In such thin foils the

thickness of a specimen can actually be spanned by a very small number of grains, possibly even by a single grain. For this reason, the crack fronts of through cracks in such materials may only sample a small amount of material microstructure no matter how large their length may be. By the transition length defined above, these cracks will never become long cracks and thus exhibit small crack behavior, including accelerated growth, for their entire lifecycle.

## **Chapter V – Bi-Modal Model of Micro Multi-Site Cracking**

In this chapter it is shown that the total population of cracks within a cluster is actually comprised of two separate statistical distributions: primary and secondary cracks. Primary cracks are those which continue to grow and can ultimately lead to failure, whereas secondary cracks will ultimately arrest. It is shown that if these secondary cracks are not removed from the data before any fatigue crack growth analysis is performed the analysis will inherently lead to erroneous non-conservative life predictions. This is shown by creating confidence limits on the mean growth of the various distributions of cracks.

Two different methods of separating the distributions are proposed. The first relies on the micro-structurally based transition point defined previously. The second method is based on the crack acceleration and requires no information other than the raw crack data.

Finally, a method is presented for the estimation of the fatigue crack propagation life in which the life is divided into two growth regimes separated at the small to long crack transition length. The long crack regime is treated by conventional LEFM methodology while the small crack regime is treated in a statistical manner utilizing the calculated confidence bounds.

### **5.1 Introduction**

It is a common observation that when a smooth surface undergoes fatigue loading, cracks will initiate in randomly oriented clusters. In the current tests many such clusters have been observed and recorded. It has also been shown [29, 36, 37] that within these clusters cracks will interact with each other in ways that do not occur for single dominant cracks such as those artificially initiated from a notch. For instance, within the clusters shielding and anti-shielding will occur causing additional transient effects in the growth

of small cracks. Additionally, as previously discussed, the phenomenon of crack coalescence can lead to significant changes in the propagation of cracks and the resultant specimen fatigue life.

It is expected that the fatiguing of service components will also lead to cracks naturally initiating from smooth surfaces. For this reason it is ideal to use cluster crack data to analyze the behavior of small cracks as it represents a close approximation to realistic situations. However, it is also found that within clusters many cracks will grow exceedingly slowly or arrest completely [36]. This can happen, for example, when a crack intersects a grain boundary which it does not have the energy to cross. These cracks behave fundamentally different than those cracks that will continue to propagate. It is only these propagating cracks that can ultimately lead to unstable failure by fracture.

The remaining non-propagating cracks are still important as they create a unique neighborhood through which each propagating crack must grow. For that reason testing of a single crack completely apart from a cluster can lead to erroneous non-realistic data. However, if the data from the many non-propagating cracks, which can often be quite small, were included in an analysis of the data from the propagating ones [28, 29, 54] they would skew the results making it appear that the distribution of cracks present is smaller than it should actually be considered to be. This result means that if secondary cracks are included in an analysis of crack growth the obtained results would be inherently non-conservative.

It is therefore evident that the total population of cracks on a smooth surface represents a bi-modal sample. The two separate distributions differ from each other in relative behavior. The propagating cracks which will be included in subsequent analyses

will be termed the primary crack distribution and the remaining cracks which will be excluded from further analysis will be termed the secondary crack distribution. It must be noted that there is not necessarily only a single primary crack per specimen. Often authors have termed the crack that causes final failure by fracture the dominant crack [55] and some consider it to be the only crack which for which the data is meaningful. While it is true that only a single crack can ultimately cause failure, discarding the data from other cracks that behave in a similar manner would be a waste of valid data. Therefore the possibility exists, and is most often the case, that there can be multiple primary cracks per specimen.

## **5.2 Separation of the Distributions**

Once it is recognized that the primary cracks must be partitioned from the total measured crack distribution the key problem becomes determining a method to perform this separation. For this method to be useful it will be beneficial for it to represent a deterministic approach, not subject to the discretion of the user. In addition, the separation method should be sufficiently general such that it can be applied to any metallic material, loading situation and crack/specimen geometry.

The situation of the separation of the distributions is significantly complicated when viewing the crack populations early in the fatigue life of a specimen. At this time in the life of a specimen all cracks will look similar and in general will be fairly small. For this reason, separation of the distributions at this stage in the life cycle of a specimen is impossible. It is instead necessary to allow for significant crack growth to take place.

Two experimental methods with the characteristics described above were developed. The first of these methods is relatively simple, utilizes the entire crack growth history and

is based upon the concept of a micro-structural transition length between small and long crack behavior that was introduced previously. This method will be described here. A second approach which is based upon the numerically evaluated second derivative of the crack length versus cycle count data will be presented in a section below.

Since it is not possible to separate the crack distributions early in the fatigue life of a specimen cracks are instead allowed to grow to significant lengths where their relative behaviors become distinguishable. This includes lengths well over the micro-structurally defined transition point where the crack front has intersected an average of 15 grains. This transition length calculation follows the same form as was described previously using all of the same simplifying assumptions. These assumptions include that all cracks have a semi-circular crack front geometry and that the average number of grains along this crack front is given by the simple linear relation presented in equation 4.8.

After it is determined which cracks reach the transition length and become micro-structurally long cracks by specimen failure the procedure is twofold. First, all cracks that have reached this length are put into the primary crack distribution with the remaining cracks being considered in the secondary distribution. Secondly a closer look is taken at all cracks whose lengths are approximately, within 10-15 percent, of the transition point at failure. This is done for several reasons. Some cracks may behave as primary cracks but due to a late initiation may still be physically small at failure. Additionally, it must be understood that the transition length is not a concrete quantity but rather a statistically defined one. The growth rates of these cracks, calculated using the secant method as described above, are compared to that of the average primary and secondary cracks. They are then placed into the distribution with which their physical behavior is more

consistent. In the current work it was always immediately apparent which distribution these borderline cracks belonged in. An example of the results of this analysis applied to all of the cracks measured on a single specimen is presented below in figure 5.1. Primary cracks are shown in red while secondary cracks are shown in blue.

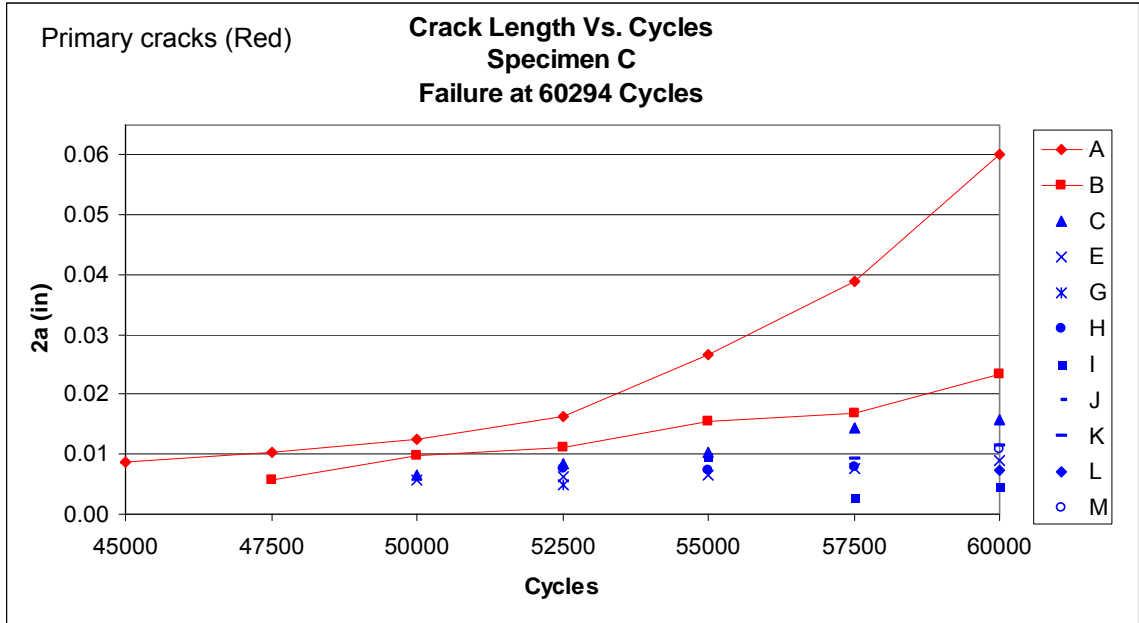


Figure 5.1: Example of the distribution separation procedure applied to specimen C

Notice how the growth of the secondary cracks tends to level off and arrest even through continued cycling. The primary cracks all continue to grow with crack A eventually leading to specimen failure. A second example showcasing the differences in the behaviors exhibited by primary and secondary cracks is shown previously in figure 4.4.

Although long cracks that are growing, and thus being loaded above the threshold SIF, are all expected to continue to grow along a predictable growth curve this method of separation is not perfect. Whether a crack is micro-structurally long or small is not a fundamental measure of the behavior of a crack. This method is therefore not completely

based upon what is physically occurring on the specimen surface. A separation algorithm that rectifies this problem will be presented below.

### **5.3 Confidence Limit Analysis**

As previously discussed, meaningful confidence limits on the growth of small cracks can only be obtained once the secondary crack distribution has been separated from the data. With this completed and only the primary cracks remaining, the results of any statistical analysis will then represent the true behavior of the crack population. The results of these analyses can then safely be used for life prediction purposes.

With this in mind the separation procedure discussed above was performed on the sum of all of the data obtained in the current tests. It was determined that out of the 57 cracks measured, the data on the 43 cracks determined to be secondary cracks would be discarded prior to statistical analysis leaving 14 primary cracks to represent the small crack growth behavior in the material. This distribution included several cracks that underwent coalescence which is beneficial in that it ensures that coalescence effects are included in the calculated behavior of the small cracks.

The first step needed to develop confidence limits on crack lengths versus loading cycle data is to calculate representative statistics of the data. Once the primary cracks had been separated it was a simple procedure to determine the population standard deviation and mean at each value of loading cycle. These values are summarized below in table 5.1 for all cycle counts where crack measurements were taken.

Table 5.1: Summary of primary crack statistics

Loading Cycle	40000	42500	45000	47500	50000	52500	55000	57500	60000
Mean, $\mu$	0.00768	0.00825	0.01052	0.01456	0.01770	0.03113	0.03485	0.05598	0.06998
S.D., $\sigma$	0.00207	0.00271	0.00413	0.00825	0.01028	0.02585	0.03427	0.05384	0.05592

The next step in the analysis is to choose a probability distribution that models the data sufficiently well. While the normal (Gaussian) distribution is extremely simple to work with, it is not appropriate in this case. The normal distribution would infer the possibility for the existence of negative crack lengths. Additionally, the normal distribution is a symmetrical distribution. This symmetry is not expected to be found in the primary crack data [36] and in fact contradicts what has been observed. The true distribution must reproduce the skewed shape of the data which places emphasis on the upper tail due to the presence of a small number of large cracks.

Related to the normal distribution, the lognormal distribution [56] is not only simple to work with but also offers a good approximation of the crack distributions observed. The utility of the lognormal distribution is that when it is transformed by the logarithm function it becomes the normal distribution. This transformation and the resulting probability density function (PDF) of the lognormal distribution are shown below.

$$X \sim \text{Lognormal}, Y \sim \text{Normal} \tag{5.1}$$

$$\ln(X) = Y$$

$$f(x) = \frac{1}{\sqrt{2\pi\sigma x}} e^{-(\ln(x)-\mu)^2/2\sigma^2} \tag{5.2}$$

$$E(X) = e^{\mu+\sigma^2/2} \quad \text{Var}(x) = e^{2\mu+2\sigma^2} (e^{\sigma^2} - 1) \tag{5.3, 5.4}$$

In these equations  $\mu$  and  $\sigma$  are the mean and standard deviation of the normal distribution associated with the lognormal, not the mean and standard deviation of the lognormal

distribution itself. The mean and variance for the lognormal distribution are shown for reference in equations 5.3 and 5.4 respectively.

It was found that the lognormal distribution provides a good fit to the primary crack length versus cycle count data. This goodness of fit can be demonstrated by plotting the logarithm of the crack length data at a specific cycle count on a normal probability plot. This is essentially a plot of the cumulative distribution function (CDF) of the logarithm of the data on normal probability paper. If the lognormal distribution is a perfect fit to the data then on this plot the data would fall on a straight line. Examples of these plots for two cycle counts, 45,000 and 55,000, are presented below in figures 5.2 and 5.3 respectively. These cycle counts represent points both early and late in the fatigue crack propagation life.

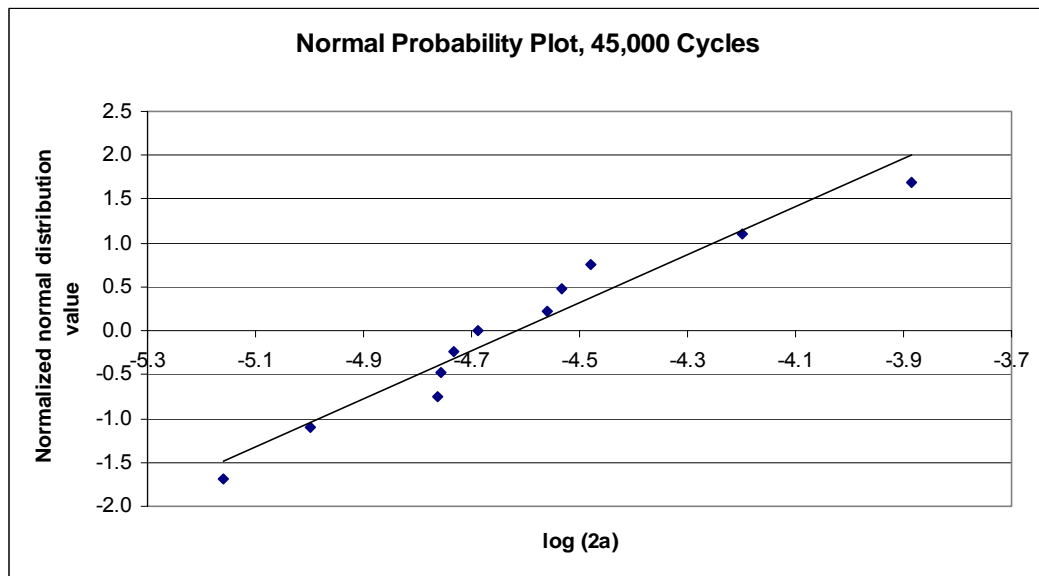


Figure 5.2: Normal probability plot of the primary crack data at 45,000 cycles

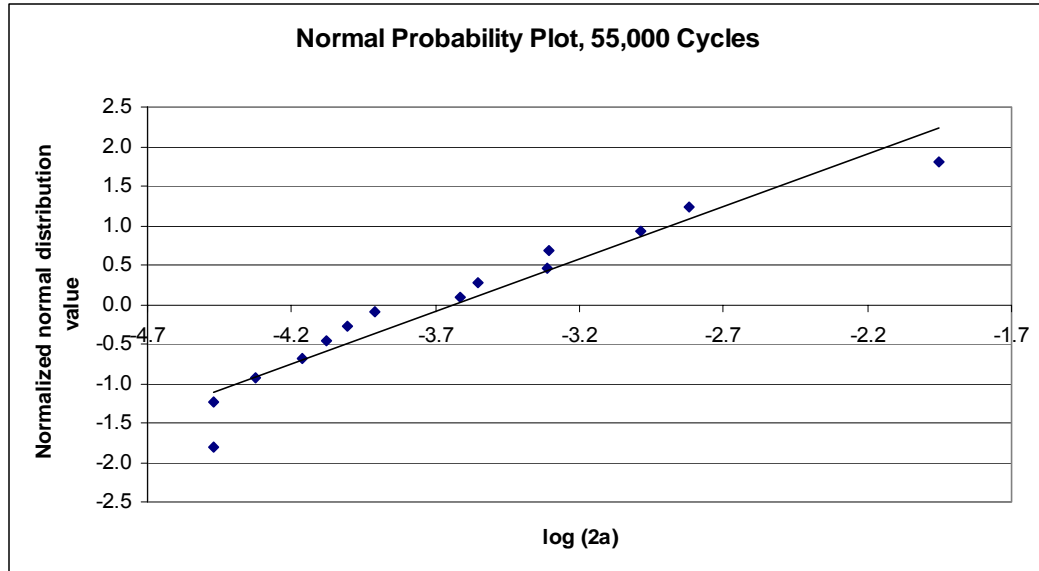


Figure 5.3: Normal probability plot of the primary crack data at 55,000 cycles

From these plots it is seen that the data do indeed lie close to straight lines. The  $R^2$  values for the fitted regression lines for the two values of the loading cycle count shown above were 0.946 and 0.926 respectively. The fact that these values are close to one provides a quantitative measure that assures that a good fit has been obtained.

The distribution of the secondary cracks is also well described by the lognormal distribution. A normal probability plot of the secondary crack data at 55,000 cycles is provided below in figure 5.4. Once again the  $R^2$  value, 0.934, is close to unity indicating a good fit. A normal probability plot of the secondary crack data at 45,000 cycles has not been provided. At this level of cycling there had not been a sufficient number of secondary cracks measured to construct a meaningful plot.

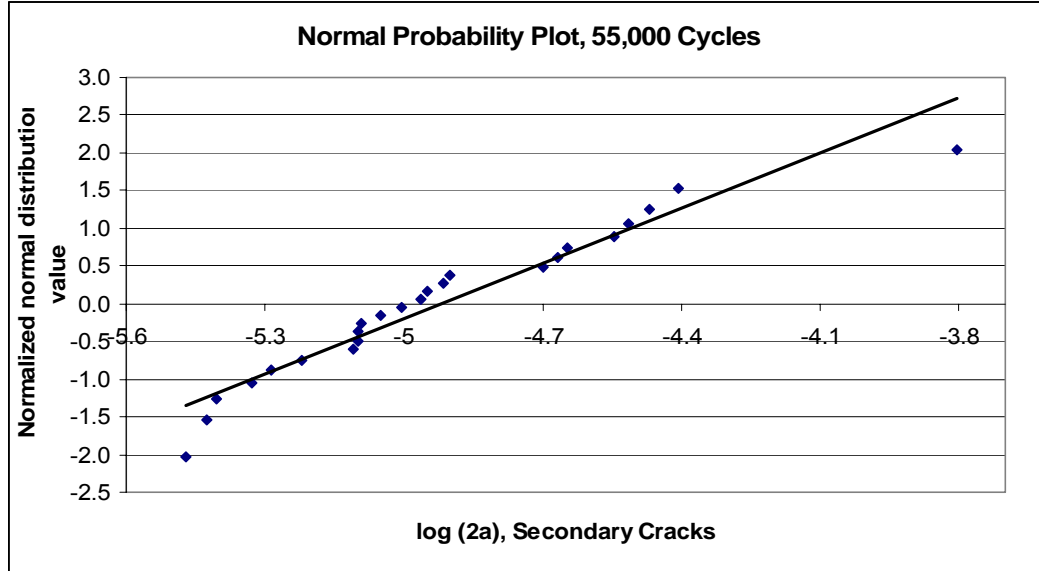


Figure 5.4: Normal probability plot for secondary cracks at 55,000 cycles

Given the assumptions that the both the primary and the secondary crack distributions are represented with a fair amount of accuracy by the lognormal distribution the PDF of the total population of cracks takes the form presented below.

$$X(x) = \frac{1}{\sqrt{2\pi x}} \left[ \frac{\beta}{\sigma_1} e^{-\frac{(\ln(x)-\mu_1)^2}{2\sigma_1^2}} + \frac{(1-\beta)}{\sigma_2} e^{-\frac{(\ln(x)-\mu_2)^2}{2\sigma_2^2}} \right] \quad (5.5)$$

In this equation  $\mu_{1,2}$  and  $\sigma_{1,2}$  are the means and standard deviations of the logarithms of the primary and secondary crack data respectively. Additionally  $\beta$  is a mixture coefficient which varies from zero to unity. It can be found at any cycle count as the proportion of the total number of cracks that have been placed into the primary crack distribution.

With the assumption that the logarithm of the primary crack data is normally distributed, confidence limits on the mean of this normal distribution ( $\mu$ ) could then easily be built using the two-sided t-interval which is presented below.

$$\mu \in \left( \bar{x} - \frac{t_{\alpha/2, n-1} S}{\sqrt{n}}, \bar{x} + \frac{t_{\alpha/2, n-1} S}{\sqrt{n}} \right) \quad (5.6)$$

In the above formula  $\alpha$  is equal to one subtracted by the selected confidence limit value. For all work contained herein a confidence limit of 95 percent was used.  $\bar{x}$  and  $s$  are the sample mean and standard deviation obtained from the data that has been transformed to come from the normal distribution, which in this case that is the logarithm of the primary crack data.  $n$  represents the number of crack measurements where the confidence limit is being built. Finally,  $t$  represents the Student-t distribution with  $n-1$  degrees of freedom. The form of this distribution is given below.

$$f(x) = c \left( 1 + \frac{x^2}{\nu} \right)^{-\frac{1}{2}(\nu+1)} \quad (5.7)$$

$$c = \frac{\Gamma\left(\frac{\nu+1}{2}\right)}{\sqrt{\pi\nu}\Gamma\left(\frac{\nu}{2}\right)}$$

Once the confidence limits on the mean of the normal distribution are found the logarithmic transformation is reversed on those limits to obtain 95 percent confidence limits on the mean of the unaltered primary crack data,  $\lambda$ . The form of these limits is shown below.

$$\lambda \in \left( e^{\bar{x} - \frac{t_{\alpha/2, n-1} S}{\sqrt{n}}}, e^{\bar{x} + \frac{t_{\alpha/2, n-1} S}{\sqrt{n}}} \right) \quad (5.8)$$

The confidence limits on the mean of the crack lengths versus loading cycle was calculated in the manner described above for all primary cracks, at each cycle count where measurements were taken. A plot of the primary crack data with the calculated confidence bounds is presented below in figure 5.5.

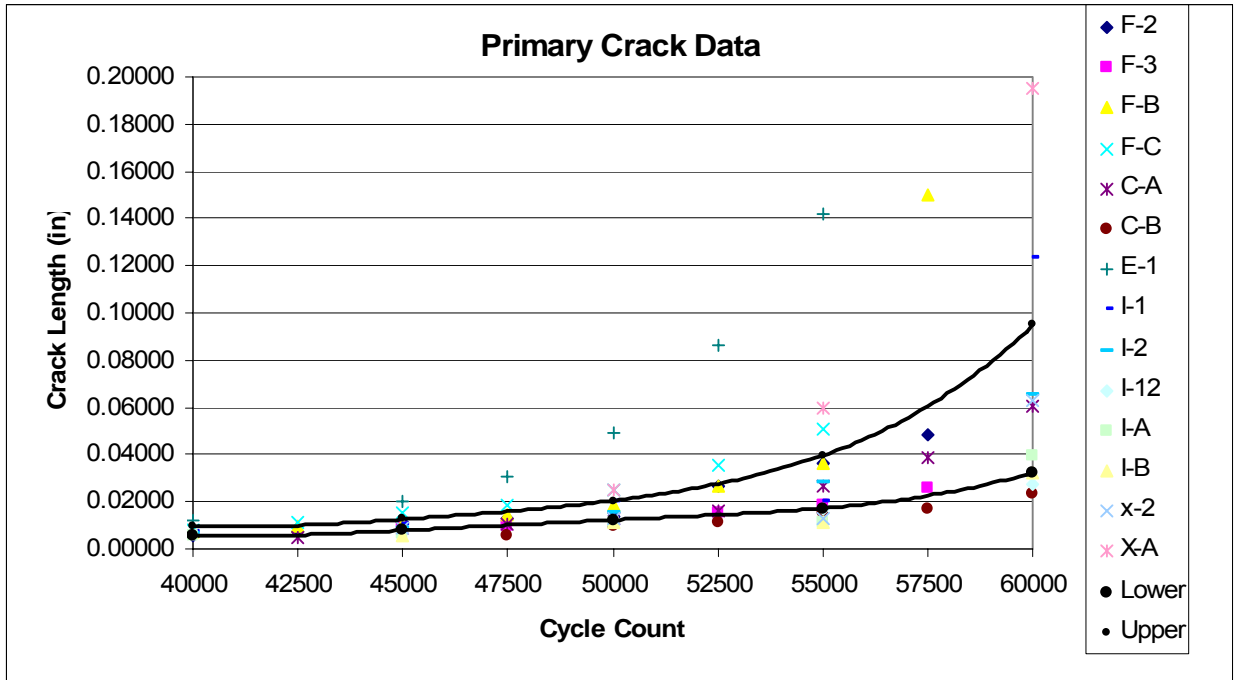


Figure 5.5: Primary crack data with confidence limits drawn on the mean

In this figure, the plotted points are the crack length data for the 14 primary cracks measured. The solid lines are fit through the calculated confidence limits on the mean at each cycle count where data was taken. It is first noted that a small number of cracks grow to very large lengths quickly and cause the positive skew seen in the large upper bound. All cracks in this small subgroup grew to these lengths through crack coalescence. This highlights the importance of dealing with clusters of cracks where coalescence is a possibility, rather than at single cracks where it cannot occur.

It should also be noted that the inclusion of secondary cracks will significantly and non-conservatively distort the calculated confidence limits. This would lead to unsafe predictions of fatigue life if these data were used due to the fact that the 53 measured secondary cracks are generally smaller than the primary cracks at any given cycle count. To illustrate how these cracks will alter the calculated confidence bounds, new confidence bounds were constructed which included them as additional data. For the purpose of this plot it was assumed that all of the data, both primary and secondary cracks could be described by a single lognormal distribution. While this assumption is not strictly valid it is a reasonable approximation for the current purposes of illustrating the effect of the additional data. This updated plot is presented below in figure 5.6. This figure also shows the same primary crack data shown in figure 5.5, but for the sake of clarity the large number of secondary cracks have not been plotted.

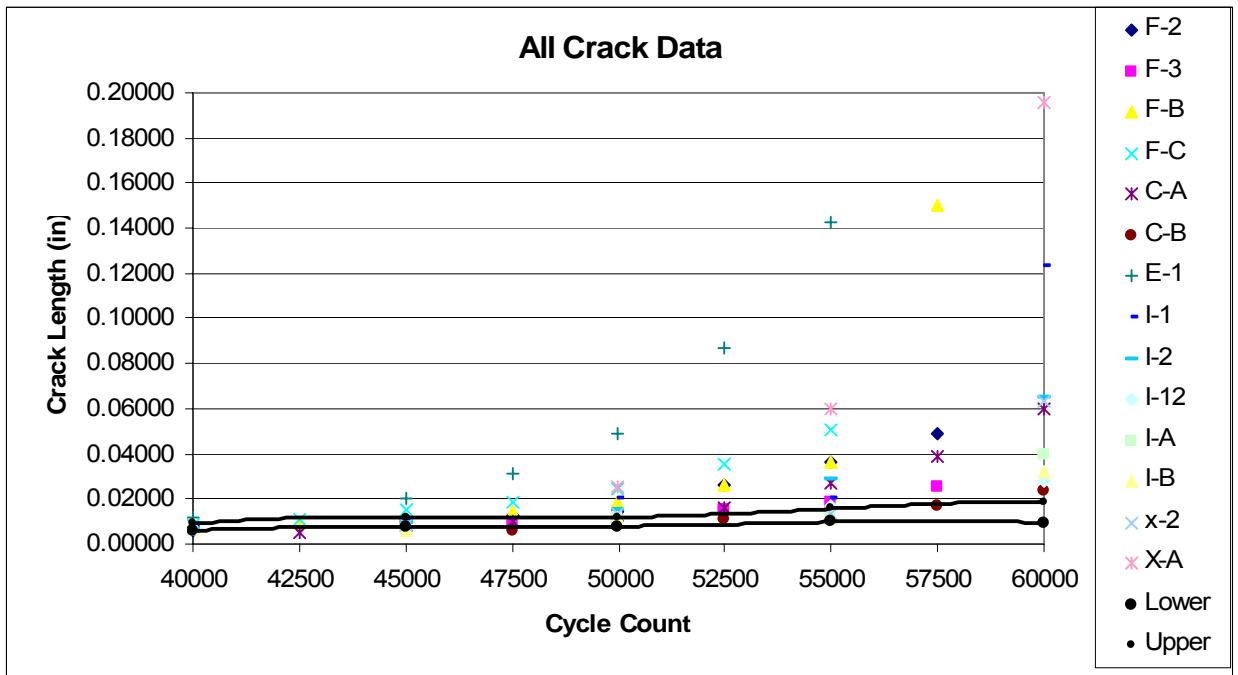


Figure 5.6: Primary crack data with confidence limits drawn on the mean behavior of both the primary and secondary cracks

It is clear that from the inclusion of the secondary crack data the confidence limits have dropped significantly. These limits no longer adequately describe the cracks which are growing on the specimen surface and will thus offer an unrealistic prediction of fatigue life.

#### **5.4 Life Prediction**

The statistical analysis detailed above is useful not only to study the behavior of small cracks but also in that it can be applied to the durability analysis of aerospace structures. It is the goal of such analyses to predict the failure of components subject to cyclic loading. This is often performed as a twofold procedure. First an initiation life is calculated using methods such as the Strain Life formulation. Initiation is assumed to occur when a crack of some critical size has appeared. The remainder of the fatigue life is then found by propagating this crack until a second critical crack size for unstable fracture is reached.

As has been discussed, the growth of small cracks can be difficult to predict. Not only does the similitude of fracture mechanics parameters break down at these length scales but the crack data is also subject to large levels of scatter. The ability to account for this region of crack growth in the initiation life rather than having to construct a growth prediction for them would therefore be beneficial. For this reason it is suggested that one possibility for an initiation crack size would be the transition length from micro-structurally small to long crack behavior. The initiation and small crack growth regimes will then be analyzed together. Due to the scatter found in the growth of small cracks it will be necessary that this analysis be non-deterministic in nature. These concepts will be

illustrated below in a simplified analysis of the fatigue life of the specimens used in the current tests.

The first step in the process will be to obtain 95 percent confidence bounds on the small crack growth regime. This analysis was performed above in section 5.3 and the results were presented in figure 5.5. These limit curves will be truncated at the cycle count where the primary cracks reach the transition length and can thereafter be considered to grow as long cracks. In this case for the current tests this occurs at approximately 45,932 cycles for the upper bound and 51,844 cycles for the lower.

At this point a deterministic long crack analysis will begin starting from the transition crack size. These long crack analyses will be continued through failure, ultimately providing predicted confidence limits on the number of cycles until failure by fracture.

For purposes of the illustration of this technique a simplistic long crack analysis will be developed. Cracks will be assumed to grow with a semi-circular geometry as has previously been discussed. Additionally the cracks will be assumed to grow in the center of a plate of finite thickness and width as shown below in figure 5.7.

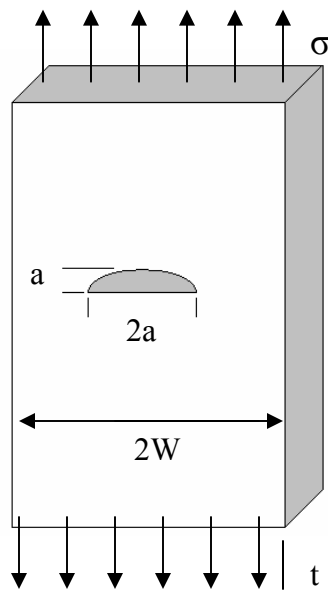


Figure 5.7: Assumed crack geometry

These assumptions are reasonable as for several reasons. First, the notch radius of the specimen is sufficiently mild to allow approximating it as a flat surface. Secondly, even micro-structurally long cracks are frequently small when compared to the specimen width. This allows an average crack to be modeled as growing in the center of the plate. Thirdly, by the time most primary cracks grow to long crack status they have outgrown much of the cluster where they have initiated and are thus growing in a more homogeneous medium. In order to achieve a truly accurate model of long crack growth a significantly more complex analysis would have to be developed rather than the admittedly simplistic one used here. This analysis however is only being suggested to illustrate the general methodology of treating the small and long crack regimes separately.

Given the assumptions discussed above, the SIF for the tips of the growing thumbnail cracks was given above in equation 4.9. The common assumption of Paris law growth in the long crack regime will be used here. Values for the Paris constants  $C$  and  $m$  for 7075-T7351 aluminum alloy were obtained from the literature [58] to be  $1.71 \times 10^{-9} \text{ in}(\text{in}^{3/2}/\text{kip})^m$  and 3.54 respectively. Numerically integrating the Paris law from the initial crack sizes is a simple matter.

The crack growth curves obtained from this analysis are then combined with the confidence limit curves from the small crack analysis. The results of the procedure are shown as solid lines below in figure 5.8. The primary crack data was also included on this plot. The small crack regime is shown in red while the long crack regime is black.

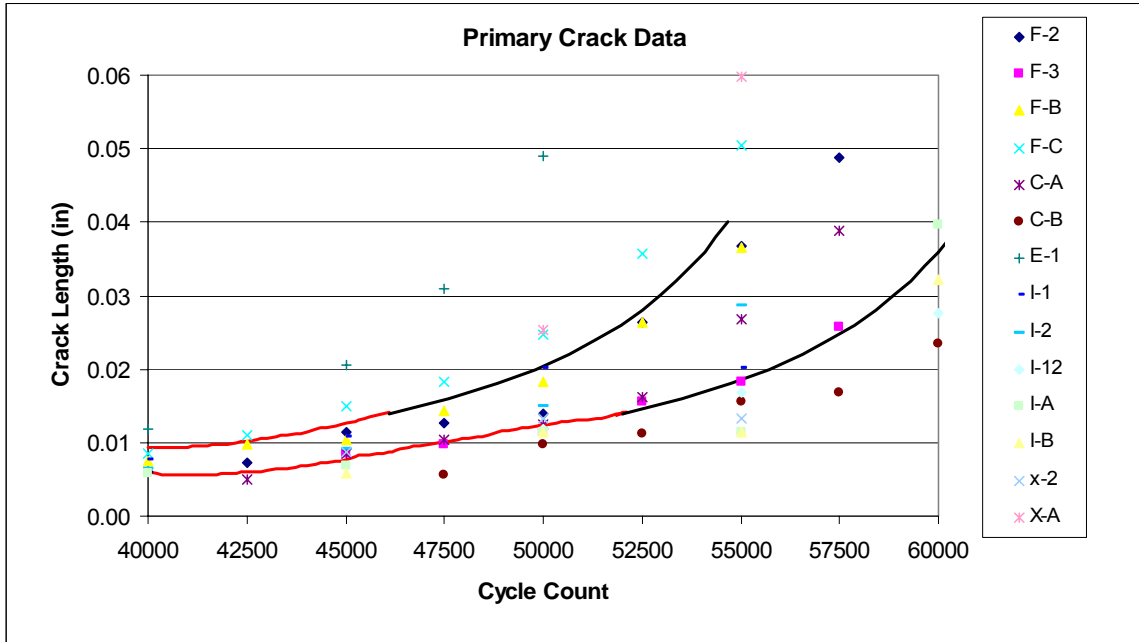


Figure 5.8: Results of the life prediction analysis

A final unstable failure criterion, such as  $K_{IC}$ , was not modeled in the current analysis. This would have led to significant complexities as the crack geometry was found to change near failure as cracks impinge on the extremities of the specimen gage section.

It can be noted that several cracks lie outside the upper and lower limits. However, it must be understood that the confidence limit analysis used to determine bounds for the small crack growth regime was conducted about the mean behavior. To create curves which instead bound 95 percent of the data the statistical analysis would have to be modified slightly.

### **5.5 Crack Acceleration Analysis**

The method developed for separating the primary and secondary crack distributions that was used above is simple and easy to apply. It does however suffer from several inadequacies. First it requires material- and orientation-specific information in the micro-

structural grain size. Additionally, since the method requires knowledge of significant length of the crack growth history it cannot separate the distributions completely until near or at the specimen failure point. Finally, this method separates the distributions based upon a measure of crack growth, not directly on the crack growth behavior itself. It would instead be beneficial to separate the distributions by direct observations of what is physically occurring on the specimen surface.

A numerical method which addresses these concerns has been developed. This method relies directly upon the observed behavior of secondary cracks. As these cracks grow larger they begin to arrest. In other words, their growth rates tend towards zero. Conversely, primary cracks generally accelerate with growth. This suggests that the two distributions can be differentiated by observing the values of the second derivative of the crack length versus cycle count data.

The first derivative of the crack length versus cycle count data represents the crack growth rate. These values were found to often be similar for primary and secondary cracks of a given length. However, the second derivative, which represents the crack acceleration, will be different for such cracks.

This principle was tested on the current cluster crack data. Discrete crack growth rates for all cracks were calculated using the secant method as described above in chapter IV. Starting from the crack growth rates the crack accelerations were then found utilizing the same method. Cracks which had negative crack accelerations for extended periods of cycling were put into the secondary crack distribution. This is stated mathematically below.

$$\frac{d^2 a}{dN^2} \leq 0 \quad \text{Secondary Cracks} \tag{5.9}$$

$$\frac{d^2 a}{dN^2} > 0 \quad \text{Primary Cracks}$$

Short periods of negative crack acceleration were allowed for primary cracks. These regions occur when the crack is still small and thus subject to acceleration/deceleration transients.

To illustrate this procedure, the crack accelerations of all of the cracks on single specimen, specimen F in this case, are presented below in figure 5.9.

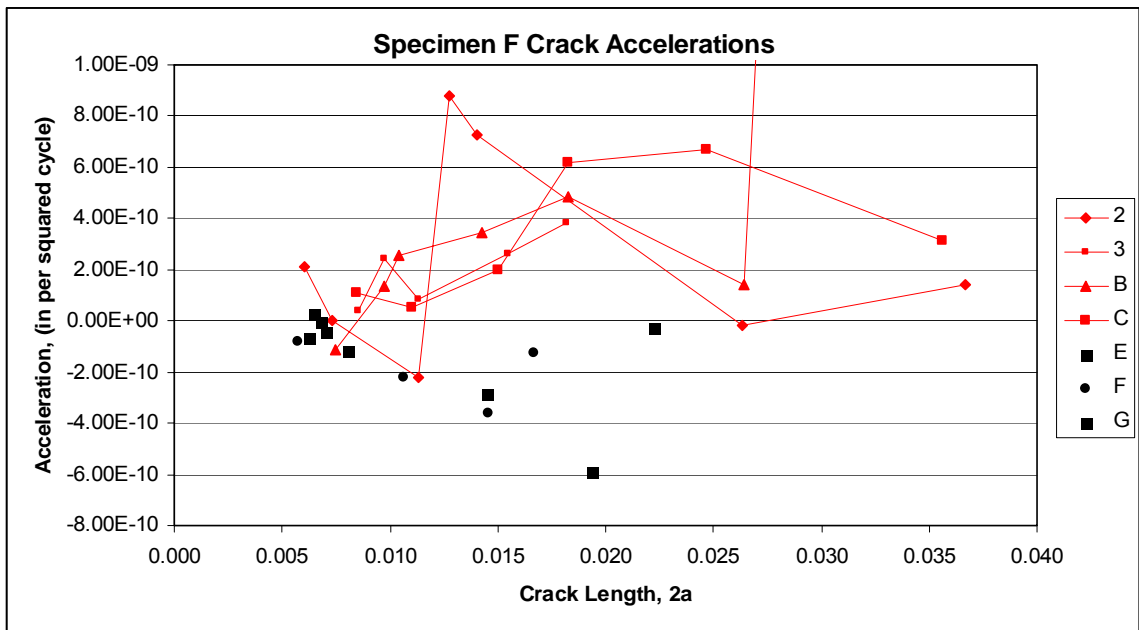


Figure 5.9: Crack accelerations for all cracks on specimen F

Cracks with less than two data points were not included on this plot. For these cracks it was not possible to numerically evaluate crack accelerations. However, cracks such as these are all found late in the fatigue life of the specimen and due to their delayed

initiation are still small at failure. For this reason they can simply be placed in the secondary crack distribution.

In figure 5.9 the two crack distributions are shown separated. Primary cracks are shown connected while secondary cracks are not. This separation of distributions was completed apart from any other data including any other crack data as well as material parameters such as the grain size and even the loading conditions under which the tests were conducted. However, even without any additional information the crack acceleration analysis separates the primary and secondary cracks in a matter that is identical to the previously described analysis which relies on material parameters and additional testing. Additionally, the acceleration method accomplished this utilizing only the intrinsic crack behavior rather than artificially defined parameters. Similar results were found for the remainder of measured cracks.

## Chapter VI - Continuing Research

The current work has addressed the relatively simple case of constant amplitude sinusoidal loading on a carefully prepared specimen. Material used in aerospace applications will not benefit from such simple conditions. For this reason the effects of more realistic load spectra and surface finishes should be investigated. Additionally, the aluminum alloy chosen for the current tests contained a simple single-phase microstructure. The applicability of the obtained results should also be investigated on other materials, such as those containing more complex dual-phase microstructures. For this reason work is currently underway on a titanium alloy, Ti-6Al-4V. Finally, as the density of crack clusters will control the relative importance of cluster effects such as crack coalescence, the effect of notch size on crack density also warrants further investigation.

### **6.1 Operational Condition Issues**

In the experiments presented in this work, constant amplitude sinusoidal loading at a single R-ratio was applied to all specimens. During service however, components will be subjected to variable amplitude loading which will significantly complicate the analysis. The effects of random amplitude loading or of the many industry developed spectra on the observed behavior of small fatigue cracks would be a fruitful topic for further research.

The situation can be simplified by instead investigating the effects of overloads and underloads on the growth of small cracks in fatigue. For long cracks the acceleration and deceleration of growth after such load excursions is believed to be a function of the size of the plastic zone [50, 59]. The behavior of small cracks under such loading can then be

expected to differ from the behavior observed in long cracks because, as has been previously discussed, the plastic zones developed by small cracks may be contained within a small number of grains. For this reason, cracks of similar size will not have similar plastic zones. It can then be expected that significant scatter will be found in the reactions of small crack growth to such loading.

In addition, the effects of the R-ratio on the growth of small cracks could be investigated with additional constant amplitude tests. It has been suggested that when loaded to high R-ratios, small cracks can exhibit behavior similar to that of long cracks [28]. However at small R-ratios the situation can be quite different. A systematic study of these effects is needed.

Changes in load level itself are also expected to affect both the transition behavior of small cracks as well as the separation of the primary and secondary crack distributions. At higher loads the average crack driving force will be larger and therefore able to overcome a greater proportion of micro-structural barriers such as grain boundaries. This increases the proportion of the total population of cracks that will overcome the micro-structurally dominated small crack regime and thus become primary cracks. Higher driving forces which overcome micro-structural barriers easier may also shrink the small to long crack transition length as cracks under higher loads will transition away from crystallographic growth sooner [60].

In addition to loading, the effect of material orientation on the growth and transition behavior of small cracks can be studied. As discussed previously the microstructure of the plate form of material used in the current experiments differs greatly depending on orientation of crack growth. It can then be expected that crack growth and transition

behavior will differ depending on orientation as well [60]. Through systematic testing of multiple material orientations the applicability of the methods developed here can be evaluated. Additionally, other forms of the material such as extruded rods, forgings or castings can be investigated.

For all of the experiments performed in the current body of work specimens were diligently polished to a one micron finish glass-like finish. This level of surface preparation limits the number and type of crack initiation sites leading to an overall increase in fatigue life. Obviously however, aerospace components cannot be prepared to such high standards as the costs to do so would be prohibitive. In order to quantify the effects of realistic surface preparations tests can be run with more representative surface preparations. This testing would not have to be limited simply to increased surface roughness. The effects of residual stress producing procedures such as traditional and laser shot-peening can be investigated.

## **6.2 Dual Phase Alloys**

The definition of the transition crack length defined above has been shown to be accurate when applied to several aluminum alloys. However, for any definition of transition length to be truly useful with wide applicability, it must be accurate for multiple material systems. This would include simple single-phase alloys such as aluminum as well as more complex dual-phase ones.

Work is currently underway on a beta-annealed Ti-6Al-4V titanium alloy. This alloy is widely used for aerospace applications. However in this material, significant scatter is observed in the growth of both small and long cracks. This behavior may be a function of the complex microstructure found in this alloy.

The aluminum alloy studied in the current work contained only a single phase, a face centered cubic (FCC) crystal structure and will thus have primarily only a single microstructural parameter, the grain size. However, beta-annealed Ti-6Al-4V is a dual phase metal containing both a hexagonal close packed (HCP) alpha phase and a body centered cubic (BCC) beta phase. These phases combine in a complex Widmäsatten/Colony type microstructure containing several key parameters. These include the prior beta-grain size, the alpha colony size within prior beta grains and the width of the individual alpha and beta lamellae. The relative sizes of these micro-structural features, some of which can often be fairly large, are primarily controlled by adjusting the rate at which the material is cooled during heat treatment. An example of how the microstructure can be altered by cooling rate is shown below in figure 6.1 [61]. In these micrographs the white material is the HCP alpha phase while the black represents the BCC beta phase. As one moves towards the right with increasing cooling rate the microstructure can be seen to become finer. However, the size of the large grains which contain colonies of alpha and beta lamellae, which are the prior beta grains are not affected to the same extent.

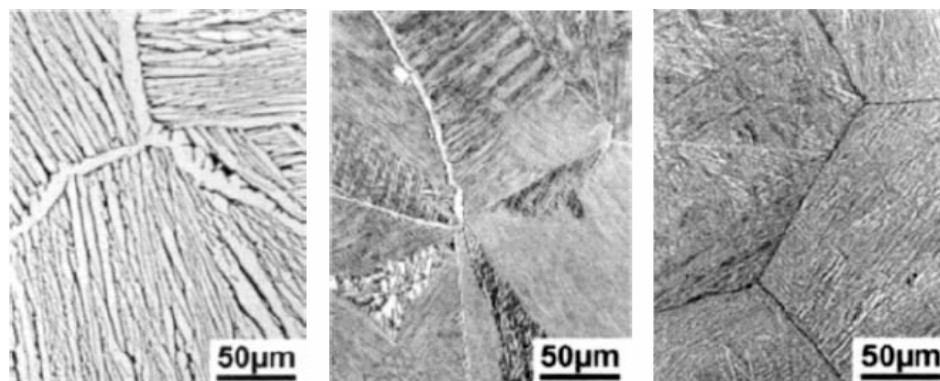


Figure 6.1: Effects of cooling rate on the microstructure of Ti-6Al-4V

The intrinsic complexity and length scales of this microstructure can be expected to affect the level of microstructure a small crack front must sample before the effects of individual micro-structural features will begin to average out. This will thus affect the transition length between small and long crack behavior. Additionally, as the beta grains can often be fairly large this may be able to explain the scatter observed in the growth of physically long cracks as they may in fact actually be micro-structurally small.

### **6.3 Cluster Density**

In the current experimental work cracks grew in clusters as a result of natural crack initiation from smooth surfaces. However, the locations of these clusters was somewhat localized by the specimen geometry. While the radius of the notch was fairly large cracks were found in a region near the center of the notch. This localization led to crack clusters with certain crack densities.

It can be expected that the crack cluster density will be a function of, among other variables such as load level, the notch radius. For instance, for the limiting case of a sharp notch only a single crack will grow. However as that radius grows it would be reasonable to assume that at first clusters of high density would appear. As the radius continues to grow towards becoming a flat surface the clusters will spread apart, possibly approaching a characteristic cluster density for a given material/loading system.

Since it can be expected that the importance of cluster related effects such as crack shielding and coalescence will be of higher importance for cracks which are packed closer together, the behavior of crack cluster density with varying notch radius is an important area of study.

## Chapter VII – Conclusions

- Cracks initiated from smooth surfaces in 7075-T7351 aluminum alloy were observed to grow in randomly oriented clusters. While a portion of the cracks were observed to grow with complex morphologies the majority of cracks were observed to grow with semi-circular crack fronts.
- Within the crack clusters several crack interactions were observed to take place. These included crack shielding and anti-shielding as well as crack coalescence. These effects led to additional scatter in the crack data, especially in the small crack regime.
- It was found that the scatter in crack growth rate data decreases until approximately 15 grains are intersected by the growing crack front. From this point forward scatter was found to assume a constant long crack value. Therefore the point at which the growing crack front intersects 15 grains has been defined as a micro-structurally based transition point between small and long crack behavior. This point has been shown to apply for several aluminum alloys and crack geometries.
- Discrete crack growth rates for the cluster crack data were computed. These data showed a chaotic behavior containing growth acceleration/arrest transients in the small crack regime. After cracks reach the small to long crack transition length the behavior was significantly more predictable.
- It has been shown that the total population of cracks in crack clusters is a compilation of two separate distributions. The first of these distributions is that of the *primary* cracks. These cracks can grow to ultimately cause component failure. The second distribution consists of *secondary* cracks. These cracks will ultimately arrest; however, their importance lies not in their growth but in the fact that they create a unique

environment through which primary cracks must grow. This includes the possibility of their coalescence with primary cracks.

- Two separation methods were developed to separate the primary and secondary crack distributions, both achieving similar results. The first method utilizes the definition of transition length. The second method can be used without any additional data, material or loading information. This method relies on the numerically calculated crack acceleration. Cracks with primarily negative acceleration are placed into the secondary crack distribution while cracks with primarily positive acceleration are designated as primary cracks.
- It was shown that the secondary cracks must be removed from the data prior to any fatigue crack growth analysis to achieve meaningful conservative results. This was shown by developing confidence limits on the mean crack growth behavior.
- It was shown that a fatigue life analysis could be constructed by separating the life into two regimes, small and long crack growth. These regimes are separated at the microstructural transition point. The small crack growth regime is treated using the previously developed confidence bounds on the mean crack behavior. The long crack regime analysis utilizes traditional LEFM methods to append crack growth curves to the ends of the small crack confidence bounds.
- It has been suggested that the current work be extended to include the effects of various operational conditions. These include the effects of varying R-ratios, variable amplitude loading, material orientation effects and the effects of surface preparation. Additionally, since the current tests were performed on single phase alloys only it had been suggested

that the growth of small cracks in dual-phase alloys such as Ti-6Al-4V titanium be investigated as well.

## Appendix A – Micro-structural Characterization

### Micrographs

What follows are a series of micrographs showing the microstructure of the 7075-T7351 aluminum alloy studied in the current work. The photographed material was taken from the same plate used to manufacture all test specimens. Prior to photographing the microstructure in each of the three planes defined below in figure A.1, the sample surface was etched to reveal grain boundaries.

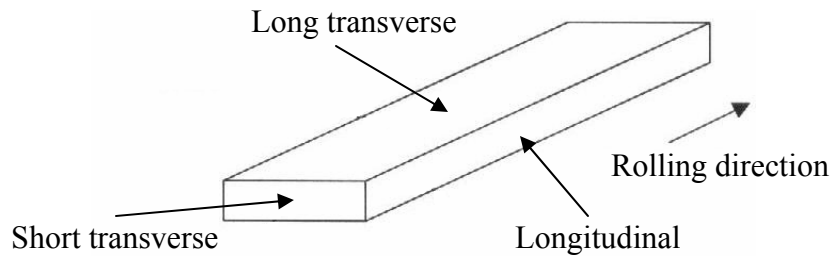


Figure A.1: Schematic defining the material planes

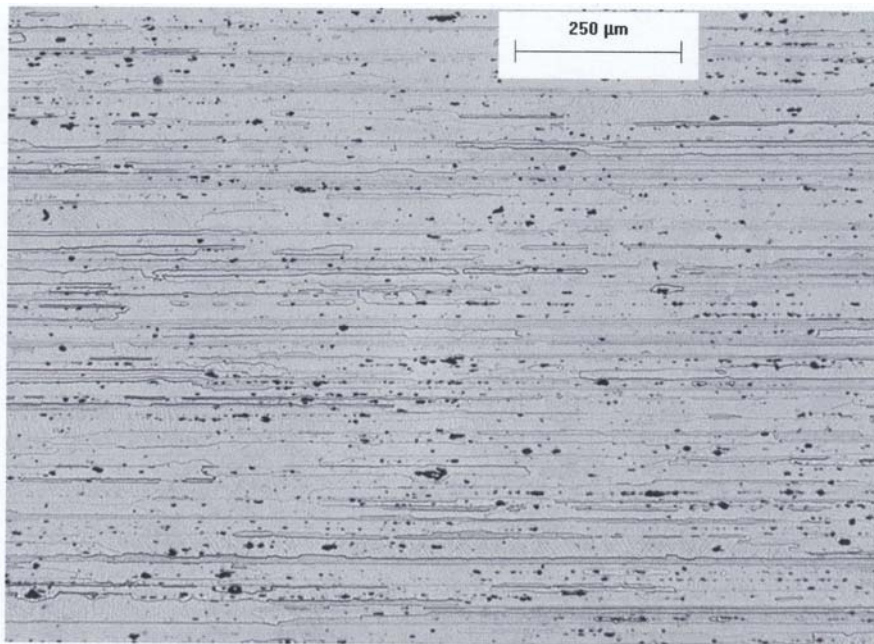


Figure A.2: Longitudinal section, 5x zoom

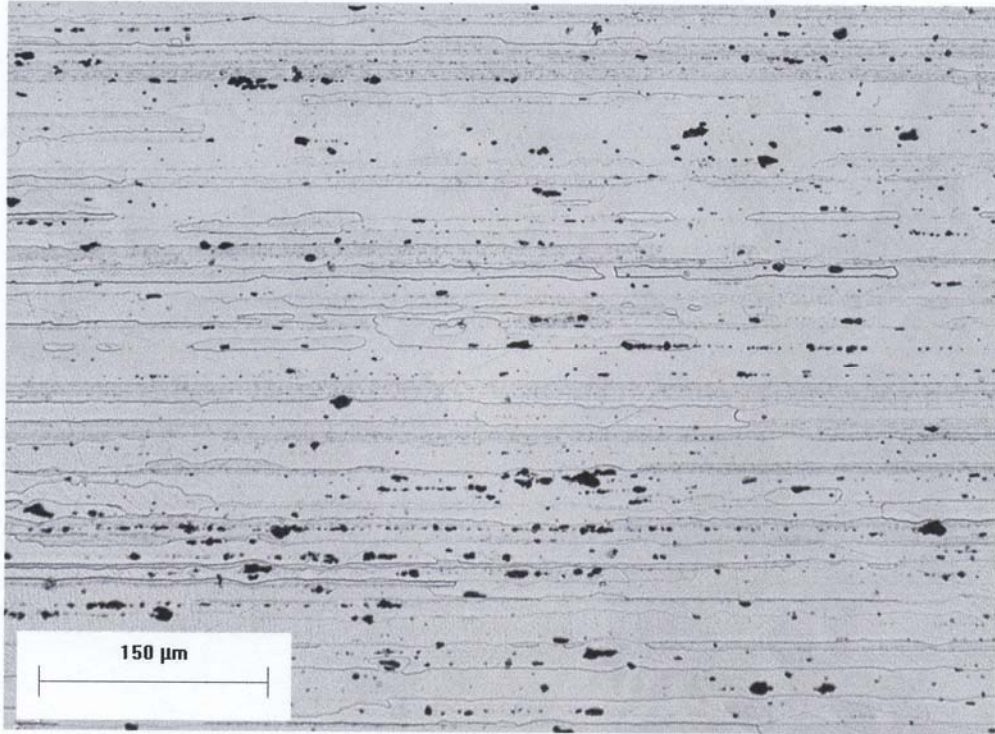


Figure A.3: Longitudinal section, 10x zoom

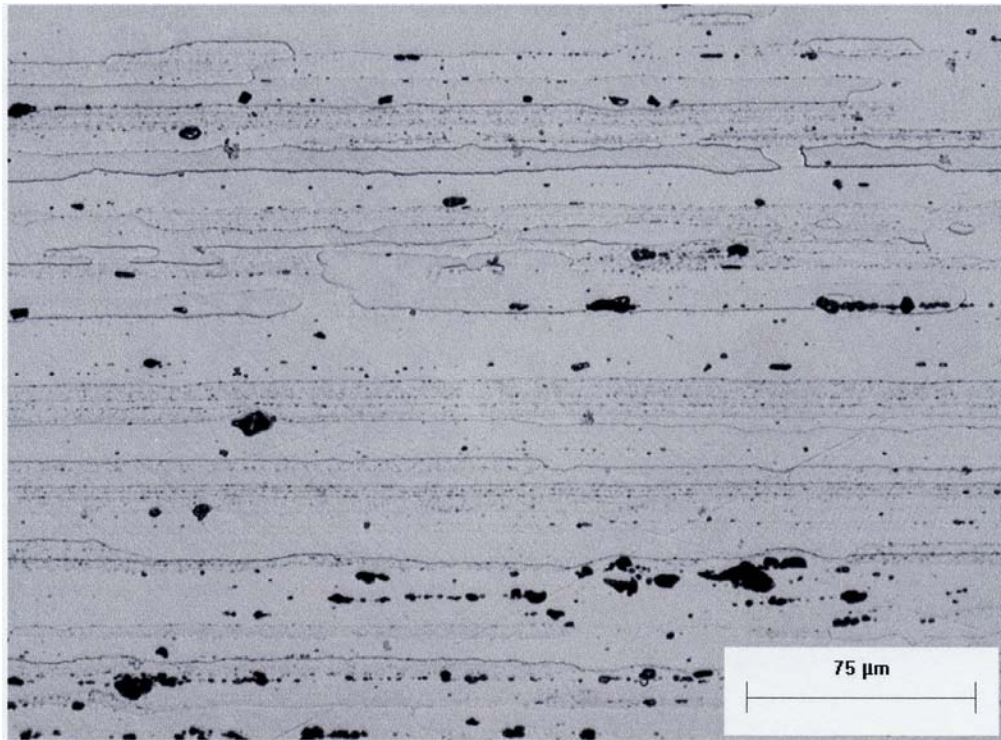


Figure A.4: Longitudinal section 20x zoom

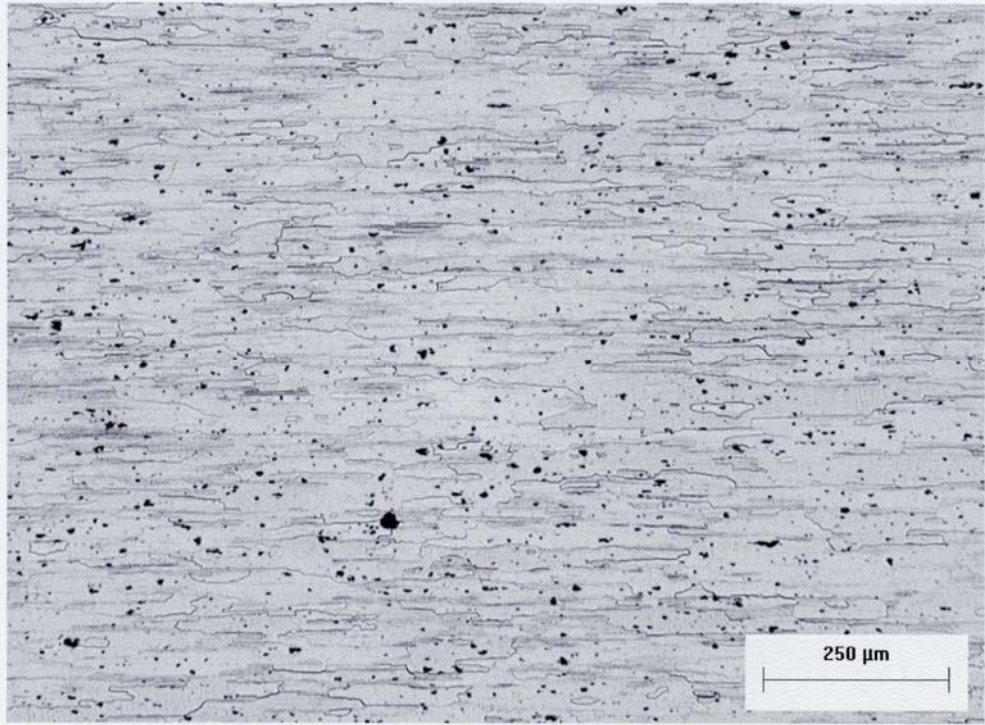


Figure A.5: Short Transverse section, 5x zoom

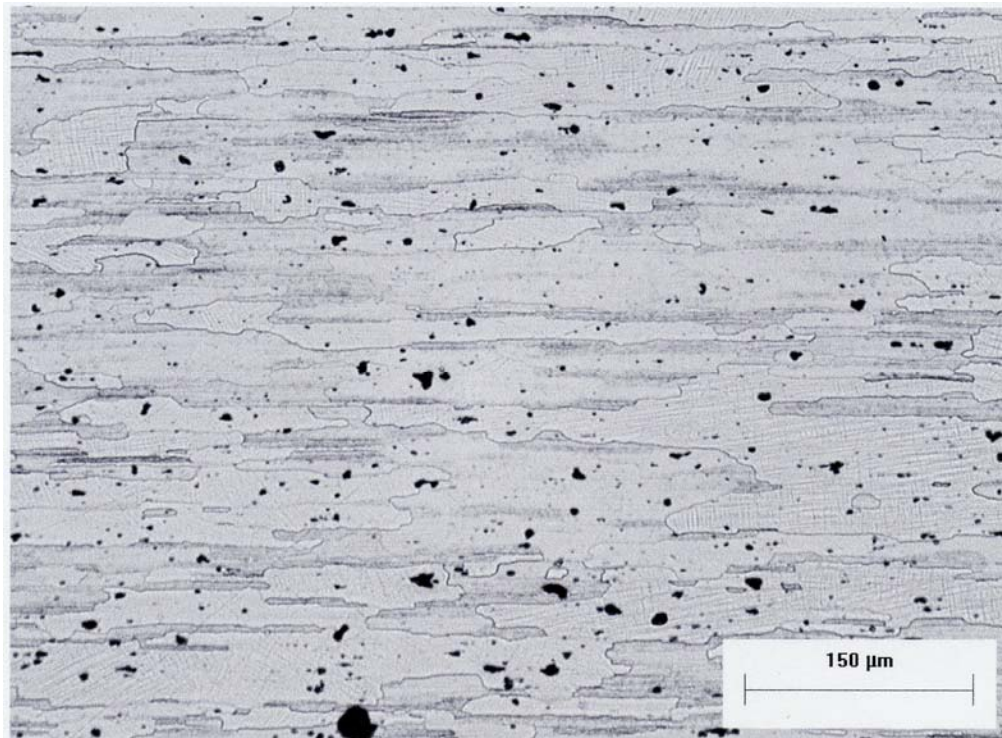


Figure A.6: Short Transverse section, 10x zoom

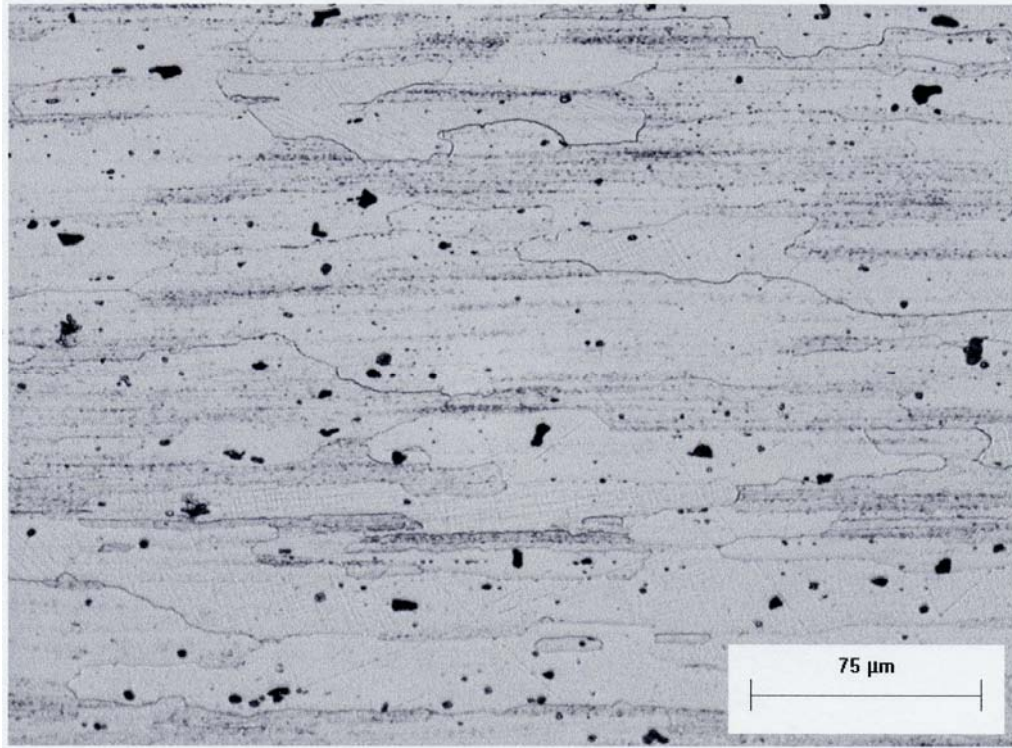


Figure A.7: Short Transverse section, 20x zoom

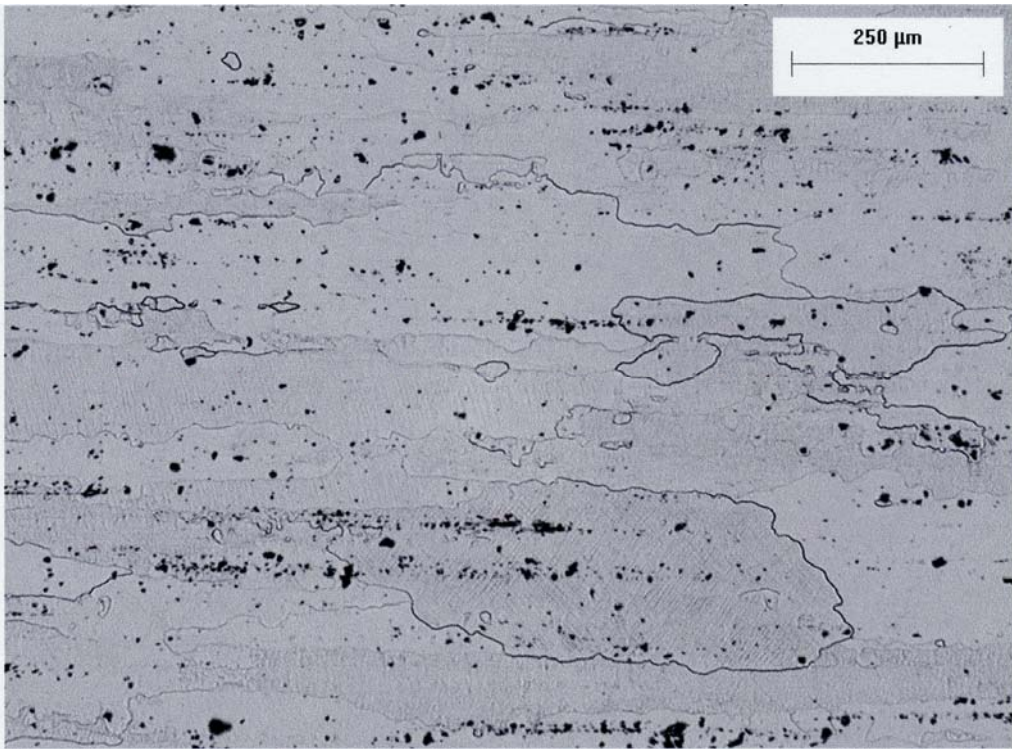


Figure A.8: Long Transverse section, 5x zoom

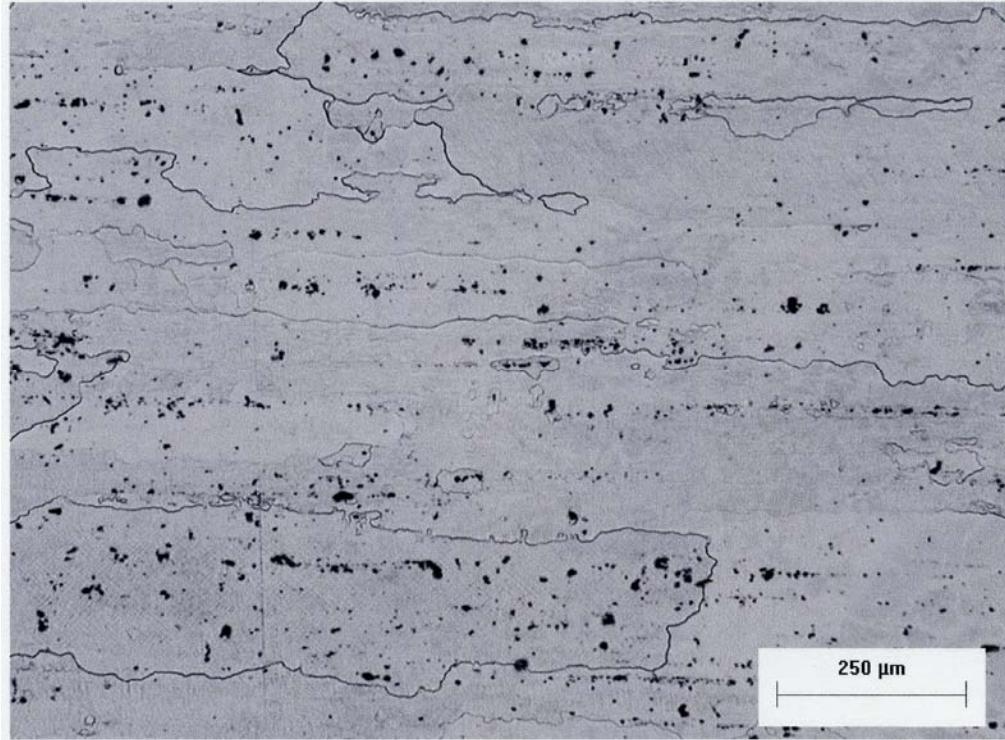


Figure A.9: Long Transverse section, 5x zoom

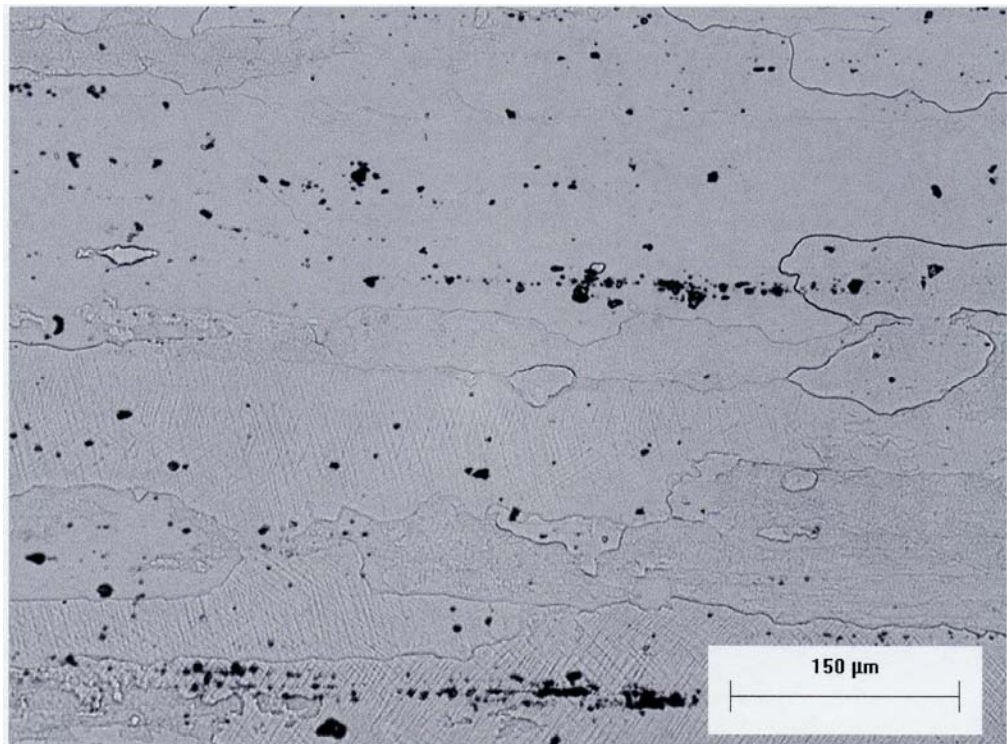


Figure A.10: Long Transverse section, 10x zoom

## Particle Size Distributions

What follows are a series of distribution plots describing the populations of inter-metallic particles found in the aluminum matrix. The particles were divided into two classes,  $Mg_2Si$  and Fe-Al. The data in these plots was determined from the micrographs shown above.

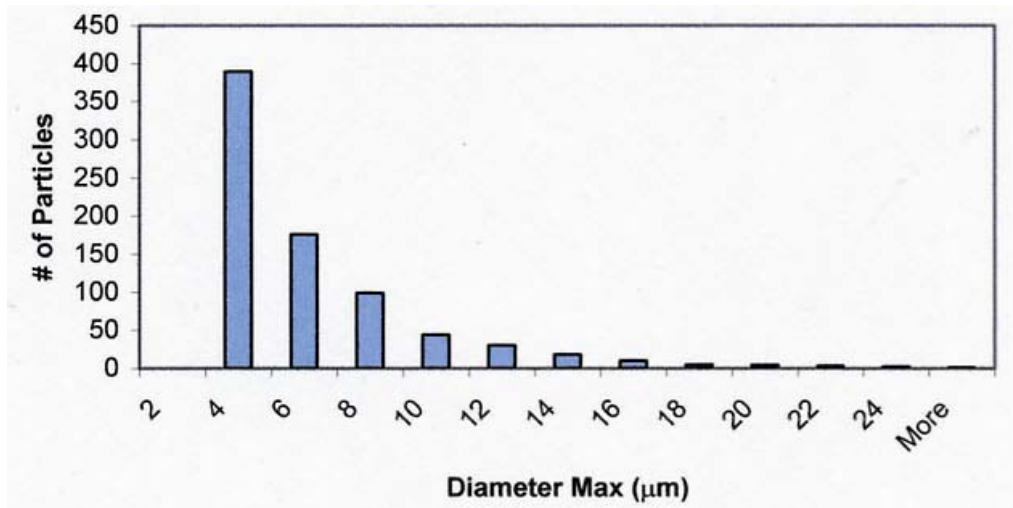


Figure A.11: Distribution of Fe-Al particles in the longitudinal section

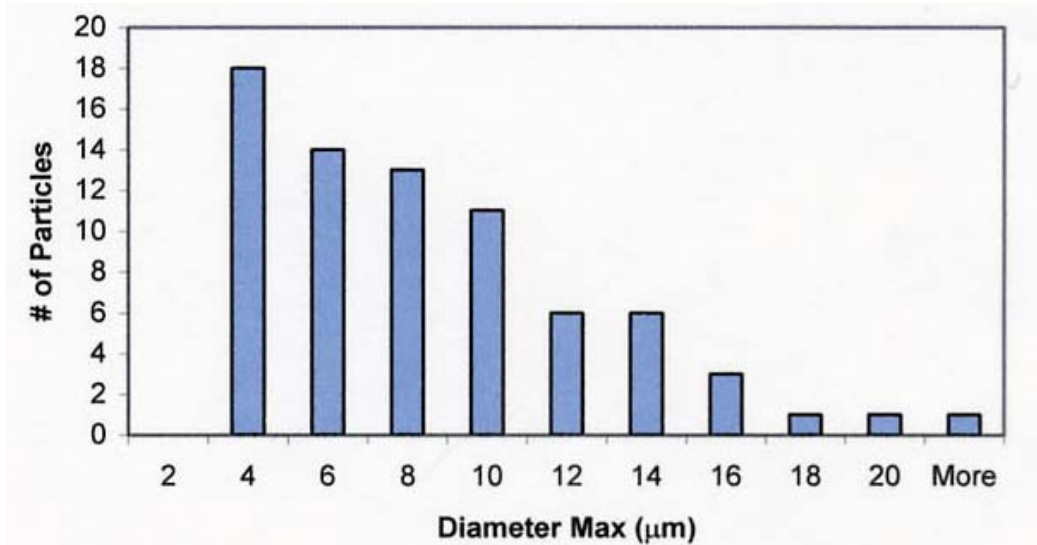


Figure A.12: Distribution of  $Mg_2Si$  particles in the longitudinal section

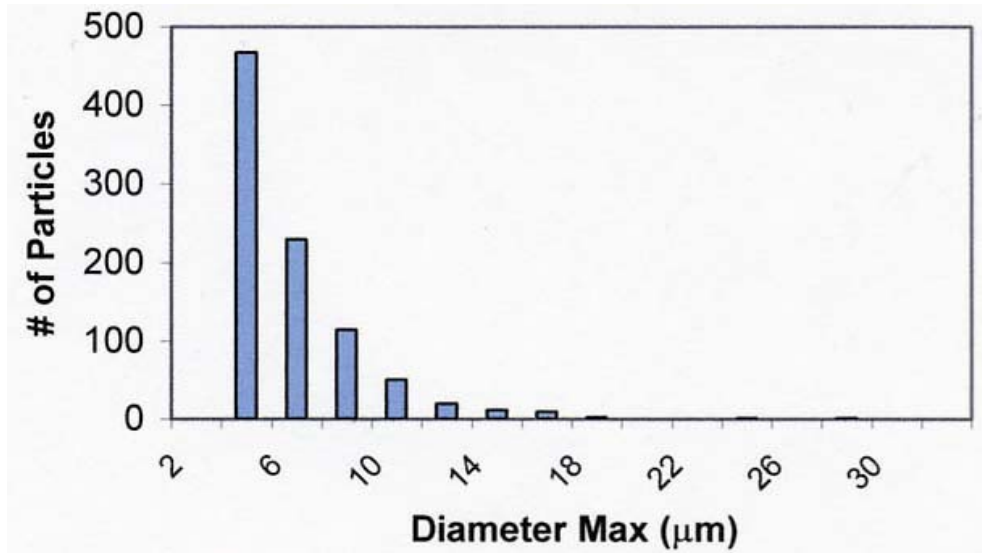


Figure A.13: Distribution of Fe-Al particles in the short transverse section

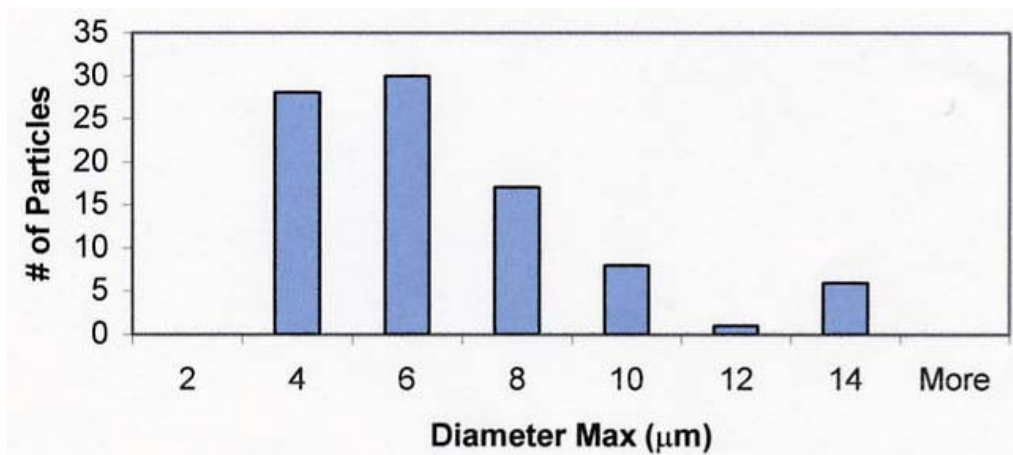


Figure A.14: Distribution of Mg<sub>2</sub>Si particles in the short transverse section

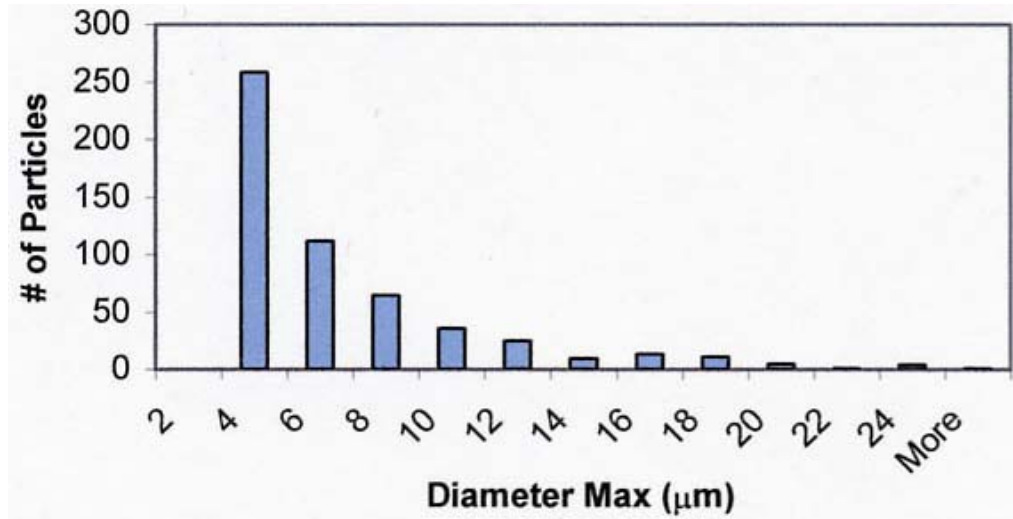


Figure A.15: Distribution of Fe-Al particles in the long transverse section

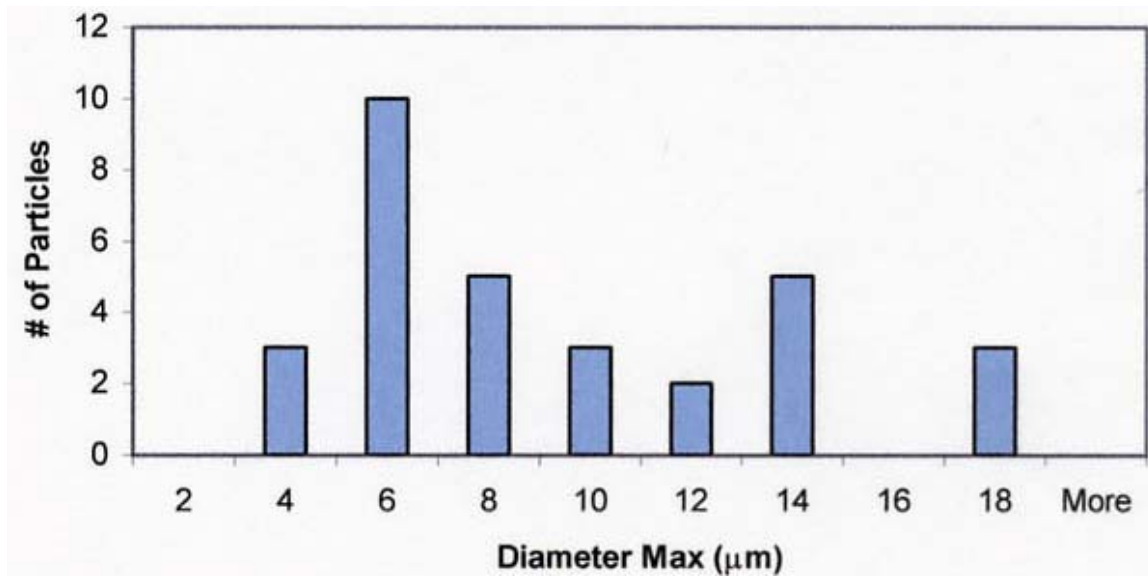


Figure A.16: Distribution of Mg<sub>2</sub>Si particles in the long transverse section

## Appendix B – Specimen Preparation

### Polishing Procedures

What follows are the exact procedures used to prepare the gage sections of all specimens tested in the current work. The portions of the gage section which would not be viewed for cracks were polished in only one direction along the specimen longitudinal axis. As portions of sandpaper were exhausted they were replaced and the specimen rinsed with water before polishing was restarted. All diamond pastes were applied with a low nap cloth and lubricated with olive oil.

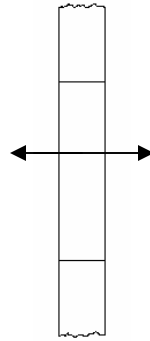


Figure B.1: Illustration of horizontal polishing

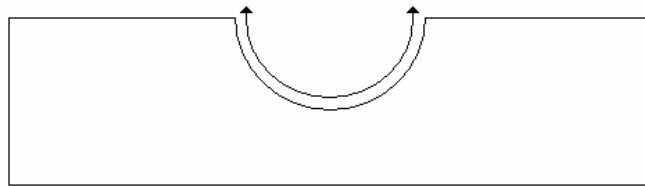


Figure B.2: Illustration of vertical polishing

1) Using 240 Grit SiC sandpaper roughen non-viewed surfaces. Using wooden dowel and 240 Grit SiC sandpaper, horizontally roughen the test surface as shown in figure B.1. Clean specimen with soap and water.

- 2) Using 320 Grit SiC sandpaper wet-sand non-viewed surfaces. Wet-sand the test surface vertically using 320 Grit SiC sandpaper as shown in figure B.2. Clean specimen with soap and water. View specimen surfaces under magnification. If horizontal marks remain from the 240 Grit paper then continue working vertically with 320 Grit paper.
- 3) Using 600 Grit SiC sandpaper wet-sand non-viewed surfaces. Wet-sand the test surface horizontally using wooden dowel and 600 Grit SiC sandpaper as shown in figure B.1. Clean specimen with soap and water. View specimen surfaces under magnification. If vertical marks remain from the 320 Grit paper then continue working horizontally with 600 Grit paper.
- 4) Using 15 micron diamond paste polish non-viewed surfaces. Using 15 micron diamond paste and drill press, polish the test surfaces vertically as shown in figure B.2. Clean specimen with soap and water. View specimen surfaces under magnification. If horizontal marks remain from the 600 Grit paper then continue working vertically with 15 micron paste.
- 5) Using 6 micron diamond paste polish non-viewed surfaces. Using 6 micron diamond paste and wooden dowel, polish the test surfaces horizontally as shown in figure B.1. Clean specimen with soap and water. View specimen surfaces under magnification. If vertical marks remain from the 15 micron paste then continue working horizontally with 6 micron paste.
- 6) Using 1 micron diamond paste polish non-viewed surfaces. Using 1 micron diamond paste and drill press, polish the test surfaces vertically as shown in figure B.2. Clean specimen with soap and water. View specimen surfaces under magnification. If

horizontal marks remain from the 6 micron paste then continue working vertically with 1 micron paste.

## Appendix C – Crack Cluster Topographical Measurements

### **Topographical Plots**

What follows are a series of plots similar to figure 3.5 which is described in chapter III. They represent the evolution of the topography of crack clusters. As in figure 3.5, secondary cracks are shown in blue and primary cracks in red.

*40,000 Cycles*  
*Cycles*

*45,000 Cycles*

*50,000 Cycles*

*55,000 Cycles*

*60,000*

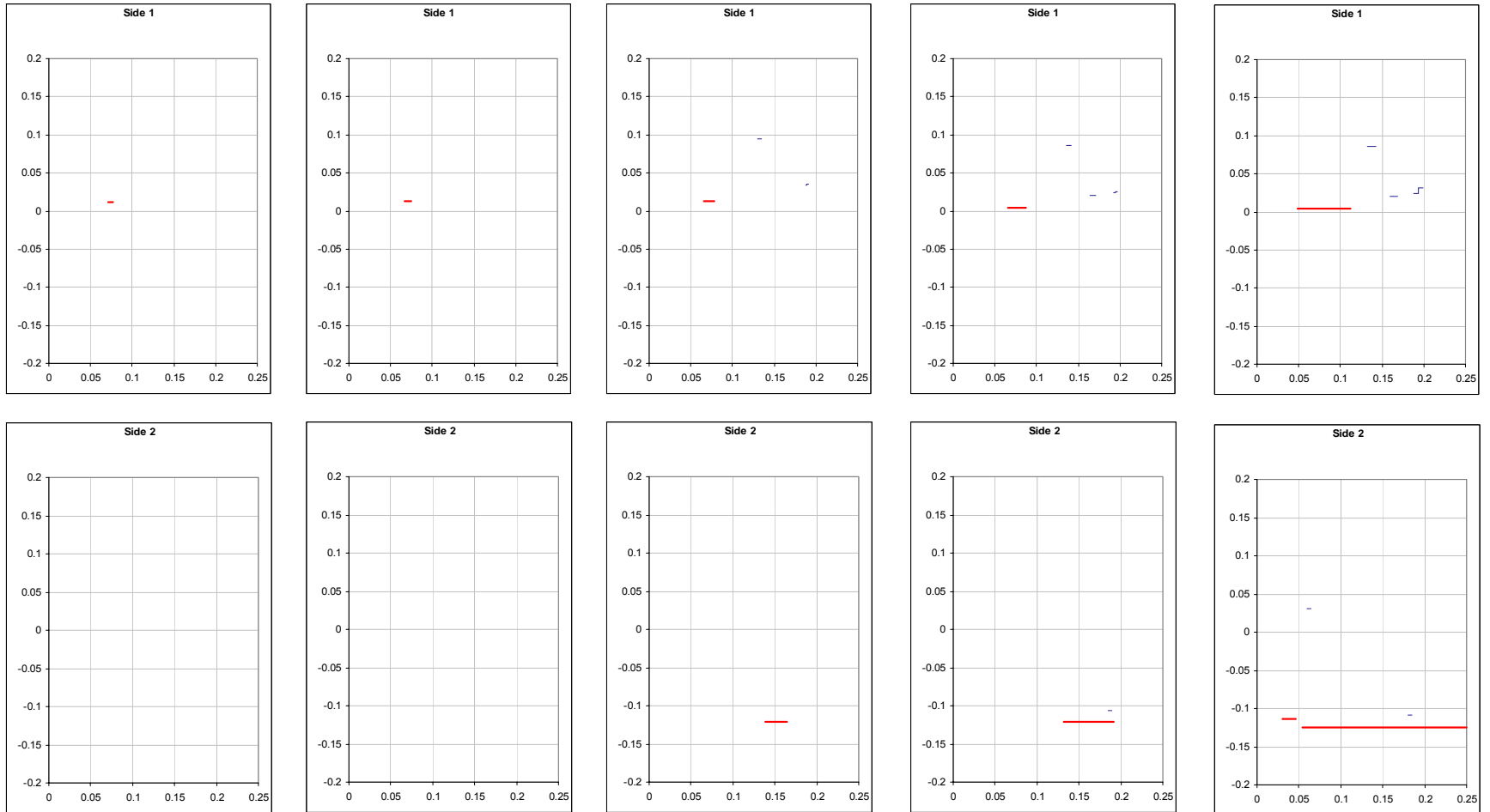


Figure C.1: Topography of the multi-site crack growth on specimen 6

*40,000 Cycles*  
*Cycles*

*45,000 Cycles*

*50,000 Cycles*

*55,000 Cycles*

*60,000*

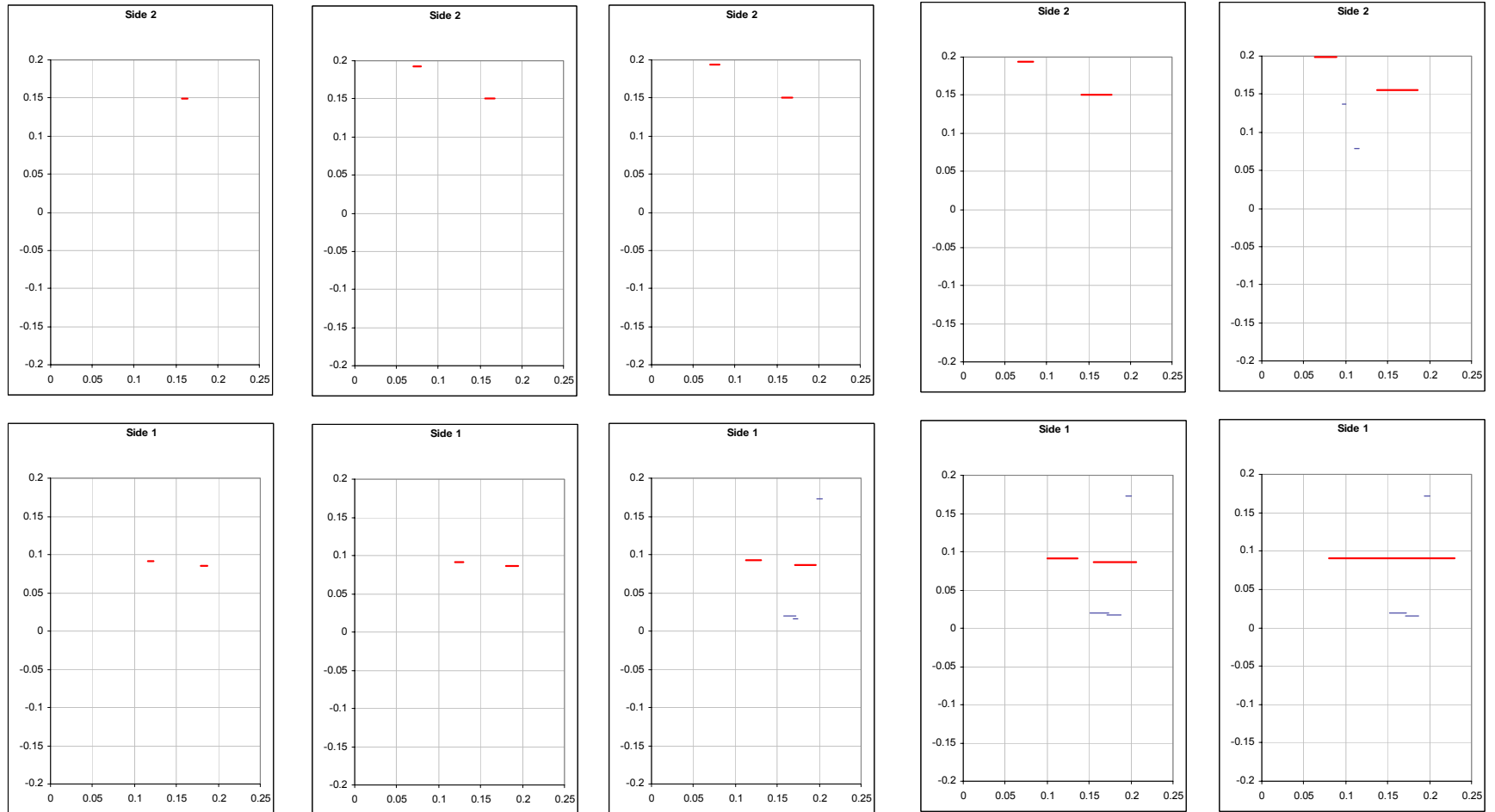


Figure C.2: Topography of the multi-site crack growth on specimen F

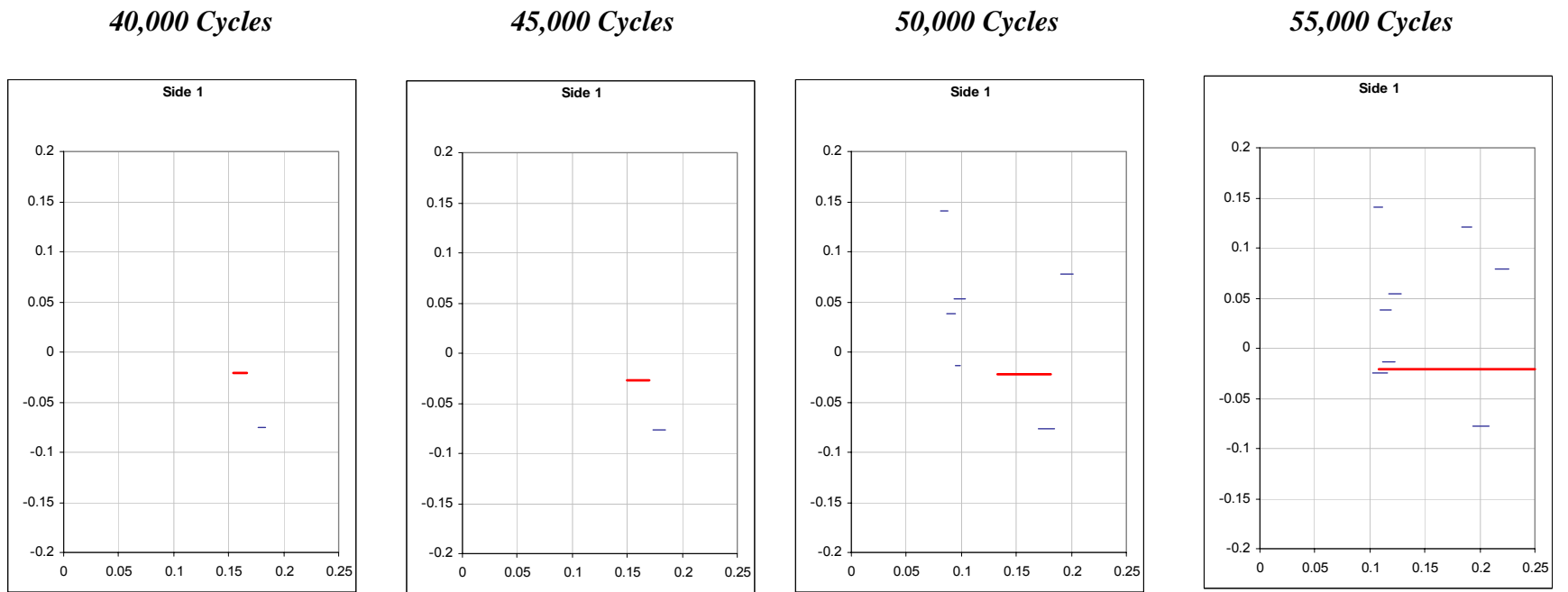


Figure C.3: Topography of the multi-site crack growth on specimen E

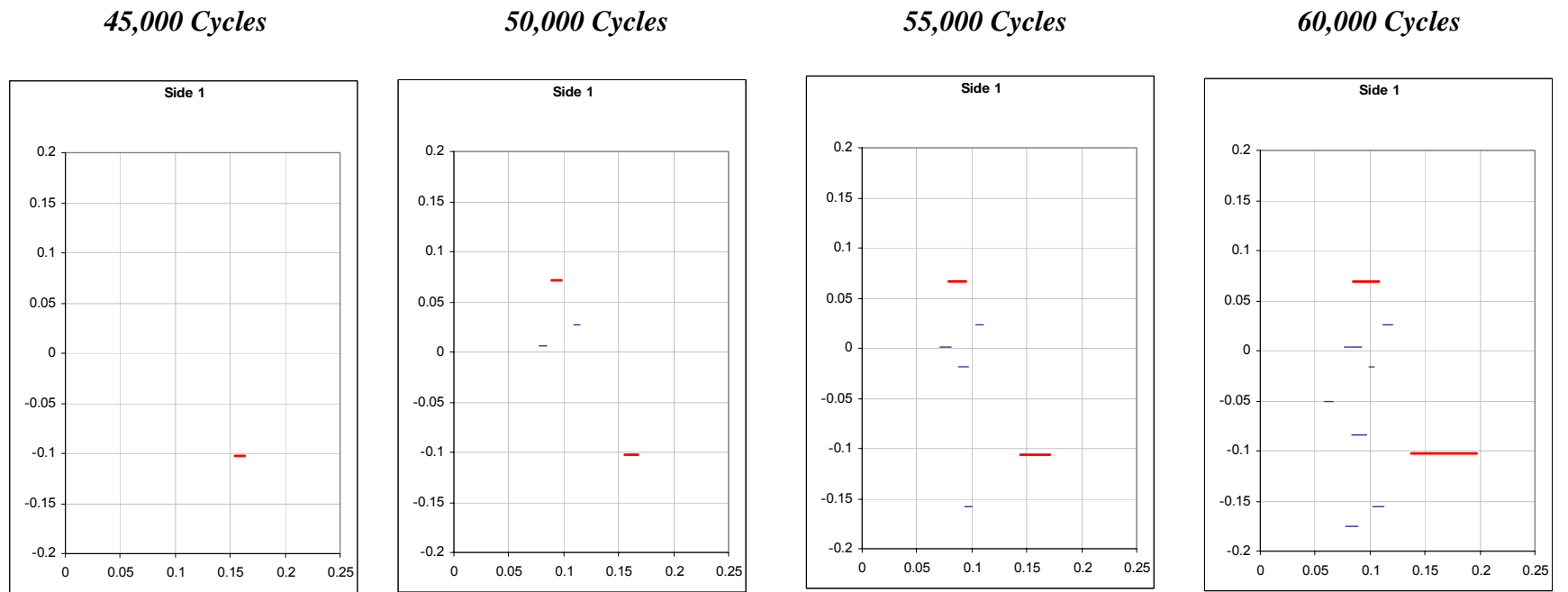


Figure C.4: Topography of the multi-site crack growth on specimen C

## References

- [1] Schijve, J, *Fatigue of Structures and Materials*, Kluwer Academic Publishers, Dordrecht, The Netherlands, 2001.
- [2] Carlson, R.L., Kardomateas, G.A., *An Introduction to Fatigue in Metals and Composites*, Chapman and Hall, 1996.
- [3] Pearson, S., “Initiation of Fatigue Cracks in Commercial Aluminum Alloys and the Subsequent Propagation of Very Short Cracks”, *Engineering Fracture Mechanics*, Vol. 7, 1975, p 235-247.
- [4] Suresh, S., *Fatigue of Materials*, Cambridge University Press, New York, 1998.
- [5] Lankford, J., “The Growth of Small Fatigue Cracks in 7075-T6 Aluminum”, *Fatigue of Engineering Materials and Structures*, 1982, Vol. 5, No 3, p 233-248.
- [6] Lankford, J., “Initiation and Early Growth of Fatigue Cracks in High Strength Steel”, *Engineering Fracture Mechanics*, Vol 9, 1977, p 617-624.
- [7] Tanaka, K., Hojo, M., Nakai, Y., “Fatigue Crack Initiation and Early Propagation in 3% Silicon Iron”, *Fatigue Mechanisms: Advances in Quantitative Measurements of Physical Damage*, ASTM STP 811, J. Lankford, D.L. Davidson, W.L. Morris, R.P. Wei, Eds., American Society for Testing and Materials, 1983, p. 207-232.
- [8] Sadananda, K., Vasudevan, A.K., “Non-Propagating Incipient Cracks from Sharp Notches Under Fatigue”, *Acta Materialia*, 52, 2004, p 4239-4249.
- [9] Kitagawa, H., Takahashi, S., “Applicability of Fracture Mechanics to Very Small Cracks or Cracks in the Early Stage”, *Proceedings 2<sup>nd</sup> International Conference on Mechanical Behavior of Materials*, American Society for Metals, Metals Park, OH, 1976, p 627-631.
- [10] Picu, C., “Interface Crack Impinging on a Triple Junction”, *International Journal of Solids Structures*, 1996, 33, 1563.
- [11] Picu, C., Gupta, V., “Stress Singularities at Triple Junctions with Freely Sliding Grains”, *International Journal of Solids Structures*, 1996, 33, 1535.
- [12] Halliday, M.D., Poole, P., Bowen, P., “In Situ SEM Measurements of Crack Closure for Small Fatigue Cracks in Aluminum 2024-T351”, *Fatigue and Fracture of Engineering Materials and Structures*, Vol 18, No 6, 1995, p 717-729.
- [13] Morris, W.L., “The Noncontinuum Crack Tip Deformation Behavior of Surface Microcracks”, *Metallurgical Transactions*, 1980, Vol 11A, p1117-1123.

- [14] Newman Jr., J.C., "A Crack-Closure Model for Predicting Fatigue Crack Growth Under Aircraft Spectrum Loading", *Methods and Models for Predicting Fatigue Crack Growth Under Random Loading*, STP 748, J.B. Chang, C.M. Hudson Eds., American Society for Testing and Materials, Philadelphia, 1981, p 53-84.
- [15] Morris, W.L., "Microcrack Closure Phenomena for Al 2219-T851, Metallurgical Transactions", 1979, Vol 10A, p5-11.
- [16] Taylor, D., Knott, J.F., "Fatigue Crack Propagation Behavior of Short Cracks: The Effect of Microstructure", *Fatigue of Engineering Materials and Structures*, Vol 4, No 2, 1981, p147-155.
- [17] El Haddad, M.H., Dowling, N.E., Topper, T.H., Smith, K.N., "J-Integral Application for Short Fatigue Cracks at Notches", *International Journal of Fracture*, Vol 16, No 1, 1980, p 15-30.
- [18] Newman Jr., J.C., Swain, M.H., Phillips, E.P., "An Assessment of the Small-Crack Effect for 2024-T3", *Small Fatigue Cracks*, Santa Barbara, CA, Jan. 1986, p 427-452.
- [19] Newman Jr., J.C., "Fracture Mechanics Parameters for Small Fatigue Cracks", *Small-Crack Test Methods*, ASTM STP 1149, J.M. Larsen and J.E. Allison, Eds., American Society for Testing and Materials, 1992, p 6-33.
- [20] Suresh, S., "Crack Deflection: Implications for the Growth of Long and Short Fatigue Cracks", *Metallurgical Transactions*, Vol 14A, 1983, p 2375-2385.
- [21] De Los Rios, E.R., Mohamed, H.J., Miller, K.J., "A Micro-Mechanics Analysis for Short Fatigue Crack Growth", *Fatigue and Fracture of Engineering Materials and Structures*, Vol 8, No 1, 1985, p 49-63.
- [22] McDowell, D.L., "Multiaxial Small Fatigue Crack Growth in Metals", *International Journal of Fatigue*, Vol 19, No 1, 1997, p S127-S135.
- [23] Kulkarni, V.G., *Modeling and Analysis of Stochastic Systems*, Chapman and Hall/CRC, New York, 1995.
- [24] Gansted, L., Brincker, R., Hansen, L.P., "Fracture Mechanical Markov Chain Crack Growth Model", *Engineering Fracture Mechanics*, Vol 38, No 6, 1991, p 475-489.
- [25] Ortiz, K., Kiremidjian, A.S., "Stochastic Modeling of Fatigue Crack Growth", *Engineering Fracture Mechanics*, Vol 29, No 3, 1988, p 317-334.
- [26] Cox, B.N., Morris, W.L., "A Probabilistic Model of Short Fatigue Crack Growth", *Fatigue and Fracture of Engineering Materials and Structures*, Vol 10, No 5, 1987, p 419-428.

- [27] Cox, B.N., Morris, W.L., “Model-Based Statistical Analysis of Short Fatigue Crack Growth in Ti-6Al-2Sn-4Zr-6Mo”, *Fatigue and Fracture of Engineering Materials and Structures*, Vol 10, No 6, 1987, p 429-446.
- [28] Halliday, M.D., Cooper, C., Poole, P., Bowen, P., “On Predicting Small Fatigue Crack Growth and Fatigue Life from Long Crack Data in 2024 Aluminum Alloy”, *International Journal of Fatigue*, Vol 25, 2003, p 709-718.
- [29] Kitagawa, H., Nakasone, Y., Miyashita, S., “Measurement of Fatigue Damage by Randomly Distributed Small Cracks Data”, *Fatigue Mechanisms: Advances in Quantitative Measurement of Physical Damage*, ASTM STP 811, J. Lankford, D.L. Davidson, W.L. Morris and R.P. Wei, Eds., American Society for Testing and Materials, 1983, p 233-263.
- [30] Sobol', I.M., *A Primer for the Monte Carlo Method*, CRC Press, New York, 1994.
- [31] Lawson, L., Chen, E.Y., Meshii, M., “Micro-structural Fracture in Metal Fatigue”, *International Journal of Fatigue*, 1997, Vol. 19, Supp. No. 1, S61-S67.
- [32] Cox, B.N., Morris, W.L., “Monte Carlo Simulations of the Growth of Small Fatigue Cracks”, *Engineering Fracture Mechanics*, Vol 31, No 4, 1988, p 591-610.
- [33] Cox, B.N., “Inductions From Monte Carlo Simulations of Small Fatigue Cracks”, *Engineering Fracture Mechanics*, Vol 33, No 4, 1989, p 655, 670.
- [34] Murakami, Y., Nemat-Nasser, S., “Growth and Stability of Interacting Surface Flaws of Arbitrary Shape”, *Engineering Fracture Mechanics*, Vol 17, No 3, 1983, p 193-210.
- [35] Steadman, D.L., “Growth-Arrest Behavior of Small Fatigue Cracks”, PhD Thesis, Georgia Institute of Technology, 1997.
- [36] Chen, E.Y., Lawson, L., Meshii, M., “Comparison of the Growth of Individual and Average Microcracks in the Fatigue of Al-SiC Composites”, *Metallurgical and Materials Transactions*, Vol 26A, 1995, p 3163-3176.
- [37] Chen, E.Y., Lawson, L., Meshii, M., “The Effect of Fatigue Microcracks on Rapid Catastrophic Failure in Al-SiC Composites”, *Materials Science and Engineering*, A200, 1995, p 192-206.
- [38] Laz, P.J., Craig, B.A., Hillberry, B.M., “A Probabilistic Total Fatigue Life Model Incorporating Material Inhomogeneities, Stress Level and Fracture Mechanics”, *International Journal of Fatigue*, 2001, S119-S127.
- [39] Laz, P.J., Hillberry, B.M., “Fatigue Life Prediction from Inclusion Initiated Cracks”, *International Journal of Fatigue*, Vol 20, No 4, 1998, p 263-270.

- [40] Newman, J.C. Jr., FASTRAN II – A fatigue crack growth structural analysis program. NASA-TM-104159, Hampton, VA; NASA Langley Research Center, 1992.
- [41] Suresh, S., Ritchie, R.O., “Propagation of Short Fatigue Cracks”, *International Metals Reviews*, Vol 29, No. 6, 1984.
- [42] Detter-Hoskin, L., Patel, G., “Measurement of Particle Size and Grain Size in Al 7075 Hot-Rolled Sample”, GTRI Sub. Project No. A7542-000, 2004.
- [43] Morris, B.R., Gokhale, A.M., Vander Voort, G.F., “Grain Size Estimation in Anisotropic Materials”, *Metallurgical and Materials Transactions*, 1998, Vol 29A, p. 237-244.
- [44] Pilkey, W.D., *Peterson's Stress Concentration Factors*, Wiley, New York, USA, 1997.
- [45] Young, W.C., Budynas, R., *Roark's Formulas for Stress and Strain*, McGraw Hill Professional, USA, 2001.
- [46] Carlson, R.L., Steadman, D.L., Kardomateas, G.A., “An examination of Small Fatigue Crack Morphology”, *International Journal of Fracture*, 108, 2001, p 63-72.
- [47] Swain, M.H., “Monitoring Small-Crack Growth by the Replication Method”, *Small-Crack Test Methods*, ASTM STP 1149, J.M. Larsen and J.E. Allison, Eds., American Society for Testing and Materials, 1992, p 34-56.
- [48] Carlson, R.L., Steadman, D.S., Kardomateas, G.A., “Fatigue growth of Small Corner Cracks in Aluminum 6061-T651”, *International Journal of Fatigue*, Vol. 19, Supp. No. 1, 1997, p S119-S125.
- [49] Carlson, R.L., Halliday, M.D., “An Extrapolation Method for Estimating Crack Growth Rate Confidence Intervals from Small Fatigue Crack Data”, *Journal of Testing and Evaluation*, May 2002, Vol 30 No. 3, p 179-185.
- [50] Bannantine, J. A., Comer, J.J., Handrock, J.L., *Fundamentals of Metal Fatigue Analysis*, Prentice Hall, NJ, 1990.
- [51] Anderson, T.L., *Fracture Mechanics: Fundamentals and Applications*, CRC Press, New York, 1995.
- [52] ASTM 647 Standard Test Method for Measurement of Fatigue Crack Growth Rates
- [53] Lamberson, L.E., "Fatigue and Fracture of Thin Metallic Foils with Aerospace Applications", Masters Thesis, Georgia Institute of Technology, 2006.

- [54] Chen, E.Y., Sauer, S., Meshii, M., Tucker, W.T., "Fatigue Microcrack Distributions and the Reliability of a Nickel Base Superalloy", *International Journal of Fatigue*, Vol 19, No 1, 1997, p S75-S82.
- [55] Miller, K.J., "The Short Crack Problem", *Fatigue of Engineering Materials and Structures*, Vol 5, No 3, 1982, p 223-232.
- [56] Hald, A., *Statistical Theory with Engineering Applications*, John Wiley and Sons, New York, 1952.
- [57] Hayter, A., *Probability and Statistics for Engineers and Scientists*, Thomson, USA, 2007.
- [58] *Military Handbook 5H: Metallic Materials and Elements for Aerospace Vehicle Structures*, DOD, 1998.
- [59] Carlson, R.L., Kardomateas, G.A., "Effects of Compressive Load Excursions on Fatigue Crack Growth", *International Journal of Fracture*, Vol 16, 1994, p 141–146.
- [60] Plumtree, A., O'Connor, B.P.D., "Influence of Microstructure on Short Fatigue Crack Growth", *Fatigue and Fracture Mechanics of Engineering Materials and Structures*, Vol 14, No 2/3, 1991, p 171-184.
- [61] Lütjering, G, Williams, J.C., *Titanium*, Springer-Verlag, NY, 2003.
- [62] Saxena, A., *Nonlinear Fracture Mechanics*, CRC Press, New York, 1998.
- [63] Samuels, L. E., *Metallographic Polishing by Mechanical Methods*, American Society for Metals, Metals Park, OH, 1982.
- [64] Hertzberg, R.W., *Deformation and Fracture Mechanics of Engineering Materials*, John Wiley and Sons, New York, 1976.
- [65] McDowell, D.L., "An Engineering Model for Propagation of Small Cracks in Fatigue", *Engineering Fracture Mechanics*, Vol 56, No 3, 1997, p 357-377.